


CHARLES UNIVERSITY
First Faculty of Medicine

MUDr. Pavel Hála

Department of Physiology

Hemodynamic adaptation mechanisms of heart failure to percutaneous venoarterial extracorporeal circulatory support

Mechanismy adaptace hemodynamiky při uplatnění perkutánní venoarteriální mimotělní podpory oběhu u srdečního selhání

Dissertation thesis

Supervising tutor:
Prof. MUDr. Otomar Kittnar, CSc., MBA

Study program:
Human Physiology and Pathophysiology

Praha, 2020

Declaration:

I declare that I carried out this dissertation thesis independently and that all sources were cited correctly. This thesis has not been submitted previously for the award of any other academic degree or diploma.

Prohlášení:

Prohlašuji, že jsem závěrečnou práci zpracoval samostatně a že jsem řádně uvedl a citoval všechny použité prameny a literaturu. Současně prohlašuji, že práce nebyla využita k získání jiného nebo stejného titulu.

Souhlasím s trvalým uložením elektronické verze mé práce v databázi systému meziuniverzitního projektu Theses.cz za účelem soustavné kontroly podobnosti kvalifikačních prací.

In ..... date ....

Author's signature

Identification record:

HÁLA, Pavel. Hemodynamic adaptation mechanisms of heart failure to percutaneous venoarterial extracorporeal circulatory support. Praha, 2020. Dissertation thesis (PhD). Charles University, First Faculty of Medicine, Department of Physiology. Supervising tutor: KITTNAR, Otomar.

Identifikační záznam:

HÁLA, Pavel. Mechanismy adaptace hemodynamiky při uplatnění perkutánní venoarteriální mimotělní podpory oběhu u srdečního selhání. Praha, 2020. Dizertační práce (PhD). Univerzita Karlova, 1. lékařská fakulta, Fyziologický ústav. Vedoucí práce: KITTNAR, Otomar.

Acknowledgments

First of all, I would like to thank my tutor – professor Otomar Kittnar – who kindly supervised my postdoctoral studies and supported and motivated me in my work.

While learning about the principles of circulatory supports, facilities of the Experimental laboratory at Albertov became an amazing place where our initial ideas were transformed into real practice. In team cooperation with fellow laboratorians, scientists, and doctors, we were able to design and set novel experiments to help me understand and explain pathophysiological mechanisms of circulatory supports. It was a school of great value and pleasant nature at the same time.

I can hardly imagine to acquire better practical skills and medical knowledge than during my fellowship at Na Homolce Hospital. I found here inspiration for research and source of clinical observations, which come together with perfect leadership for my training.

An important period of my postdoctoral studies were connected to the Extracorporeal life support laboratory at the University of Michigan. During a long-term research fellowship, a valued cooperation was established and I was offered to participate in a broad spectrum of projects including cardiopulmonary resuscitation, organ preservation, or the applications of nitric oxide.

I endlessly value the facts that on this long and winding road many of my close friends helped and many of my colleagues became my friends. Without their little help, the presented work would never get by. The passion for physiology, medicine, and research became our common motivation on every day in the life.

Contents

Abbreviations

ANP, BNP – atrial and brain natriuretic peptides
CO – cardiac output
dP/dt_{max} – maximal positive pressure change
dP/dV – diastolic stiffness
Ea – effective arterial elastance
EBF – extracorporeal blood flow
ECLS - extracorporeal life support
ECMO – extracorporeal membrane oxygenation
EDA, ESA – end-diastolic and end-systolic area
EDD – end-diastolic diameter
EDP, ESP – end-diastolic and end-systolic pressure
EDV, ESV – end-diastolic and end-systolic volume
Ees – slope of ESPVR
EF – ejection fraction
ELSO – Extracorporeal Life Support Organization
FAC – fractional area change
HF – heart failure
HR – heart rate
LV – left ventricle
LVAD – LV assist device
MVO_2 – myocardial oxygen consumption
PE – myocardial potential energy
PI – pulsatility index
PV (loop) – pressure-volume (loop)
PVR – pressure-volume relationship
rSO_2 – regional tissue oxygenation
RV – right ventricle
SV – stroke volume
SvO_2 – mixed venous blood saturation
SW – stroke work
TAPSE – tricuspid annular plane systolic excursion
VPO – ventricular power output

1 Introduction

Patients suffering of heart failure (HF) require intensive and highly specialized management from the onset of disease. Combination of life style, medication and implantable electrical devices is considered conventional therapy. Despite of full supportive treatment, patient's hemodynamic status can change abruptly into circulatory decompensation and cause severe prognosis (Jackson et al. 2000).

In situations when circulatory failure may not be possible to treat with conventional methods, extracorporeal life supports (ECLS) can temporarily substitute the function of heart and lungs and provide time for treatment of underlying disease (Abrams et al. 2014, Brogan et al. 2017). These advantages in combination with ease of circuit introduction led to wide spread of ECLS (Brogan et al. 2017).

Artificial circuit can substitute the pump function of heart (Pranikoff et al. 1994, Combes et al. 2008), but due to changes in hemodynamics, its flow increases afterload of left ventricle (LV) and puts higher demands on heart work (Seo et al. 1991, Aissaoui et al. 2012, Burkhoff et al. 2015, Broome and Donker 2016, Truby et al. 2017). Further hemodynamic complications like LV dilation or pulmonary edema were described but their risk factors remain unclear (Barbone et al. 2011, Soleimani and Pae 2012, Boulate et al. 2013).

Therefore, monitoring and better understanding of heart hemodynamics during ECLS might improve prognosis (Soleimani and Pae 2012, Truby et al. 2017, Na et al. 2019). This text will focus on the current use and effects of ECLS during acute decompensation of HF and available methods of hemodynamic assessment.

1.1 Heart failure

The performance of the heart depends on the following components: stroke volume (SV; influenced by contractility, preload, and afterload) and heart rate. HF describes situations when the heart is not able to maintain adequate cardiac output (CO) to meet body requirements. Common classification distinguishes between acute and chronic HF by the speed of symptoms onset.

1.1.1 Causes of HF

HF results from a decline in SV that is due to systolic dysfunction, diastolic dysfunction, or a combination of the two. Typically, causes for HF can lie in impaired myocardial contractility itself or in long-lasting ventricular volume or pressure overload. Coronary hypoperfusion is the underlying cause in majority of patients. Arterial hypertension has been reported as the cause of HF with or without other factors in over 70%. It predisposes to the development of HF through several pathological mechanisms, including LV hypertrophy, ischemia, and predisposition to arrhythmias. Cardiomyopathies are primary diseases of heart muscle and their classification distinguishes three basic types: dilated, hypertrophic, and restrictive cardiomyopathies. All of them can progress into symptomatic HF. Valvular diseases, both regurgitation and stenosis, put higher preload or afterload to

ventricular hemodynamics and lead to dilation and failure of overloaded chambers. Severe rhythm disturbances and conduction blocks also participate to inefficient heart work (Jackson et al. 2000).

1.1.2 Pathophysiology of acute HF

Acute HF is defined by an abrupt reduction in CO. Mechanisms like extremely high or low frequencies, contractile dysfunction (ischemia, toxic), pericardial tamponade, acute heart valve failure, or acute increases to ventricular afterload or preload can immediately progress into the symptoms of HF.

1.1.3 Pathophysiology of chronic HF

Chronic HF or insufficiency occurs by long-lasting volume or pressure overload of heart muscle. With progressive exhaustion of heart muscle, increased afterload or preload can slowly progress into reduction of CO. Chronic HF is associated with neurohormonal activation and allows to fully develop systemic adaptation mechanisms (Ošťádal and Vízek 2005).

In typical scenario of chronic HF with slow progression, the body can tolerate more profound decreases in CO as compensatory mechanisms have enough time to develop. Most prominent symptoms include dyspnea, fatigue, and lethargy as a consequence of tissue hypoperfusion. Fluid retention and capillary hydrodynamic pressure increase lead to edemas in predisposing tissues, effusions, and in severe cases to pulmonary edema. Physical signs include elevated jugular venous pressure, tachypnea, orthopnea, reduced exercise tolerance, pulmonary crepitation, swelling.

1.1.4 Integration of Cardiac and Vascular Changes

Both systolic and diastolic heart failure lead to changes in systemic vascular resistance, blood volume, and venous pressures. These changes, which can be examined by using cardiac and vascular function curves (Figure 1), help to compensate for the loss of cardiac performance. However, these compensatory responses cause a large increase in venous pressure that can lead to edema. Furthermore, the increase in systemic vascular resistance increases the afterload on the LV, which can further depress its output.

1.1.5 Compensatory mechanisms in HF

If CO is reduced but allows temporary survival, compensation mechanisms to improve organ perfusion are activated. They initially improve contraction and maintain integrity of the circulation in order to mitigate the depressed hemodynamics. Although these mechanisms provide valuable support, they also have an important role in the development and progression of HF. Also, in cases of their exhaustion or additional negative impact, compensated HF can progress into acute heart decompensation with an CO insufficient to meet requirements (Ošťádal and Vízek 2005). Hence, can arrhythmias, myocardial ischemic events, or just weakening of compensatory mechanisms initiate a vicious cycle of cardiogenic shock which leads to death if not adequately supported (Figure 2).

Following compensatory mechanisms play important roles in HF pathophysiology.

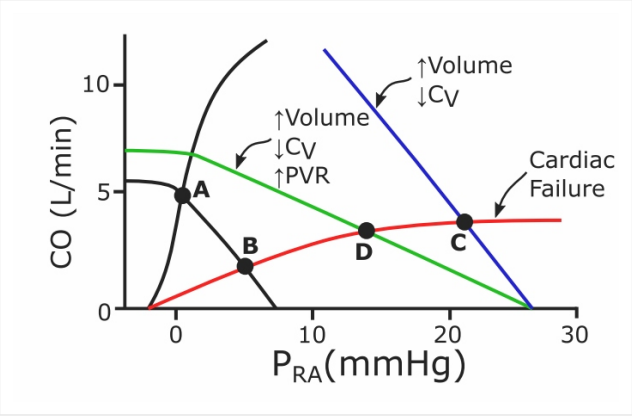

Figure 1. Changes in cardiac output (CO) and right atrial pressure (P_{RA}) in response to cardiac failure. Cardiac and vascular function curves at normal state (black) meet at an equilibrium point **A**. With reduction in contractility, cardiac curve shifts downwards (red) and moves the equilibrium point to **B**. When these changes are coupled with compensatory increase in blood volume and decreased venous compliance (C_V), rightward shift of vascular curve (blue) generates new equilibrium point at **C**. Finally, with increase of peripheral vascular resistance (PVR) the vascular curve reduces its slope (green) and results in equilibrium point **D**.

Sympathetic nervous system

The sympathetic nervous system is quickly activated via chemo- and baroreceptors as an early compensatory mechanism in an attempt to maintain cardiac output. Rise in plasma catecholamines leads to a chronotropic stimulation and accelerated resting heart rate. Consequently, higher oxygen consumption is demanded by the myocardium, but the diastolic time shortens and limits the coronary perfusion. Elevated resting heart rate is considered one of independent prognostic factors of HF (Reil and Bohm 2008).

In long-term, chronic high catecholamine concentrations lead to down regulation of beta receptors on cardiomyocytes, so the sympathetic effects are attenuated and reduction in heart rate variability can be observed. In addition, vagal parasympathetic activity to the heart is reduced. Another pathophysiological mechanisms reducing contractility in chronic HF would be the force-frequency relationship. In contrast to a healthy heart, this relation becomes flat or negative in chronic HF (Davies et al. 1995).

Renin-angiotensin-aldosterone system

Stimulation of renin-angiotensin-aldosterone pathway increases concentrations of plasma renin, angiotensin II, and aldosterone. Angiotensin II is a potent vasoconstrictor of renal efferent arterioles and systemic circulation. It also stimulates sympathetic, but suppresses vagal tone, which contributes to endothelial dysfunction. Further, aldosterone effects on sodium retention add to extracellular fluid expansion, thus it elevates both ventricular filling pressures and afterload (Packer 1992).

Natriuretic peptides

Several natriuretic peptides, of similar structure, have been isolated and their function on the heart, kidneys, and nervous system described. Atrial and brain natriuretic peptides (ANP, BNP) are released from the atria and ventricles, respectively, in response to stretch. The main effects are vasodilation and natriuresis. ANP and BNP concentrations increase in response to volume expansion and act as physiological antagonists to the effects of angiotensin and aldosterone. This fact allows to use concentration of the natriuretic

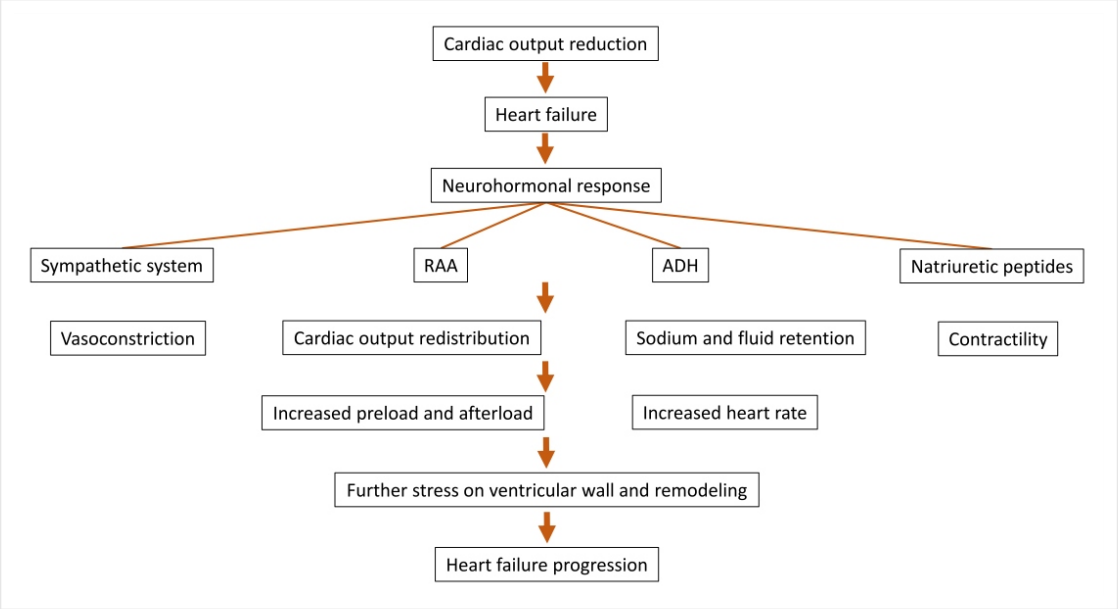

Figure 2. Neurohormonal activation and compensatory mechanisms in heart failure. Other factors include endothelin or intrinsic nitric oxide release. RAA – Renin-angiotensin-aldosterone system, ADH – Antidiuretic hormone/vasopressin.

peptides in plasma as diagnostic and prognostic markers (Gardner et al. 2003).

Antidiuretic hormone

Antidiuretic hormone (vasopressin) concentrations are also increased in severe chronic heart failure. It has a fluid retention effect and in high concentrations is a strong vasoconstrictor.

Other hormonal mechanisms

Several other hormones have been recognized to participate in the pathophysiology of HF. Endothelin is secreted by endothelial cells and is a potent vasoconstrictor. Up to some extend, this is opposed by endogenous nitric oxide, prostaglandins E2 and I2, or bradykinin from kallikrein-kinin system.

In summary, key neurohormonal systems maintain cardiac output with an increase in heart rate, contractility, and peripheral vasoconstriction, and increase in blood volume with retention of salt and water. Temporarily, compensatory mechanisms help for the cost of higher energy demands, but when persisting, these systemic responses have detrimental effects on the heart and systemic organs. On the other hand, when these mechanisms are not sufficient and fail, acute decompensation of heart failure occurs and requires immediate treatment.

1.1.6 Clinical presentation

In typical scenario of chronic HF with slow progression, the body can tolerate more profound decreases in CO as compensatory mechanisms have enough time to develop. Most prominent symptoms include dyspnea, fatigue, and lethargy as a consequence of tissue underperfusion. Fluid retention and capillary hydrodynamic pressure increase lead to edemas in predisposing tissues, effusions, and in severe cases to pulmonary edema.

Physical signs include elevated jugular venous pressure, tachypnea, orthopnea, reduced exercise tolerance, pulmonary crepitation, swelling.

Classification of HF severity is traditionally based on exercise capacity and is used to monitor the response to treatment. New York Heart Association (NYHA) classification distinguishes between four groups: I) asymptomatic with no limitation of normal physical activity, II) mild limitations, III) moderate, and IV) severe with symptoms at rest.

Killip classification grades the severity of decompensated HF into four classes: I) no signs of LV dysfunction, II) pulmonary congestion, III) pulmonary edema, and IV) shock syndrome. Associated hospital mortality increases from 6% for class I to 90% for class IV.

1.1.7 Therapy and prognosis

Prognosis of HF

In the Framingham Heart Study, the overall survival at 8 years for all NYHA classes was 30% while over 60% one-year mortality was observed in class IV (Watson et al. 2000). Predictors of poor outcome include reduced LV systolic function, low peak oxygen consumption, increased LV filling pressure, low cardiac index, comorbidities like diabetes mellitus, and raised plasma catecholamine and natriuretic peptide concentrations. Acute decompensation or in the worst case sudden death most often arise from ventricular arrhythmias, although asystole and new coronary thrombosis is another common event in severe HF (Uretsky et al. 2000, Watson et al. 2000).

HF therapy

Therapy of HF and its progression is complex. Salt and fluid restriction, exercise training in combination with advances in pharmacological management and implantable electric device therapies all improve quality of life and survival.

1.1.8 Acute management strategies

Acute HF decompensation represents a medical emergency and its management strategies include oxygen therapy in hypoxemic patients, diuretics to reduce intravascular volume, nitrates with vasodilating effect in volume overload, or vasopressors such as norepinephrine or dobutamine to raise blood pressure to redistribute CO to vital organs. However, these are potentially hazardous due to generation of increased ventricular afterload and myocardial oxygen demands and can further worsen peripheral tissue perfusion (Werdan et al. 2014). Vasopressoric agents and volume expansion place an added burden on the heart, increase cardiac work, and may cause myocardial ischemia (Fuhrman et al. 1999). Immediate correction of underlying etiology remain the ultimate treatment for severe shock states (Millane et al. 2000).

In cases when full compensating mechanisms and available conventional treatment fail to stop HF progression, non-conventional treatment represented by implantable ventricular assist devices or extracorporeal circulatory supports remain the only modalities to temporarily substitute heart or heart and lung functions. For acute clinical presentations, implantation of intracorporeal devices is too complex and only devices allowing percutaneous access are suitable due to their fast initiation (Werdan et al. 2014). These

are referred to as extracorporeal life support (ECLS) systems and underwent a massive development in recent decades.

1.2 Heart failure models

Modeling HF in experimental settings has been a common practice of research to understand hemodynamic effects of circulatory supports (Power and Tonkin 1999, Dixon and Spinale 2009). In general, the availability and variety of animal models used for hemodynamic studies is wide and offers choice for many specific needs. For these experiments, mostly porcine, canine, ovine or with smaller settings frequently murine models are being chosen offering a good simulation of expected human body reactions (Power and Tonkin 1999). Furthermore, forms of single organ experiments (Trahanas et al. 2016, Church et al. 2017) or computer HF modeling (Broome and Donker 2016) are becoming more frequent. To reliably mimic pathophysiology of HF, circulation is being artificially deteriorated. Damage to the heart can be caused by various tactics, often by one of ischemia, arrhythmia, pressure overload or cardiotoxic effects of drugs, any of these leading to hemodynamic deterioration of the model (Power and Tonkin 1999, Dixon and Spinale 2009, Ostadal et al. 2016, Lacko et al. 2018). To produce a true model of chronic HF, time has to be provided for developing the long-term adaptation of the whole organism.

Most of the published experiments on left ventricular (LV) performance and hemodynamics of mechanical circulatory support have been studied on experimental models of acute HF (Bavaria et al. 1988, Shen et al. 2001, Mlcek et al. 2012, Ostadal et al. 2014, Ostadal et al. 2015, Ostadal et al. 2016) or even on completely intact hearts. On the other hand, in clinical practice mechanical circulatory supports are often being applied in status of circulatory decompensation which develops on grounds of previously already present chronic heart disease. In such situations the adaptation mechanisms are fully developed and can play important role in inconsistency of outcomes observed according to the "acuteness or chronicity" of underlying cardiac disease (Tarzia et al. 2015). Although there are reasons why the use of chronic HF models is scarce – time-consuming preparations, instability of heart rhythm, high mortality rates, ethical questions – the advantages of using chronic HF models are evident as they offer prolonged neurohumoral activation, general systemic adaptation, functional changes of cardiomyocytes, and structural alterations of heart valves (Howard et al. 1988, Moe and Armstrong 1999, Power and Tonkin 1999, Schmitto et al. 2011).

Such a reliable and stable model is well represented by tachycardia-induced cardiomyopathy (TIC) which can be produced by rapid cardiac pacing in experimental animal (Hala et al. 2018). Porcine, canine or ovine TIC models were repeatedly prepared to study the pathophysiology of heart failure (Power and Tonkin 1999). Changes to the left ventricle mimic the entity of dilated cardiomyopathy (Spinale et al. 1990). Well described are hemodynamic characteristics – increased ventricular end-diastolic pressures, decreased cardiac output, increased systemic vascular resistance and dilation of both ventricles. In contrast, wall hypertrophy is not observed consistently and even wall thinning was described by some researchers (Chow et al. 1990, Howard et al. 1991). With progression of ventricular dimensions, regurgitation on atrioventricular valve develops (Howard et al. 1991).

1.3 ECLS

1.3.1 Definition of ECLS

In order to maintain life in an organism with failing oxygen delivery, we need to support circulation, gas exchange, or both. Extracorporeal life support (ECLS) is a treatment modality that provides prolonged blood circulation and gas exchange and can partially support or fully substitute functions of heart and lungs in patients with severe but potentially reversible cardiopulmonary failure refractory to conventional therapy. The system consists of intravascular cannulas connected to tubing set which is attached to mechanical pump. The extracorporeal circuit is then closed in a loop with a gas exchange unit, also called the artificial lung. Gas blender enables adjustment of the gas flow and oxygen fraction in the oxygenator. The functions of heart pump and lungs are transferred outside the body until the native organs recover. Due to this typical setting, ECLS is also referred to extracorporeal membrane oxygenation (ECMO) and went through thorough research and development in the last century. Although the main concepts remain, important improvements have been achieved, ECMO widespread globally, and its benefits are being applied in different fields of clinical and experimental medicine.

1.3.2 History of ECLS

The remarkable story of ECLS development can be traced for over three hundred years in the past and, as usual in medical field, its clinical use was preceded by sleepless nights ending with brilliant ideas. British physician, Benjamin Ward Richardson, MD, in 1860s demonstrated how oxygen and blood can be injected by a syringe to the right heart to create artificial circulation in animal experiments. In those early years, lack of anticoagulation did not allow to extend the research and limited the use of extracorporeal circuits due to excessive clot formations.

After loss of a young patient with pulmonary embolism in 1931, Doctor John Gibbon came to the revolutionary idea, that even short-term substitution of the human cardiopulmonary functions during an acute illness could save lives. He collaborated with his wife Mary at Jefferson Medical School in Philadelphia and they together developed a free-standing roller pump for extracorporeal support. In their heart-lung machine, which was the size of a small piano, thin films of deoxygenated blood were passing over a screen exposed to oxygen (Lillehei 1993, Bartlett 2014). After long 22 years Dr. Gibbon was able to use the device in practice. In May 1953 he performed the first successful extracorporeally assisted repair of atrial septal defect in the history (Figure 3). At similar times Richard DeWall and Dr. Walton Lillehei invented and firstly used a bubble oxygenator (Lillehei 1993, Kanto and Shapiro 1995).

Collaboration between biomedical engineers, physiologists, physicians, and surgeons finally led to reducing complications and development of blood gas machines for extended time periods. Important steps were machines working without a blood gas interface, controlled anticoagulation, and invention of silicone. Silicone rubber membrane lung invented in the 1960s by Theodor Kolobow revolutionized the artificial lung (Kolff et al. 1956, Kammermeyer 1957) as this material holds the hydrostatic pressure while remain permeable for gas. ECMO suddenly became feasible for days at a time (Bartlett et al. 1969).

Introduction of the ECMO to heart surgery and general clinical practice happened

Figure 3. John H. Gibbon, MD and patient Cecilia Bavolek, who underwent the landmark repair of an atrial septal defect utilizing an extracorporeal circuit. Source: Bloom et al. "John H. Gibbon, Jr., M.D.: surgical innovator, pioneer, and inspiration." (2011). Department of Surgery Gibbon Society Historical Profiles.

Figure 4. Esperanza, in 1975, the first successful neonatal application of ECMO, and, later in 1996, as an adult lady with Robert Bartlett and Theodor Kolobow. Source: ECLS Lab, University of Michigan.

soon after. The very first use for a traumatic ARDS by Don Hill in 1971 in Santa Barbara (Hill et al. 1972) and growing number of other cases were presented (Bartlett et al. 1976, Bartlett et al. 1977). Initially, ECMO was applied to children and adults to overcome circulatory failures and respiratory distress syndromes, later in 1975 Dr. Robert Bartlett, who is called the father of modern extracorporeal support, introduced ECMO also to neonates by rescuing a newborn baby dying from persistent pulmonary hypertension (Figure 4) (Bartlett 2017). At those times ECMO promoted improved survival rates in the surgical and intensive care community from only 10% to 75% (Bartlett et al. 1976) but the initial clinical study reported conflicting results (Zapol et al. 1979).

Soon major randomized clinical trials on effectivity of ECMO lead by Dr. Bartlett at University of Michigan and Dr. Pearl O'Rourke in Boston Children's Hospital revealed convincing superiority of ECMO therapy and ECMO progressed from a concept to clinical. Many centers were founded and a voluntary alliance of these active centers emerged. In 1989 the Extracorporeal Life Support Organization (ELSO) was established in Michigan. Its purpose is to gather data on ECMO support, exchange ideas, and, with the cooperation of its other four branches, help to maneuver ECLS intentions around the globe.

1.3.3 Indications and incidence of ECMO

The ECMO system consists of multiple components so different settings of ECMO are available and can be applied to various diseases of cardiorespiratory systems. With

different sizes of cannulas, tubing sets, pumps, and membrane lungs, ECMO serves in neonate, infant, and adult patients. In general, the basic principles for providing ECMO are 1) Reversible pathology which can be treated during the ECMO support and 2) The risks associated with ECMO are less than those of not providing it (Brogan et al. 2017).

Indications for ECMO

Typical cardiac indication would be an acutely decompensated HF with low cardiac output (cardiac index below 2 L/min/m^2) and hypotension despite adequate volumotherapy, inotropic agents, and other conventional methods (Makdisi and Wang 2015) but many more indications emerged during the years.

Neonatal and pediatric respiratory diseases

Neonatal respiratory diseases that can progress into respiratory failure were the initial indication for ECLS use and include mainly persistent pulmonary hypertension and hypoxic respiratory failure due to congenital diaphragmatic hernia, meconium aspiration, pneumonia, or sepsis.

When conservative therapy fails, many of these patients require ECMO. Commonly, these are due to insufficient pulmonary blood flow (Brogan et al. 2017). In the 1995 report from ELSO Registry (Bartlett 1997) 11 out of total 14 thousand ECMO applications were for neonatal respiratory failure. These were reported to have 80% survival. From the early 1990s the newer therapies such as surfactant, high frequency oscillator ventilation, and inhaled nitric oxide improved the survival of neonatal respiratory failure and reduced the use of ECMO (Haines et al. 2009). In 2015, there were 813 ECMO runs with 63% survival to hospital discharge (Thiagarajan et al. 2017).

In the pediatric respiratory category, pathologies of alveolar gas exchange by infections are the leading cause of respiratory failure. In 2015, there were 561 ECMO runs with 60% survival to hospital discharge according to the ELSO Registry (Thiagarajan et al. 2017).

Neonatal and pediatric cardiovascular diseases

Congenital heart disease, cardiomyopathy, myocarditis, or cardiac arrest were the most common diagnoses for ECMO therapy. In 2015, over a thousand of neonates and children needed ECMO with the survival between 45-61%, strongly depending on the age (Thiagarajan et al. 2017).

A specific case would be ECMO for maintaining fetal circulation when miniaturized extracorporeal circuit is used to support circulation of preterm newborns. This is sometimes referred to as artificial placenta and is still in the phase of pure experimental testing (Church et al. 2018, McLeod et al. 2019).

ECMO for respiratory disease in adults

Still in 2004, the adult respiratory failure was reported to be the smallest group in ELSO reports with less than 100 cases per year, but this number increased dramatically in 2009 due to the influenza pandemic and strongly positive results from CESAR trial favoring ECMO therapy (Peek et al. 2009). 2,046 runs were reported in 2015. Common causes are viral or bacterial pneumonia, ARDS and the average survival was 57%.

ECMO for cardiovascular disease in adults

With 2,167 cases reported to the registry, this was the largest group of adult patients in 2015. The most common cause for cardiac indication has been cardiogenic shock, cardiomyopathy, myocarditis, or congenital heart defects. Average duration of ECMO support was 5 to 8 days and survival 37-65%, both strongly depending on the diagnosis.

In cardiac arrest unresponsive to conventional cardiopulmonary resuscitation (CPR), ECMO can be used to provide time to restore spontaneous circulation (Swol et al. 2016). The ELSO registry has reported thousands of both pediatric and adult applications. With this indication, referred to as extracorporeal CPR (ECPR), the survival remains low at 28% (Haas et al. 2017, Richardson et al. 2017), but without the ECMO, none of these patients would be rescued. Despite intensive experimental research (Spinelli et al. 2016) and several clinical studies indicating possible benefit of ECPR (Chen et al. 2008, Wang et al. 2014), evidence remain limited and results from randomized trials are currently being awaited (Belohlavek et al. 2012, Lamhaut et al. 2017).

Other ECMO indications

ECMO can also be used in less common and more specific indications like massive pulmonary embolism, septic shock, severe trauma (Jacobs et al. 2015), primary graft failure after heart or lung transplantation, or periprocedural support for high-risk percutaneous cardiac interventions. In this scenario ECMO support of the native circulation is initiated preemptively in patients undergoing cardiac interventions when severe hemodynamic instability is expected. Applications with electro-anatomical mapping, catheter ablations, coronary interventions, or valve replacement were reported (Baratto et al. 2016).

In summary, when considering the ECMO therapy, the potential to recover from underlying disease, expected time frame of circulatory support requirement, skills of ECMO team, and ethical questions must all be taken into account. There will always remain some degree of uncertainty, but ECMO should not be started when there is 1) no chance, 2) no purpose, or 3) no ability to provide good quality of extracorporeal circulation.

Incidence and survival of ECMO use worldwide

Indications for ECMO can be divided into three categories according to the supported organ. Cardiac, respiratory, or the combination of the two. According to the data from the annual international ELSO Registry through January 2019, over total of 112,231 patients received ECLS. The majority of patients were adult patients 40%, 37% were neonates and 22% infants. The distribution of ECLS included 60,560 (54%) cases for respiratory failure, 39,256 (35%) cases for cardiac failure and 12,415 (11%) case for ECPR (ELSO Registry 2019).

Highest survival rate to discharge or transfer is steadily among neonatal ECMO population (66%), followed by pediatric (53%) and adult (48%) populations (Figure 5)(ELSO Registry 2019).

Trends of ECMO use worldwide

From the inception of the registry in 1989, some interesting trends can be tracked. In the 1995 report neonatal and pediatric indications formed vast majority of all cases, and even more interestingly, the cumulative total count of adults supported by ECMO was only 246. From the historical reports, massive increase in use for adult patients and cardiac diagnoses is observed since 2009. This boom of ECMO use in adult population for both respiratory and cardiac diagnoses was fueled mostly by the previously mentioned CESAR study results and global introduction of ECPR to resuscitation guidelines (Soar et al. 2015).

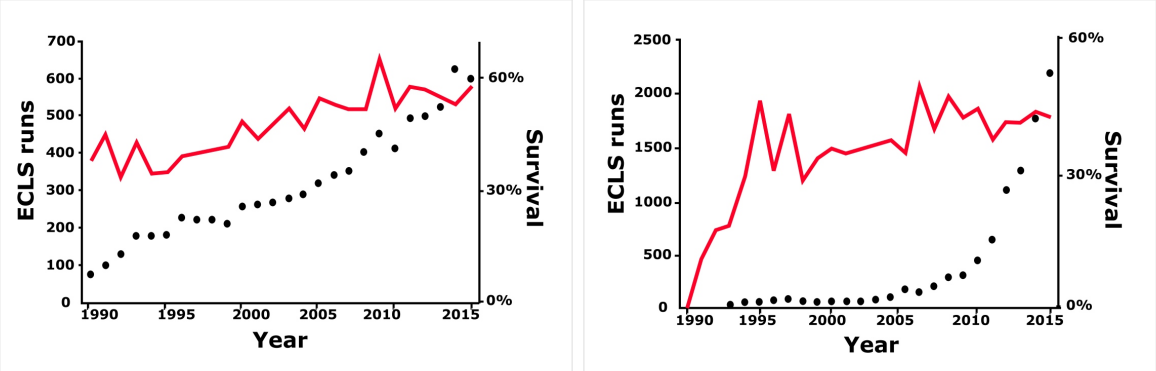

Figure 5. Extracorporeal life support use (black dots) and survival (red line) in cardiac disease in neonates (left) and adult patients (right) between the years 1990 and 2015. Modified from Thiagarajan et al. (2017).

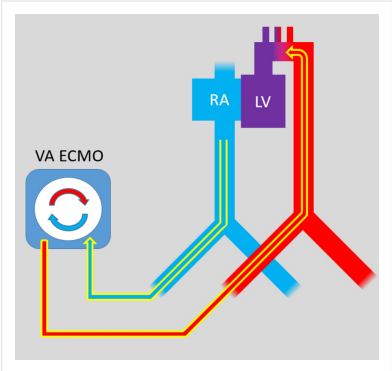

Figure 6. Femoro-femoral VA ECMO scheme. Venous blood is drawn by inflow cannula from right atrium (RA). It then continuous through the gas exchange unit by the force of blood pump and oxygenated is returned to the descending part of thoracic aorta. LV – left ventricle.

1.3.4 Anatomy of ECMO

Venovenous ECMO (VV ECMO)

In VV ECMO, both drainage and reinfusion are located in veins. Either a two separate cannulas or a single dual-lumen cannula can be introduced. Blood is usually drained from the common femoral vein and after gas exchange reinfused to internal jugular or femoral vein. In this case, ECLS does not support the circulation, so the patient must have stable hemodynamics. Thus, VV ECMO is indicated in patients with respiratory failure.

Venoarterial ECMO (VA ECMO)

VA ECMO provides both respiratory and hemodynamic support; native and extracorporeal circuits are connected in parallel. Blood is being drained from right atrium or vena cava and reinfused to arterial system or aorta (Figure 6).

The use of VA ECMO is well established and increasingly used in refractory cardiogenic shock due to post-cardiotomy syndrome, myocardial infarction, fulminant myocarditis, or other myocardial pathologies, massive pulmonary embolism (Abrams et al. 2014), or during cardiac arrest (Swol et al. 2016).

Technologically advanced pulsatile ECMO (PECMO) flow is supposed to improve hemodynamic parameters in acute HF (Itoh et al. 2016, Ostadal et al. 2018).

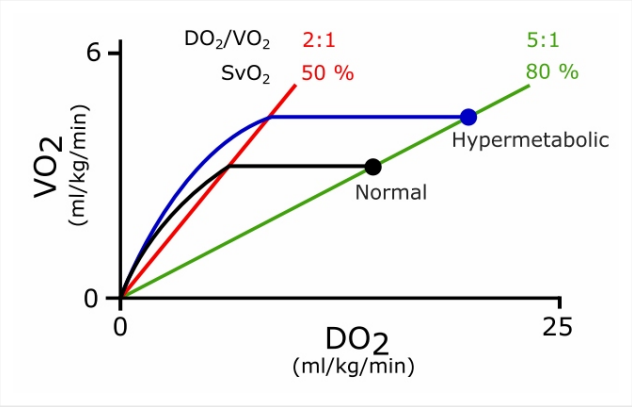

Figure 7. DO_2/VO_2 relationship during normal and high metabolic state. In both normal (black) and hypermetabolic (blue) state DO_2/VO_2 ratio of 5:1 (green) represents adequate tissue oxygen delivery. Low DO_2/VO_2 ratio of 2:1 (red) is unsustainable and progresses to anaerobic metabolism and shock. DO_2 – tissue oxygen delivery, VO_2 – oxygen consumption, SvO_2 – mixed venous saturation.

Venoarteriovenous ECMO (VAV ECMO)

In situations of combined lung and heart failure, an additional reinfusion cannula is placed to the jugular vein. This setting provides oxygenated blood to pulmonary circulation and subsequently this blood is ejected by the left ventricle and can perfuse coronary arteries.

Arteriovenous ECMO (AV ECMO)

Membrane lung can also be perfused from patient's arteries, fully avoiding blood pump. Its specific application is extracorporeal CO_2 removal ($ECCO_2R$) offering significant CO_2 elimination and decreasing the need for mechanical ventilation (Brodie et al. 2019).

1.3.5 Pathophysiology of VA ECMO

To patients with severe cardiorespiratory failure ECMO provides time to recover heart and lung functions but its technical nature also changes common physiological mechanisms. This chapter summarizes a review of cardiopulmonary physiology, pathophysiology, and ECMO physiology related to mechanical replacement of heart and lung function.

ECMO supplied oxygenation

Blood oxygen content is the sum of oxygen bound to hemoglobin and oxygen dissolved. Product of blood oxygen content and cardiac output (CO) equals to oxygen delivery to tissues (DO_2). Normal resting DO_2 is 600 mL/min/m^2, but the tissues consume (VO_2) only about 20% of the offered oxygen (Brogan et al. 2017). That is why hemoglobin in mixed venous blood saturation is about 80%. DO_2 and VO_2 variables are strongly affected by exercise, fever, other stress, catecholamine administration, respiration, cardiac output, or hemoglobin concentration. When oxygen extraction increases to 50% (i.e. DO_2/VO_2 ratio 2:1), tissues are not receiving enough oxygen to maintain aerobic metabolism (Figure 7). This situation is not sustainable, leading to metabolic collapse (Bartlett 2016, Brogan et al. 2017).

A goal of managing any critically ill patient is to maintain DO_2/VO_2 ratio close to normal or at least more than the critical 2:1 (Brogan et al. 2017). Indication for ECMO

is when DO_2 is inadequate or when the interventions needed are harmful (high dose catecholamines, high ventilatory pressures, high oxygen fraction). ECMO circuit in its venoarterial form drains most of the venous blood, pumps it through gas exchange unit, and returns it oxygenated into the systemic circulation. This provides time for the disease to be diagnosed and treated while maintaining sufficient DO_2.

ECMO blood flow

Blood pump generates the hydrodynamic force for the extracorporeal blood flow (EBF). The pressure has to push blood though the gas exchange unit, overcome all tubing and cannula resistances, and eject the blood back to the patient – against the aortic pressure. Importantly, most pump types create also negative pressure on the drainage site. This suction is harmful to blood cells, so pressures no more negative than -50 mmHg are targeted to prevent hemolysis. Pumps can be of centrifugal, servo-modified roller, or peristaltic design. Worldwide, centrifugal pumps are most commonly used and apart from few experimental exceptions, ECMO flow is continuous with no or minimal pulse pressures. Introduction of head wash-out in centrifugal pumps significantly reduced heat generation and consequently thrombus formation. Appropriate flow range must be chosen for to reflect individual patient needs.

Cannula size is the main limiting factor of EBF. The blood flow resistance depends on length and the fourth power of its inner diameter (Augustin et al. 2010). Blood viscosity being another independent parameter. Variation of cannula sizes and designs have been introduced. Material engineering developed cannulas with thin but durable walls as kinking, chugging, and clot formation strongly limit effectivity.

ECMO gas exchange

Gas exchange unit, also known as membrane or artificial lung or oxygenator, is the artificial organ where venous blood is being perfused through dense grid of hollow fibers filled with continuously blowing sweep gas. This gas can be pure oxygen or its mixture with air or CO_2. Blood and gas are sealed, so they do not appear in direct contact. Gas exchange is based on the same principles of solubility, diffusibility, and partial pressure gradients as on the alveolocapillary membrane. In order to meet requirements, the gas exchange unit must be able to transfer the amount of oxygen consumed, as well as the amount of CO_2 produced by the patient. The amount of gas exchange is a function of the membrane lung surface area, the gradient between the inlet and sweep gas concentrations. Oxygen gradient is generally higher, but its diffusibility and solubility are lower compared to CO_2. CO_2 clearance is generally managed by controlling the sweep gas flow; capacity of blood oxygenation of individual unit is described by the concept of "rated flow" – the maximum blood flow with which the venous blood is oxygenated to 95% (Figure 8). If water vapor condenses excessively on the membrane lung, gas exchange through membrane will be reduced – a similarity to the pathophysiology of pulmonary edema. Current generation of centrifugal pumps, polymethylpentene or polyolefin hollow fiber oxygenators, and biocompatible circuit materials significantly reduced problems commonly associated with older ECLS systems. Designing the exchange units for fast gas equilibration, while maintaining low pressure drop, low priming volume, and clot prevention are crucial aspects of current development. Experimental use of microfluidic artificial lung is promising for the future of membrane oxygenation (Thompson et al. 2019). The trend towards simplicity

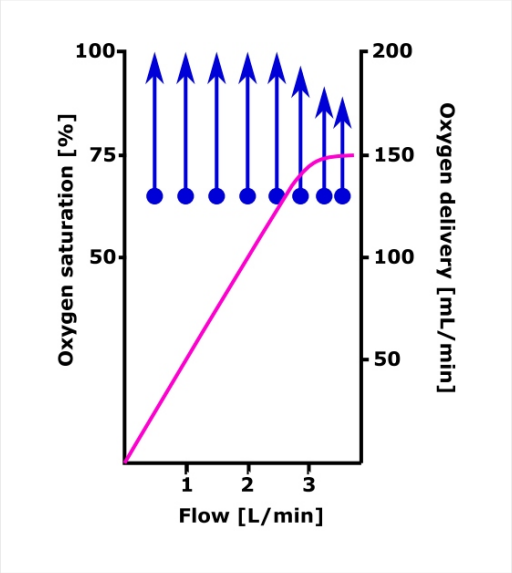

Figure 8. The concept of rated flow. Desaturated venous blood (points) is passed through the gas exchange unit and exits (arrow tips) at 100% saturation until the flow reaches a limit and full saturation is not feasible. This capacity of the gas exchange unit is described as "rated flow" (purple curve) and characterizes each artificial lung.

and integrated component systems further allow wide use of extracorporeal supports also in out-of-hospital settings.

1.3.6 Monitoring of ECMO circuit

Last, but important parts of every ECMO circuit are hemodynamic sensors for drainage and reinfusion cannula, pre and post oxygenator pressure registering. Electricity supply, heat exchange unit, blood gas analysis, and clot recognition devices all help to adjust the circuit settings to achieve the best performance and prevent complications.

1.3.7 Complications of ECMO

The benefits of ECMO must be weighed against possible risks. As it is an invasive therapy, multiple complications have been associated with the use of ECMO. These events participate on increased morbidity and mortality of ECMO treated patients (Abrams et al. 2014, Wang et al. 2014, Makdisi and Wang 2015).

Bleeding and coagulopathies

Commonly reported adverse events include significant bleeding. Even though bleeding is mostly located in cannulation sites and is associated with the necessary systemic anticoagulation, no universally accepted protocols are available and anticoagulation is being individualized. In meta-analysis, the incidence of bleeding complications is reported to >40% (Cheng et al. 2014). Heparin-induced thrombocytopenia and consumption of thrombocytes lead to reduced platelet count. Coagulation factors deficiencies (factor XIII, von Willebrand factor and fibrinogen) appear especially in long-term ECMO therapies (Makdisi and Wang 2015).

Thrombosis

Thromboses with risk of systemic embolization and stroke increases with long-term

ECMO use. Elevated pressure drop on the oxygenator and echocardiographic assessment can reveal potential clot formation in the circuit and heart. Prevention can be potentiated with anticoagulant-coated oxygenator and tubing surfaces or introducing nitric oxide into sweep gas. Risk of stroke during ECMO is reported to 6% and its pathophysiology has been well documented in experiments (Janak et al. 2017).

Limb ischemia

Arterial occlusion distally to reinfusion cannula and subsequent limb ischemia occurs in 10-20% of cases and depends on the cannulation technic. To prevent this complication, limb perfusion is ensured by additional antegrade sheath to the superficial femoral artery.

Others

Air embolism, hemolysis, and, more recently, complications associated with changes of hemodynamics have been described.

1.3.8 Hemodynamics of VA ECMO

As mentioned earlier, VA ECMO is an established method extensively being used to support circulation in the most severe conditions of HF decompensation like rapidly progressing cardiogenic shock or refractory cardiac arrest (Abrams et al. 2014, Werdan et al. 2014). When used properly, the ECMO system replaces part or all of heart and lung function, maintaining systemic perfusion while the damaged organs can recover or be replaced.

Interaction of multiple circulations

Unlikely to VV ECMO, the extracorporeal and native circulations in VA ECMO are connected in parallel. If some degree of CO is preserved, and thus the extracorporeal bypass is partial, both heart and ECMO are pumping blood into the aorta. Perfusate blood mixes in the aorta with left ventricular blood which passed through the lungs. Therefore, the arterial blood is a combination of blood from these two sources (Brogan et al. 2017) – aortic root is being filled antegradelly from the LV and descending aorta is receiving blood from the reinfusion cannula. The mixing site depends on the ratio of native CO and EBF and the position of cannula tip.

If the site of mixing happens in the aortic arch or descending aorta, coronary circulation and carotid arteries receive blood that passed through the lungs and was ejected by the left ventricle (Kinsella et al. 1992, Kamimura et al. 1999). In these situations, managing the lung ventilation is very important. If the lungs are working well, the LV ejects blood with optimal oxygen content. If the lungs are oxygenating poorly or not at all, the LV blood will have lower saturation. As a result, hypoxia of the tissues supplied by native cardiac output may occur. This is referred to as the "Harlequin syndrome" or differential cyanosis as the upper body parts are receiving less saturated blood. To prevent this severe condition of VA ECMO in cardiorespiratory failure, additional reinfusion cannula is placed into the right atrium, forming a combination of venoarterial and venovenous ECMO circuits and providing oxygenated blood to the pulmonary circulation and subsequently to the LV and coronary arteries.

Aortic pressure waveform

Hemodynamic effects on the aortic pressure waveform depend on the portion of extracorporeal support. With 100% flow support, LV is not contributing to blood stream and pulse pressure becomes flat. In such a case all tissues are perfused by artificial circuit and if heart valves are competent, blood stagnates in lungs and heart, producing risk for clot formation. Additionally, with no or severely limited heart ejection, LV gradually fills with blood from bronchial and Thebesian venous flows causing the ventricular end-diastolic pressure to increase. Aortic valve insufficiency can contribute to this phenomenon too (Sidebotham et al. 2012). With reducing the ECMO support and increasing the left ventricular contribution, pulse pressure increases. With support of 80%, pulse pressure of 10 mmHg is commonly observed (Brogan et al. 2017).

Cardiac hemodynamics on VA ECMO

VA ECMO supports systemic circulation by taking over part of cardiac workload, but it does not automatically reduce cardiac work (Fuhrman et al. 1999). Instead, reinfusion of blood from extracorporeal circuit increases systemic afterload. Especially with high EBF this increase becomes significant and LV ejection is competing with higher aortic pressure (Shen et al. 2001, Shen et al. 2001). The impairment of cardiac performance with increased EBF during VA ECMO has been well documented in several experimental and clinical studies (Seo et al. 1991, Aissaoui et al. 2012, Burkhoff et al. 2015, Broome and Donker 2016, Truby et al. 2017).

Impaired contractility reduces ejection, ventricles retain blood and dilate. Thereby LV end-diastolic pressure and wall tension rises which relates to sarcomere stretch throughout the myocardium. The contractility force will increase according to the Frank-Starling law, unless it becomes exhausted. In this setting, coronary perfusion may not keep pace with myocardial metabolic demands and initiates a vicious cycle.

To eject blood into the aorta, LV must exceed aortic diastolic pressure. If the LV is not capable of doing so, the aortic valve will not open. Although the heart would generate pressure, systemic arterial pressure trace will appear flat.

On the opposite site, right atrial pressure is reduced by draining blood into the venous cannula, decreasing ventricular preload (un-preloading of LV). This, by itself, improves organs perfusion at any aortic pressure. Draining the right heart should also reduce pulmonary artery pressure and allow remodeling of vascular smooth muscle (Fuhrman et al. 1999).

Multiple sources of blood for left atrium and LV are recognized - bronchial arterial flow, aortic regurgitant flow, right ventricular ejection, Thebesian veins, and flow through possible shunts. Left ventricular filling is then resultant combination of all these complex processes. At the moment when sources outweigh LV ejection, further increase in end-diastolic pressure, left atrial hypertension, and heart chambers dilation has to be expected.

Theoretically, if heart retains enough power, it can compete with VA ECMO-caused afterload and no congestion is to be awaited. But, if systolic function is severely compromised, VA ECMO can progress to left atrial hypertension and pulmonary congestion even with venous cannula drainage.

Progression to pulmonary congestion

With progression of this pathophysiology, increased pressure propagates to the left atrium. Left atrial hypertension adds to risk of pulmonary congestion and possibly edema development. This feared complication of VA ECMO can lead to irreversible lung damage within hours. Regular monitoring of pulmonary capillary wedge pressure can inform of venous congestion.

Myocardial perfusion

Myocardial oxygen demand is largely proportional to ventricular systolic pressure (Buckberg et al. 1972). Myocardial oxygen supply is directly proportional to coronary artery diastolic pressure and to duration of diastole (Brazier et al. 1974) and is inversely proportional to coronary sinus (subepicardial myocardium) and LV end-diastolic pressures (subendocardial myocardium) (Fuhrman et al. 1999). These are general rules, but with VA ECMO flow their parameters are significantly altered.

In general, VA ECMO flow increases perfusion of all systemic tissues. Nevertheless, its effect on myocardial perfusion is yet unclear (Werdan et al. 2014). Aortic reinfusion increases the LV afterload associated with higher arterial blood pressure, and thus it impacts myocardial work. It is a subject of research whether increasing stroke work caused by extracorporeal flow is accompanied by adequate myocardial oxygen supply. It has been suggested that as LV becomes distended, higher pressure is applied on the endocardial surface during diastole, potentially limiting perfusion of subendocardial myocardium (Kamimura et al. 1999). In animal experiments, higher VA ECMO flow was associated with lower coronary perfusion which was not accompanied by reduction of myocardial oxygen consumption (Kato et al. 1996). Even with low native cardiac output and dominant VA ECMO flow, more than 90% of the coronary blood flow is distributed from the LV ejection (Kinsella et al. 1992) and in a clinical study increase in coronary flow was observed with introduction of pulsatile form of VA ECMO (Cremers et al. 2015). Similarly, pulsatility of VA ECMO flow improved coronary perfusion in a model of hypoxemic acute HF at all degrees of circulatory support (Ostadal et al. 2018).

Left ventricular mechanics

By instantaneous measuring of pressure and cavitary volume, a typical pressure-volume (PV) loop depicts well ventricular mechanics of a single cardiac cycle. Under normal conditions, the PV loop is roughly trapezoidal, delimited by end-diastolic and end-systolic volume and pressure points (EDV, ESV, EDP, and ESP). Four sides connecting them then represent 1) isovolumic contraction; 2) ejection; 3) isovolumic relaxation; and 4) filling. Beginning after the isovolumic relaxation, LV volume starts to increase during diastole, and becomes maximal at end-diastole. Then the isovolumic contraction begins, LV pressure exceeds aortic pressure, and blood is being ejected while the LV volume decreases until the aortic valve closes. Stroke volume is represented by the width of the PV loop. Multiple load-dependent and load-independent indexes, like end-systolic and end-diastolic pressure-volume relationships (ESPVR and EDPVR), maximal positive pressure change (dP/dt_{max}), diastolic stiffness (dP/dV), and preload recruitable stroke work, can be calculated under various loading conditions. Without changes in contractile function and diastolic properties, PV loops will fit within the boundaries of ESPVR and EDPVR.

Ventricular afterload is determined by the vascular system (depicted as Ea - effective arterial elastance) against which the ventricle contracts; during VA ECMO support, this is strongly influenced by reinfusion blood flow.

$$Ea = \frac{ESP}{SV}$$

The intercept of Ea and ESPVR then determines ventricular-vascular coupling, the concept of ventricular preload, afterload, contractility, and blood circulation relations. Specifically, stroke volume (SV) can be estimated by the formula, where V_0 is ESPVR volume axis intercept, and Ees is the slope of ESPVR:

$$SV \approx (EDV - V_0) \,/\, \left(1 + \frac{Ea}{Ees}\right)$$

LV stroke work (SW) can be calculated as the integral of left ventricular transmural pressure (P) and cavitary volume (V) over each cardiac cycle as described by the formula:

$$SW = \int_{Vs}^{Vd} P \,\mathrm{d}V$$

Where Vs and Vd are systolic and diastolic ventricular volumes, respectively. By definition, SW is depictured as the area encircled by PV loop. To reflect the heart frequency (HR) on myocardial demands, ventricular power output (VPO) can be calculated (Glower et al. 1985):

$$VPO = SW * HR$$

Concept of PV loop also provides a platform to estimate myocardial oxygen consumption (MVO_2) which is linearly related to sum of SW and myocardial potential energy (PE):

$$MVO_2 \approx constant * (PE + SW)$$

In states of profound myocardial dysfunction, ventricular contractility is reduced. Increase in filling pressures is observed, but lowering Ees reflects impaired contractility. To compensate for low ejection, the ventricle operates in higher volumes but SV stays abnormally low. In the PV diagram this is demonstrated by a rightward shift and narrowing of the loop volume and pressure ranges (Figure 9).

With effects of VA ECMO cannulas suctioning and reinfusion of blood into the circulation, dramatic effects to LV hemodynamics are to be expected. Ventricular filling and peak pressures as well as contractility parameters are influenced by alterations in preload, afterload, and myocardial perfusion.

As VA ECMO reinfusion increases afterload, the Ea will increase, limiting the SV and increasing LV peak pressure (Figure 10 left). Depending on the resultant ventricular preloading and diastolic stiffness, the end-diastolic value of pressure and volume will shift the PV loop on EDPVR line. This is reflecting the LV distension. Lastly, depending on how VA ECMO will affect coronary perfusion and myocardial energetics, Ees (i.e. the ESPVR slope) will also decrease and push the end-systolic point of PV loop rightward (Burkhoff et al. 2015, Rihal et al. 2015). Increase in myocardial PE and probably also in SW must result in higher MVO_2.

In contrary, intra-aortic balloon pump reduces both LV peak and end-diastolic pressures and increases stroke volume (Figure 10 right). In a model of acute HF generated

by hypoxic myocardial perfusion Shen et al. (2001) reported decline of dP/dt_{max} and LV peak pressure associated with VA ECMO flow.

These basic hemodynamic principles are also affected by other factors like 1) right-sided factors; 2) cardiovascular substrate – e.g. a history of chronic heart failure with dilated, remodeled LV; or 3) the level of compensatory mechanisms. It is therefore important to distinguish between the primary hemodynamic effects of ECLS and the impact of secondary modulating factors invoked like changes in total peripheral vascular resistance and LV contractility (Burkhoff et al. 2015).

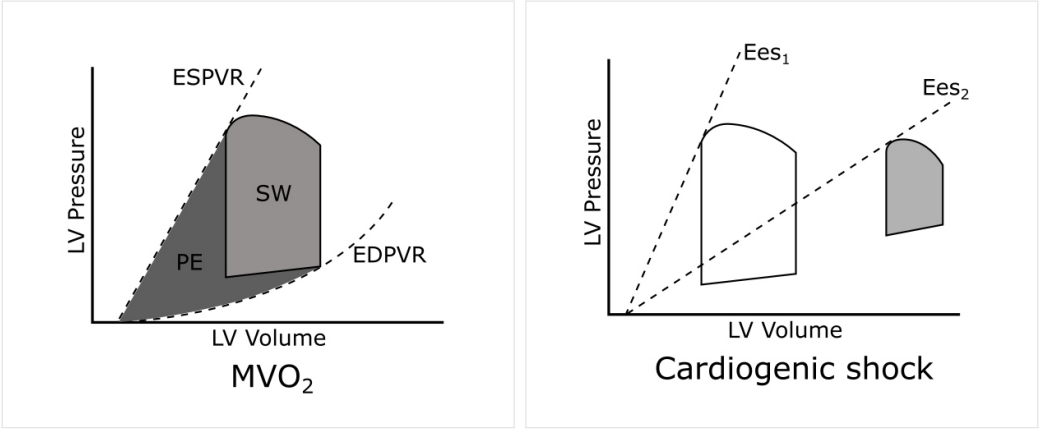

Figure 9. Pressure-volume parameters. Left - Myocardial oxygen consumption (MVO_2) is linearly correlated with pressure–volume area (PVA), which is the sum of the stroke work (SW) and potential energy (PE). Right – normal PV loop (white) and PV loop in cardiogenic shock (gray); Ees is severely reduced, LVEDV and LVEDP are increased, SV reduced.

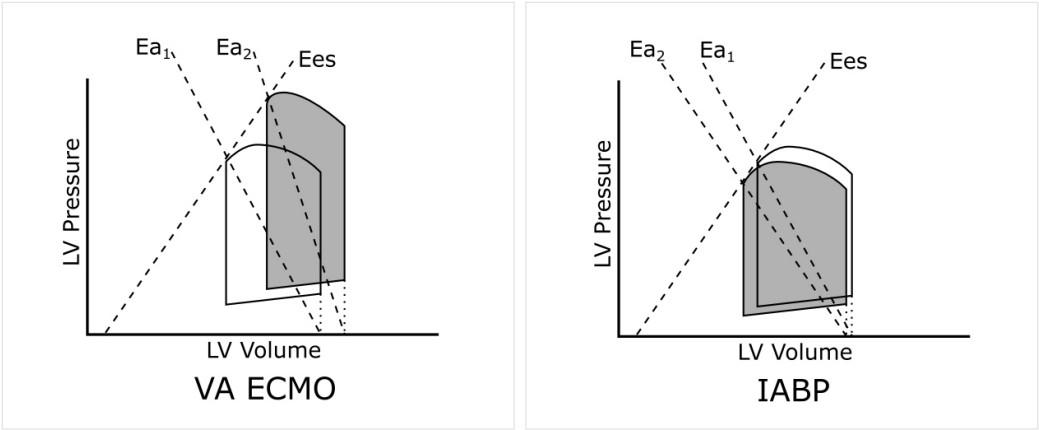

Figure 10. Changes of normal PV loop (white) by effects of mechanical supports (gray). Left – VA ECMO increases afterload ($Ea_1 < Ea_2$), reduces SV, and increases LVEDP and LVEDV. Right – Intraaortic balloon pump decreases afterload (Ea1 > Ea2) and enhances LV ejection.

Modeling the pathophysiology of ECMO circulation

Experimental animal models have become an important tool for ECMO circulation research (Table 1). On variety of conditions (healthy circulation, acute or chronic form

of HF, or cardiac arrest) improvements of hemodynamic status has been demonstrated – increases in arterial pressures, tissue saturation, or resuscitability. But it has also been revealed, that the interaction of double circulations influences myocardial perfusion (Kinsella et al. 1992, Kato et al. 1996), blood flow distribution (Kinsella et al. 1992), and most interestingly also alterations of energetic demands on the heart muscle. As a result, an undesirable hemodynamic effect of excessive VA ECMO flow was postulated (Seo et al. 1991, Aissaoui et al. 2012).

Methods of LV decompression

The use of VA ECMO in critically impaired heart function is associated with LV overload and dilation – when myocardial function cannot be instantly improved, left atrial hypertension escalates, and loss of arterial pulsation occurs. In such situations, several approaches have been suggested to decompress overloaded LV and decrease left atrial pressure (Soleimani and Pae 2012, Strunina and Ostadal 2016). Venting blood from the LV, atrium or pulmonary artery then becomes a life-saving intervention (Fuhrman et al. 1999, Oštádal et al. 2018). Besides, if right heart is drained, lymphatic drainage should also be promoted (Fuhrman et al. 1999).

Atrial septostomy

Left-to-right shunt at atrial septal defect can effectively reduce the left atrial pressure. Artificial defect created by a blade and balloon atrial septostomy has also been reported to passively decompress the left atrium and LV and relieve pulmonary congestion (Seib et al. 1999). The procedure was successful in all patients and with size of the atrial septal defect ranging between 2.5 and 8 mm, left atrial pressure fell from 16 to 30.5 mmHg.

Direct venting to reduce LV filling pressures

Surgical or mini-invasive transseptal introduction of venting cannula can be placed to left atrium or ventricle (Soleimani and Pae 2012, Boulate et al. 2013, Truby et al. 2017, Donker et al. 2019), or, in specific cases, also into pulmonary artery (Avalli et al. 2011). Cannula is then connected to the drainage site of ECMO circuit and with active suction limits ventricular overload and reduces wall stress. With the advantage of transesophageal echocardiography guidance, the left atrial cannula can be inserted during ongoing ECMO therapy (Strunina and Ostadal 2016). Direct LV venting can be done by placing a transaortic cannula or a pigtail catheter. Successful cases were reported by Barbone and Fumagalli (Fumagalli et al. 2004, Barbone et al. 2011). Although, with all these additional invasive procedures, an increased rate of complications has to be taken into account.

Intra-aortic balloon pump

Decompression of left-sided chambers is also achieved by intra-aortic balloon pump (IABP). Rapid ECG-triggered inflation-deflation of this minimally invasive balloon in the descending aorta offers a passive reduction of LV afterload and increases diastolic blood pressure. Hydrostatic pulmonary edema prevention, modest increase in stroke volume, CO, and coronary and peripheral perfusion, as well as improved survival in part of clinical studies have all been described (Doll et al. 2004, Werdan et al. 2014, Brechot et al. 2018), but the risks and benefits of combined IABP and ECMO are still being debated (Swol et al. 2016).

Percutaneous LV support

Insertion of an microaxial rotary pump during VA ECMO therapy reduces the LV

	notes	Degree of VA ECMO flow						P
		0	**1**	**2**	**3**	**4**	**5**	
Stroke work of left ventricle [mmHg*mL]								
Hala et al. 2020	chronic HF	1434 ± 941	1595 ± 987	1867 ± 1102	2014 ± 1062	2105 ± 1060	1892 ± 1036	< 0.05
Ostadal et al. 2015	acute HF	—	2096 ± 342	2510 ± 335	2752 ± 346	3031 ± 404	2884 ± 412	< 0.001
Mean arterial pressure [mmHg]								
Hala et al. 2016	chronic HF	47 ± 22	56 ± 20	67 ± 19	75 ± 16	81 ± 13	84 ± 12	< 0.001
Kato et al. 1996	normal heart conditions	84 ± 24	66 ± 14	68 ± 14	66 ± 17	66 ± 18	65 ± 21	NS
Coronary blood flow								
Kato et al. 1996	absolute [mL/min]	135 ± 46	106 ± 26	96 ± 20	89 ± 22	77 ± 18	71 ± 17	< 0.01
Ostadal et al. 2018	relative to non-pulsatile [%]	—	15.2 ± 2.6	17.0 ± 2.7	14.6 ± 2.4	7.8 ± 2.4	—	< 0.05
Kinsela et al. 1992	absolute [mL/min/100g]	186 ± 28	—	—	253 ± 44	—	244 ± 48	0.46

Table 1. Hemodynamic effects of increasing VA ECMO flow – review of experimental studies. Important hemodynamic parameters are reported at various degrees of VA ECMO support (degree 0-5). HF – heart failure.

filling pressure. This combination can improve hemodynamic status by active blood suction from LV cavity directly to the ascending aorta.

LVAD

Implantation of LV assist device (LVAD) requires open chest surgery and can be used for long-term or even destination therapy, but is not suitable in an acute presentation of cardiogenic shock (Werdan et al. 2014).

All mentioned methods of LV decompression are invasive, some requiring surgical approach, others being introduced percutaneously, and thus significantly increase risks of ECMO complications. Alternatively, reducing the EBF has been suggested, as a conservative treatment approach, if adequate tissue perfusion can still be maintained. In the past, it was a general practice to support the circulation with maximal available EBF, but as we will show in futher text, limiting the VA ECMO support to the needed minimum can spare excessive cardiac work load and is advisable for situations of acute or chronic heart failure (Seo et al. 1991, Ostadal et al. 2015, Hala et al. 2016, Hála et al. 2020).

In order to avoid possibly harmful excessive ECMO flows, broader experience of the healthcare professionals and continual monitoring of ECMO circuit hemodynamics are required. According to current opinions, decreasing the VA ECMO support to the minimal EBF necessary for tissue perfusion has been advised in situations of decompensated HF, but the optimal level of EBF remain unknown. Also, in specific situations of ECMO support for acute HF or profound decompensation of chronic HF with fully developed compensatory mechanisms, the workload put on LV is unknown. Furthermore, relieving the overloaded LV seems to alleviate the risks of lung fluid accumulation and progression to pulmonary edema (Soleimani and Pae 2012, Donker et al. 2019).

2 Hypotheses

1. Venoarterial extracorporeal membrane oxygenation causes significant changes to ventricular hemodynamics.
2. Certain extracorporeal blood flow can provide sufficient systemic perfusion and minimalize adverse effects on work of the left ventricle.

3 Aims

Based on the analyses stated above, I specified and defined the following goals:

1. Heart failure models development
   - 1.1. Develop experimental models of acute and chronic heart failure
   - 1.2. Allow for titratable severity of heart failure
   - 1.3. Aim for low mortality and reproducibility
2. Hemodynamic effects of VA ECMO
   - 2.1. Apply VA ECMO with variable extracorporeal flow to models of heart failure
   - 2.2. Assess effects of extracorporeal flow on organ perfusion
   - 2.3. Assess effects of extracorporeal flow on heart hemodynamics and ventricular work

4 Methodology

The methodology of our experimental work consisted of development of variety of heart failure (HF) models and their titration into circulatory decompensation. All necessary monitoring and instrumentation were installed and an ECMO circuit introduced. Then, a standardized ramp protocol with increasing extracorporeal blood flow (EBF) was delivered to test hemodynamics during a full spectrum of rates of extracorporeal circulatory support.

HF models utilized were:

1) chronic HF induced by long-term rapid ventricular pacing,

2) acute HF induced by regional coronary hypoxemia,

3) acute HF induced by global coronary hypoxemia,

4) right-sided HF induced by gradual occlusion of pulmonary artery.

Experimental protocols were reviewed and approved by the Institutional Animal Expert Committee and the experiments were performed at the University experimental laboratory, Department of Physiology, First Faculty of Medicine, Charles University in Prague, Czech Republic or at ECLS Laboratory, University of Michigan, Ann Arbor, USA. All animals were treated and cared for in accordance with Act No. 246/1992 Coll., on the protection of animals against cruelty, and with the Guide for the Care and Use of Laboratory Animals, 8th edition, published by National Academies Press, 2011.

4.1 Animal model of chronic heart failure

According to previous studies, TIC as a form of dilated cardiomyopathy was generated by long-term rapid cardiac pacing (Spinale et al. 1990, Nikolaidis et al. 2001, Gupta and Figueredo 2014). Details of the methodology are described in attached Document 2 (Hala et al. 2018), Figures 12, 13, 14, and Table 2.

Due to suitable anatomy five healthy crossbred female swine (Sus scrofa domestica) up to 6 months of age with initial weights of 37-46 kg were included in this study. After 1 day of fasting, general anesthesia was initiated with intramuscular administration of midazolam (0.3 mg/kg) and ketamine hydrochloride (15-20 mg/kg). Intravenous boluses of morphine (0.1-0.2 mg/kg) and propofol (2 mg/kg) were administered, and animals were preoxygenated and orotracheally intubated with a cuffed endotracheal tube. Total intravenous anesthesia was then continued by combination of propofol (6-12 mg/kg/h), midazolam (0.1-0.2 mg/kg/h), and morphine (0.1-0.2 mg/kg/h); all doses adjusted according to individual responses. Mechanical ventilation was provided by a Hamilton G5 closed-loop device (Hamilton Medical AG, Switzerland), set to adaptive support ventilation to maintain target end-tidal CO_2 of 38-42 mmHg and adequate oxygen saturation of 95-99%. All procedures were performed according to standard veterinary conventions.

Under aseptic conditions and antibiotic prophylaxis (cefazolin 1 g), a single pacing lead with active fixation was inserted transvenously by fluoroscopic guidance in the apical part

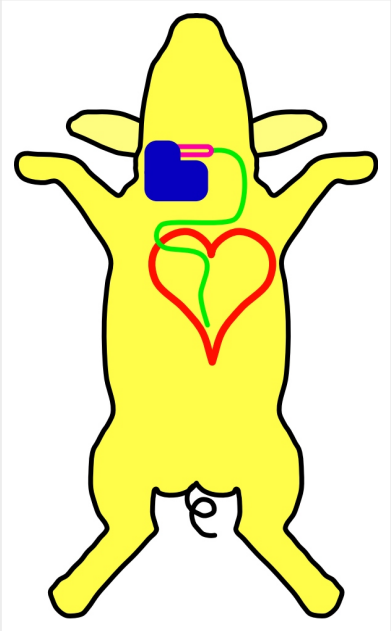

Figure 11. Heart pacing unit – the single cardiac pacing lead (green) is implanted into the apex of right ventricle (red) and subcutaneously tunneled to connect through the "Y" shaped adapter (purple) to a dual-chamber pacemaker (blue), which is then buried in the dorsal subcutaneous pocket.

of right ventricle and subcutaneously tunneled (Figure 11) to connect through an in-house modified "Y" connecting part (Lead permanent adapter, Osypka, Germany) to the heart pacemaker (Effecta, Biotronik SE & Co. KG, Germany) (Figure 12). This pacemaker unit was then buried into a dorsal subcutaneous pocket. The modified "Y" connection allowed a convergent connection of both pacemaker outputs to be joined and conducted together to the single pacing lead (Figure 13). These arrangements provide a wide range of high rate pacing frequencies and proved to prevent device-related complications.

Additional permanent catheter (Groshong PICC, Bard AS, USA or Arteriofix, B. Braun, Germany) was inserted through the marginal ear vein, and animals were kept in a chronic care facility under veterinary care. They were provided with free access to water and continued antibiotic regimen of cefazolin for total of 5 days.

Pacing protocol and chronic heart failure induction

After the necessary resting period of two to five days, reserved for recovery from the surgical procedure, a rapid ventricular pacing was started. According to previous publications (Chow et al. 1990, Hendrick et al. 1990, Tomita et al. 1991) and our own experience, the pacing protocol was defined and started at a pacing rate of 200 beats/min. The frequency was then escalated to 220 beats/min after one week, to 240 beats/min the following week, and sustained (Figure 14). Veterinary surveillance and clinical check-ups including pulse oximetry, rhythm control, and echocardiographic evaluations of myocardial contractility were performed regularly to assess the individual HF progression and pacing rate titration (Shinbane et al. 1997, Moe and Armstrong 1999). In the case of excessive HF progression, the pacing rate was reduced for a week before increasing it again. Due to interindividual differences in response to fast pacing, time needed to produce chronic HF with profound signs of decompensation varied from 4 to 8 weeks. Dilation of all heart chambers, severe systolic dysfunction, and valve regurgitations were apparent and correlated with low cardiac index and low venous blood oxygen saturation.

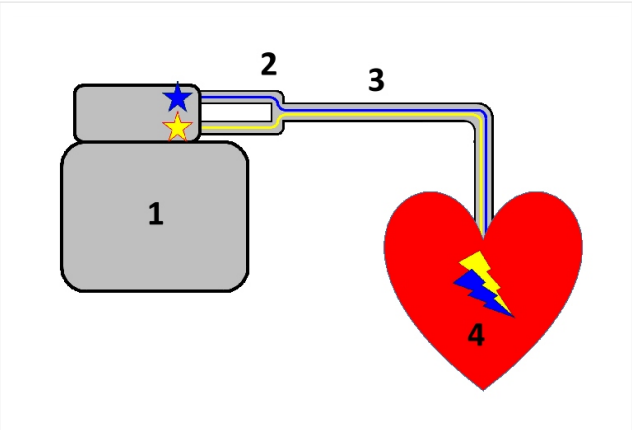

Figure 12. Heart pacing unit (scheme) – dual-chamber pacemaker (1), "Y" shaped adapter (2) conducting convergently both pacemaker outputs together to a single pacing lead (3). The tip of the lead is fixated into the apical part of RV cavity (4). This setting provides a wide range of high pacing frequencies.

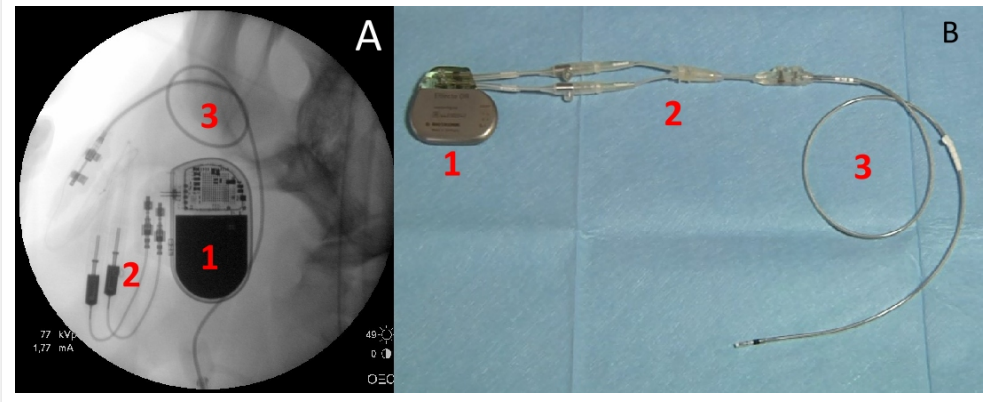

Figure 13. Heart pacing unit – X-ray (A) and photography (B) of dual-chamber pacemaker (Effecta, Biotronik SE & Co. KG, Germany, 1), "Y" shaped adapter (2) and ventricular pacing lead (3).

Desired HR	Set pacemaker rate	RR interval
beats/min	*beats/min*	*ms*
200	100	300
220	110	270
240	120	250

Table 2. Pacemaker parameters. To allow high rate cardiac pacing with the implanted in-house-modified dual-chamber pacemaker unit, the table shows the desired paced heart rate (HR) and matching RR interval values. The pacemaker must be set to D00 operation mode at rate of half of the desired HR and the AV delay set to the corresponding RR interval (pace-to-pace period) in milliseconds.

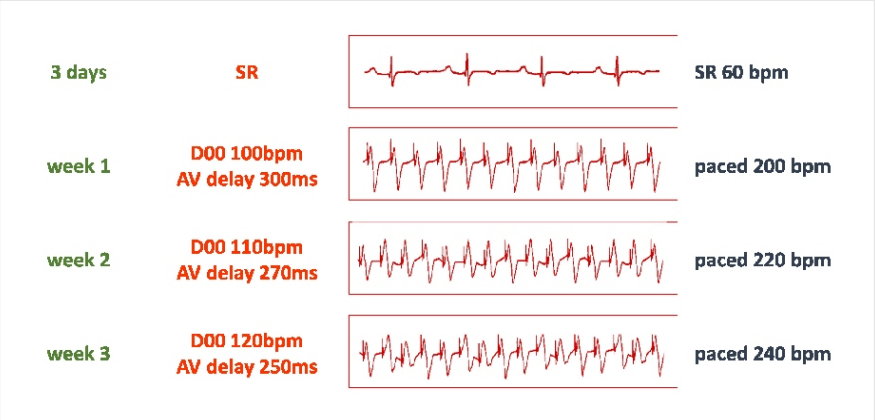

Figure 14. Pacing protocol – progressive phase of TIC induction starts after a resting period of $>$ 3 days. Then, pacemaker is set to D00 mode with pacing frequency at 50% of the desired paced frequency and AV delay is set to the matching pace-to-pace interval (see Table 2). Thanks to the "Y" shaped adapter both pacemaker outputs are conducted to a single pacing lead. This enables setting high pacing frequencies.

At that point ventricular pacing was discontinued for further hemodynamic studies and all animals were examined in sinus rhythm.

4.2 Animal model of acute HF induced by regional coronary hypoxemia

Five female swine, 4-5 months of age, with a mean bodyweight of 45 kg were included in this experiment. Additional details are described in attached Document 4 (Ostadal et al. 2015). General anesthesia, medication, and monitoring were commenced by the same principles as described above, mechanical ventilation was provided and set to Adaptive Support mode to maintain oxygen saturation (SpO_2) of 95-99% and end-tidal CO_2 pressure ($PetCO_2$) of 35-45 mmHg.

Next, coronary angiography was performed and, according to the specific coronary anatomy in each animal, the largest branch of left main coronary artery (left anterior descending artery or left circumflex artery) was identified. With the use of two coronary guide wires, a balloon catheter and an over-the-wire perfusion catheter (Medtronic, USA)

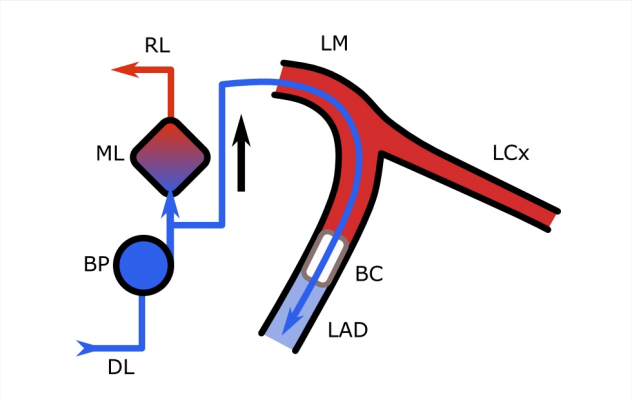

Figure 15. Induction of regional myocardial hypoxia through perfusion of selected coronary artery by desaturated venous blood. RL – reinfusion line, ML – membrane lung, BP – blood pump, DL – drainage line, BC – balloon catheter, LAD – left anterior descending, LCx – left circumflex, and LM – left main coronary artery.

were advanced into the selected artery. The perfusion catheter had its opening placed distally to the balloon and its entry was connected to the ECMO circuit between the pump and the oxygenator (Figure 15). After inflation of the balloon, the coronary artery was perfused solely with venous blood at a flow of approximately 40 mL/min.

Acute cardiogenic shock with signs of tissue hypoperfusion was defined as a drop in systolic blood pressure to < 100 mmHg and at least one of the following criteria: increase in blood lactate to > 2.0 mmol/L; decrease of mixed venous oxygen saturation to $< 50\%$; or fall in brain tissue oxygen saturation to $< 50\%$.

In cases in which the abovementioned procedure was insufficient to cause cardiogenic shock, an additional balloon catheter was introduced into the periphery of the second left main coronary artery and by its inflation myocardial infarction was induced in the respective area.

4.3 Animal model of acute HF induced by global coronary hypoxemia

Total of sixteen female swine, 4-5 months of age and a mean body weight of 45 kg, were used for this experiment. Full details of this animal model development can be found in attached Document 5 (Ostadal et al. 2016). Anesthetized and intubated animals were mechanically ventilated and heparinized to maintain an activated clotting time > 200 s. A femoral venoarterial ECMO circuit was inserted percutaneously with the tip of the outflow cannula advanced to the descending aorta. The gas exchange unit maintained pO_2 75-120 mmHg and pCO_2 30-50 mmHg in the delivered blood and the extracorporeal blood flow was set to 1 L/min.

After stabilization, the artificial ventilation was switched to continuous mandatory ventilation mode (5 breaths/min, 100 mL inspiratory volume, and fraction of inspired oxygen 21%), which caused severe desaturation of the blood in left-sided heart chambers and therefore tissue hypoxia in all organs perfused by LV ejection, including the coronary arteries. This situation resembles the clinical condition of selective cyanosis – the "Harlequin syndrome" (Figure 16). The resulting global myocardial hypoxia rapidly lowered myocardial contractility, ejection fraction of both ventricles, and arterial blood

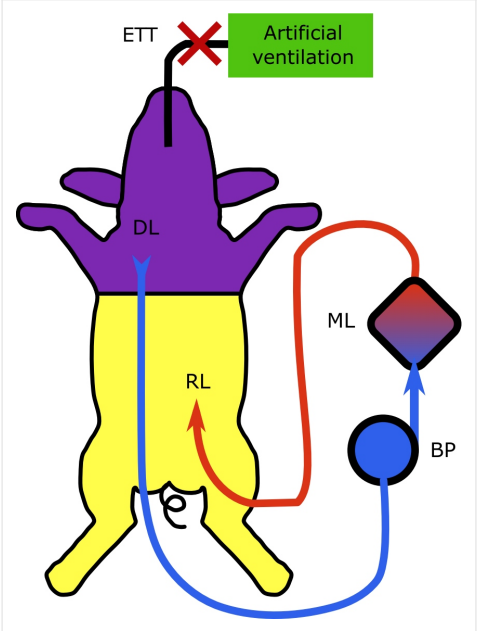

Figure 16. Schematic illustration of global coronary hypoxemia experimental settings. ETT – endotracheal intubation, DL – drainage line, RL – reinfusion line, ML – membrane lung, BP – blood pump.

pressure. At the same time, the lower part of the body was perfused with fully oxygenated blood from the ECMO reinfusion, which was gradually increased to maintain a mean arterial pressure > 60 mmHg, ensuring adequate perfusion.

The hemodynamic criteria for severe cardiogenic shock were met: LV EF $< 30\%$ and CO < 3.5 L/min. The severity of this cardiogenic shock induced by global myocardial hypoxemia could be titrated by adjusting the rate of lung ventilation.

4.4 Animal model of right-sided HF

In 5 lambs, weighing 15.7 ± 2.0 kg, right heart failure was induced by gradual occlusion of pulmonary artery (PA). As described in attached Document 7 (Carr et al. 2019), under general anesthesia intercostal thoracotomy was performed and the anterior branch of the left PA was occluded with a silk ligature. An adjustable Rummel-style tourniquet was placed around the right PA just distal to the bifurcation and tunneled to the skin (Figure 17). A perivascular flow probe was placed around the main PA and the chest closed. By adjusting the tourniquet, full occlusion of the right main PA was gradually achieved over 48 hours. The $> 50\%$ reduction of pulmonary vascular bed increased slowly the afterload of right ventricle causing its ballooned dilation and right-sided heart failure.

To assess the progression of HF, echocardiography (Siemens Acuson Cypress and cardiac probes 7V3c and 3V2c) was used to obtain standard transthoracic 2-dimensional, M-mode, and Doppler measurements at three time points: 1) before the surgery (baseline), 2) during surgery with short-time tourniquet occlusion (acute), and 3) after seven days of total occlusion (chronic). Images were acquired through intercostal windows on left side of the chest allowing to obtain analogous views to human parasternal short-axis and long-axis projections. A 4-chamber view was taken from a subxifoideal region and acquisitions of the great vessels were obtained with the chest open at thoracotomy.

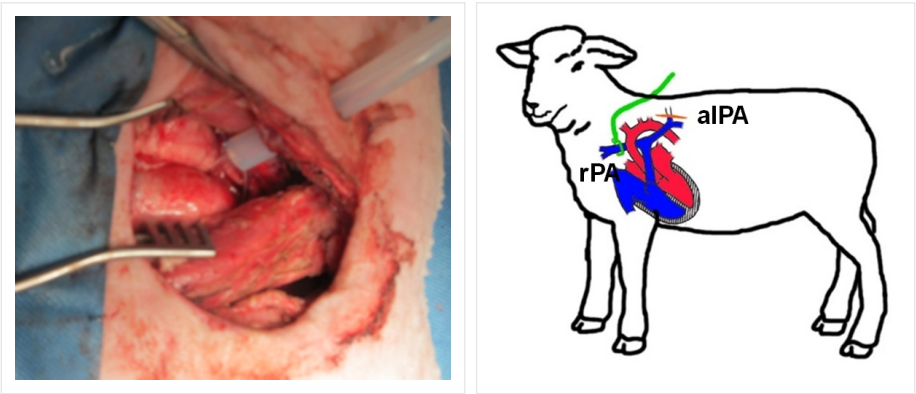

Figure 17. Surgical instrumentation of the right-sided heart failure model. Intraoperative photograph (left) and diagram (right) showing the adjustable Rummel-style tourniquet controlling the right main pulmonary artery (rPA) and ligation of anterior branch of left pulmonary artery (alPA).

Using the echocardiography, right ventricle was evaluated during end-diastole in length, basal, midventricular, and apical diameters (RV EDD). Its single plane area was measured during systole (RV ESA) and diastole (RV EDA) and RV systolic function was assessed from measured tricuspid annular plane systolic excursion (TAPSE), calculated fractional area change (FAC = (RV EDA – RV ESA) / RV EDA), and estimated ejection fraction (EF).

4.5 Experimental preparation and hemodynamic monitoring

In the porcine models of chronic HF induced by rapid ventricular pacing and of acute HF induced by regional or global hypoxemia, additional hemodynamic monitoring, experimental preparation, and VA ECMO were utilized for hemodynamic measurements of EBF effects. Details are in attached Documents 1, 3, 4, and 6 (Ostadal et al. 2015, Hala et al. 2016, Ostadal et al. 2018, Hála et al. 2020). At the stage of decompensated HF, anesthesia and artificial ventilation were maintained following principles described above, but with dosing adjusted due to low cardiac output.

Vital functions of anesthetized animals were monitored, and all invasive approaches commenced. Bilateral femoral veins and arteries, jugular vein, and left carotid artery were punctured, and intravascular accesses ensured by standard percutaneous intraluminal sheaths. Right carotid and subclavian arteries were surgically exposed, and circumjacent ultrasound flow probes of appropriate sizes attached (3PSB, 4PSB, or 6PSB, Scisense, Transonic Systems, USA), enabling continuous detection of blood flow velocities. For both arteries the pulsatility index (PI) was defined as calculated difference between the peak systolic and minimum diastolic velocities divided by the mean velocity during each cardiac cycle and as such represents the variability of arterial flow during cardiac cycle.

Intravenous anticoagulation was initiated by unfractionated heparin bolus (100 IU/kg IV), followed by continual infusion, maintaining an activated clotting time (ACT) of 200-300 s (Hemochron Junior+, International Technidyne Corporation, USA), and a set of invasive monitoring equipment was introduced. A balloon Swan-Ganz catheter was placed through femoral vein to the pulmonary artery allowing thermodilution-derived

continuous cardiac output, mixed venous oxygen saturation (SvO_2), pulmonary artery, and pulmonary wedge pressure assessments (CCO Combo Catheter; Vigilance II, Edwards Lifesciences, USA). Central venous pressure (CVP) was measured via jugular vein and arterial pressure in femoral artery using fluid-filled pressure transducers (TruWave, Edwards Lifesciences, USA). Regional tissue oxygenation (rSO_2) was monitored by near-infrared spectroscopy (INVOS Oximeter, Somanetics, USA) with sensors placed on forehead and right forelimb region representing brain and peripheral tissue oxygen saturation levels (Wolf et al. 2007).

Intracardiac and transthoracic echocardiography probes (AcuNav IPX8, Acuson P5-1 and X300 ultrasound system, Siemens, USA) were used for 2D and color Doppler imaging. ECG, heart rate (HR), pulse oximetry, capnometry, rectal temperature, and SvO_2 were measured continuously; blood gas parameters were evaluated by a bedside analysis system (AVL Compact 3, Roche Diagnostics, Germany).

In a group of eight animals with global coronary hypoxemia acute HF model, a coronary Doppler guide wire (FloWire, Volcano, USA) was placed in the proximal segment of the left anterior descending coronary artery to measure coronary flow. Average peak flow velocity was recorded during the experiment.

4.6 Left ventricular parameters and stroke work analysis

To register instant volume and pressure in the LV chamber, a pressure-volume (PV) conductance catheter (7F VSL Pigtail, Scisense, Transonic Systems, USA) was passed via left carotid arterial approach, retrogradely through the aortic valve into the LV. Its fluoroscopy and echocardiography guided position was set stable before the protocol started to obtain optimal PV loop morphology (Figure 18). Volume measurements were calibrated by thermodilution-derived cardiac output at baseline.

Measured LV parameters included end-diastolic pressure and volume (EDP and EDV), end-systolic volume (ESV), LV peak pressure (LVPP), stroke work (SW; defined as LV pressure integral with respect to volume), and maximal positive change of LV pressure, defined as first time derivative of LV pressure (dP/dt_{max}). When normalized to EDV, $dP/dt_{max}/EDV$ ratio represents a preload independent index of LV contractility (Glower et al. 1985, Little 1985, Kass et al. 1987, Burkhoff et al. 2005, Walley 2016). Additional calculated parameters were stroke volume (SV) and left ventricular ejection fraction (EF).

4.7 ECMO instrumentation

After intravenous systemic heparinization, extracorporeal circulation was maintained by a femoral VA ECMO system in all porcine hemodynamic studies. Two different ECMO circuits were used in the experiments.

In the porcine models of chronic HF induced by rapid ventricular pacing and acute HF induced by regional hypoxemia, VA ECMO system compounded of Levitronix Centrimag console (Thoratec, USA) with a centrifugal pump, hollow fiber microporous membrane oxygenator (QUADROX-i Adult, Maquet Cardiopulmonary, Germany), and tubing set with two percutaneous cannulas (Medtronic, USA) which were introduced by the Seldinger technique through punctures of the unilateral femoral vein and artery (Figure 19). The

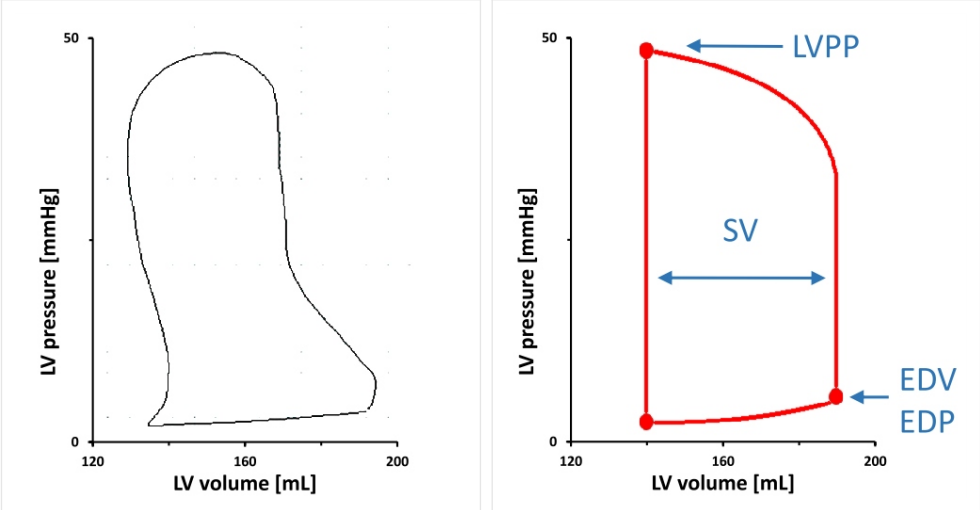

Figure 18. Pressure-Volume measurements. Sample of one representative left ventricular PV loop (left) and schematic averaged PV loop of all our TIC subjects (right). LVPP – LV peak pressure, EDP – end-diastolic pressure, EDV – end-diastolic volume, SV – stroke volume.

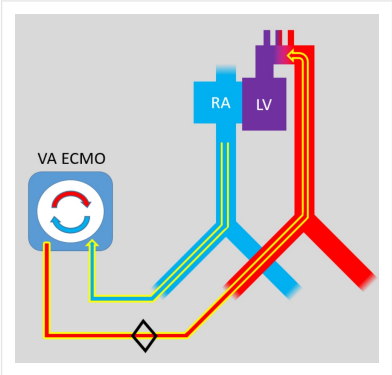

Figure 19. Femoro-femoral VA ECMO scheme. Venous blood is drawn by inflow cannula from right atrium (RA). It then continuous through the gas exchange unit by the force of centrifugal pump and oxygenated is returned to the descending part of thoracic aorta. LV – left ventricle. Black diamond showing the placement of EBF flow probe.

tip of venous inlet cannula (21 or 23 Fr) was advanced to the right atrium, and the tip of arterial outlet cannula (15 or 18 Fr) reached the thoracic descending aorta, with both positions verified by fluoroscopy.

Another VA ECMO circuit system (i-cor, Xenios AG, Germany), with ability to deliver pulsatile extracorporeal flow, was applied to the porcine model of acute HF induced by global coronary hypoxemia. Details of the protocol are to be found in attached Document 6. This ECMO circuit consisted of percutaneously inserted venous drainage (21 Fr, Maquet, Germany) and arterial reinfusion (18 Fr, Xenios AG, Germany) cannulas, diagonal blood pump, and a membrane oxygenator (Xenios AG, Germany).

Fully assembled ECMO circuits (Bartlett et al. 1977) were primed with saline solution, and extracorporeal blood flow (EBF) was initiated at flow rate of 300 mL/min to prevent thrombus formation inside the circuit while having a neglectable impact on the systemic circulation. EBF was registered by a separate circumjacent flow probe (ME 9PXL, Transonic Systems, USA) attached to the ECMO outlet.

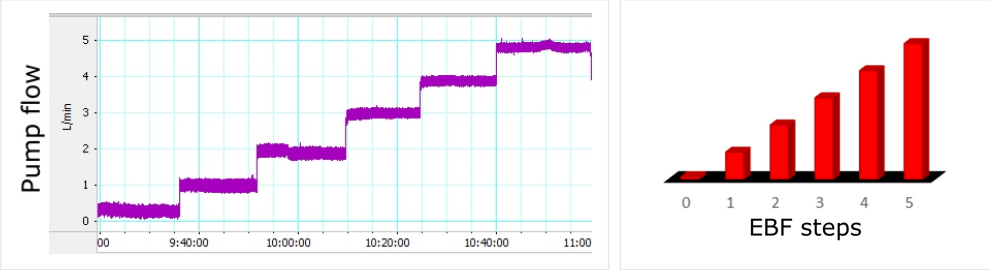

Figure 20. Experimental ECMO protocol. Example of real measured ECMO flow over a single stepwise ECMO protocol run (left) and diagram of corresponding categorized levels of EBF (right).

4.8 Experimental ECMO protocols and data acquisition

Although the ECMO protocols were similar for all studies, minor differences will be described to reflect settings of each individual experiment. The details are provided in corresponding attached documents.

Crystalloid infusion was continuously administered (2.5-5.0 mL/kg/h) to reach and maintain a mean CVP at least 5 mmHg. ACT was kept between 200 and 300 s by intravenous heparin administration, and normothermia was maintained.

Blood gas analysis was checked continuously (CDI Blood Parameter Monitoring System 500, Terumo Cardiovascular Systems Corporation, USA) throughout the whole experiment; the fraction of oxygen and air flow through the oxygenator were adjusted to maintain pO_2 100-120 mmHg, pCO_2 35-45 mmHg, and pH 7.35-7.45 in the blood leaving the oxygenator.

Under conditions of previously developed profound chronic HF or cardiogenic shock with signs of tissue hypoperfusion, the ECMO protocol was initiated. By changing the ECMO pump rotation speed, the EBF was set according to one of the standardized ramp protocols (Figure 20). EBF was gradually increased by increments of 1 L/min every 5-15 minutes from minimal flow to 5 L/min, and these stepwise categories with constant EBF were referred to as EBF 0, 1, 2, 3, 4, and 5. At each step, animals were allowed to stabilize to a steady state condition in which hemodynamic parameters including PV loop data were recorded. Sets of data were then averaged from at least three end-expiratory time points or repeated EBF steps. If present, premature beats were omitted from the analyses.

4.9 Statistical analysis

Recordings were sampled at 400 Hz by PowerLab A/D converter and continuously recorded to LabChart Pro Software (ADInstruments, Australia). Statistical analyses and graphical interpretations were performed in Prism (GraphPad, USA) and Excel (Microsoft, USA).

All data sets were tested for normality and are expressed as mean ± standard error of mean (SEM) unless stated differently. Comparisons between different levels of EBF were analyzed by using the Friedman test with Dunn's multiple comparison. Linear regression with Pearson correlation and scatter plots were used for value comparisons in between

models. In the pulsatile ECMO study, the primary experimental variables were EBF step and the mode of EBF (i.e. pulsatile or continuous). These data were analyzed using two-way repeated measures analysis of variance. When significant differences among EBF steps and/or flow modes were indicated, specific pre-planned comparisons were performed, and P-values were adjusted according to the Bonferroni method to maintain the experiment-wise α level at ≤ 0.05. In all experiments, a two-sided P-value < 0.05 was considered statistically significant.

5 Results

5.1 Characteristics of developed chronic HF model

The chronic HF model was represented by the tachycardia-induced cardiomyopathy caused by artificial ventricular pacing. At the end of the pacing protocol, physical examination revealed severe clinical signs of chronic HF in all animals. Due to interindividual differences, time to HF development varied between 4 and 8 weeks of rapid ventricular pacing. At this point, total anesthesia was administered carefully, the rapid ventricular pacing was stopped abruptly, and hemodynamic parameters were evaluated in native sinus rhythm. Detailed results are summarized in Table 3.

Initial mean heart rate of sinus rhythm was 100 ± 19 beats/min, the mean aortic blood pressure reached 47 ± 22 mmHg and CVP 14 ± 2 mmHg. Chest X-rays showed heart shadow dilation, with a cardiothoracic ratio of 0.64 ± 0.02 (Figure 21). This is in concordance with transthoracic echocardiography findings. Dilation of all heart chambers, severe systolic dysfunction of both ventricles, and significant mitral and tricuspid regurgitations were apparent on echocardiography. Mean ejection fraction of the left ventricle was below 30% in all animals, the LV wall was judged non-hypertrophic with a thickness of 7-10 mm and dyssynchrony of LV contraction was obvious (Figure 22).

Thermodilution measured cardiac output in the resting state was 2.9 ± 0.4 L/min and mixed venous blood saturation 62 ± 8% corresponded with inadequate tissue oxygen delivery in this model. Average arterial blood flow in the carotid artery was 211 ± 72 mL/min and in the subclavian artery was 103 ± 49 mL/min. Similarly, regional tissue saturation recorded transcutaneously on the head was only 57 ± 6%, and it was even lower on the right forelimb, at 37 ± 6%.

The pressure-volume loop obtained from the PV catheter illustrates the detailed hemodynamic measures and work produced by the mechanical activity of the left ventricle during each cardiac cycle (Figure 23). LV peak pressure was reduced to 49 ± 15 mmHg, but EDP remained low at 7 ± 2 mmHg. The measured volumes of the left ventricular chamber were reflective of its dilation and systolic dysfunction. EDV was increased to 189 ± 26 mL and ESV to 139 ± 17 mL. Averaged SV was 51 ± 20 mL and the mean LV ejection fraction was calculated to be 25 ± 7%. By analyzing the pressure-volume loops, LV stroke work (SW) was calculated to 1434 ± 941 mmHg*mL. In addition, preload independent index of LV contractility can be represented by the $dP/dt_{max}/EDV$ ratio, which

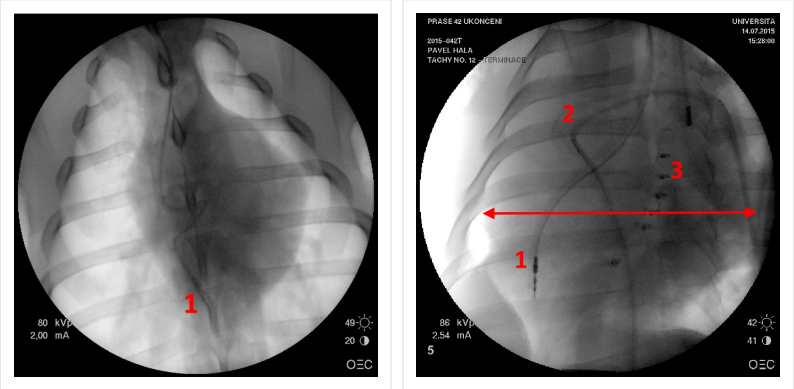

Figure 21. Chest X-ray of enlarged heart shadow (right, red arrow) and increased cardiothoracic ratio. Note the pacing lead introduced to the apex of right ventricle (1), Swan-Ganz catheter placed in the pulmonary artery (2) and PV catheter with 6 electrodes in left ventricular chamber (3). For comparison, a chest X-ray with normal heart size at the time of pacemaker implantation (left).

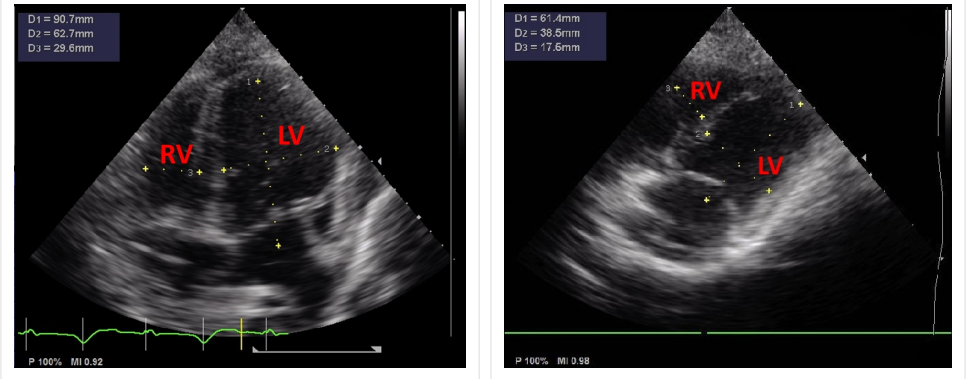

Figure 22. Transthoracic echocardiography of representative tachycardia-induced cardiomyopathy with severe dilation of all heart chambers. RV – right ventricle, LV – left ventricle. Notice the visible tip of pacing lead in RV apex.

was averaged to 2.2 ± 0.8 mmHg/s/mL.

An autopsy confirmed cardiomegaly (Figure 24) with a mean heart weight of 471 ± 127 g, which formed 0.7% of body weight. Dilation of all heart chambers and LV wall thinning were stated, and fluid collections were described in pericardial and peritoneal spaces. No shunt or other cardiac anomaly was found in any of the animals.

5.2 Characteristics of acute HF model induced by regional coronary hypoxemia

In this model, hypoxemic blood was perfused to a single coronary artery. Regional myocardial hypoxia alone led to extensive myocardial injury sufficient to cause cardiogenic shock in four out of five experimental animals. In one animal, an additional coronary artery occlusion was necessary to induce cardiogenic shock. After the development of cardiogenic shock, a low cardiac output of 2.81 ± 0.34 L/min was measured together with increased heart rate 94 ± 4 beats/min. LV ejection fraction was reduced to 43 ± 3% and LVPP to 60 ± 7 mmHg (Table 4). All animals survived myocardial injury, although two

Parameter	TIC value	*Units*
Imaging		
CTR	0.64 ± 0.02	
LV EF	< 30	*%*
LV EDD	66 ± 2	*mm*
RV EDD	40 ± 4	*mm*
AV regurgitations	severe	
Hemodynamic parameters		
HR	100 ± 19	*beats/min*
MAP	47 ± 22	*mmHg*
CO	2.9 ± 0.4	*L/min*
SvO_2	62 ± 8	*%*
rSO_2 cerebral	57 ± 6	*%*
rSO_2 right forelimb	37 ± 6	*%*
Carotid flow	211 ± 72	*mL/min*
Subclavian flow	103 ± 49	*mL/min*
CVP	14 ± 2	*mmHg*
Pressure-volume acquisition		
LVPP	49 ± 15	*mmHg*
LV EDP	7 ± 2	*mmHg*
LV EDV	189 ± 26	*mL*
LV ESV	139 ± 17	*mL*
SV	51 ± 20	*mL*
LV EF	25 ± 7	*%*
LV SW	1434 ± 941	*mmHg*mL*
dP/dtmax/EDV ratio	2.2 ± 0.8	*mmHg/s/mL*
Autopsy		
mean heart weight	471 ± 127	*g*
cardiomegaly, dilation of heart chambers, LV wall thinning, pericardial fluid collections		

Table 3. Numerical results of the TIC model after cessation of pacing protocol. All values expressed as mean ± SEM. CTR – cardiothoracic ratio, LV EF – LV ejection fraction, LV EDD/RV EDD – LV/RV end-diastolic diameter, HR – heart rate, MAP – mean aortic pressure, CO – cardiac output, SvO_2 – mixed venous hemoglobin saturation, rSO_2 – regional tissue saturation, CVP – central venous pressure, LVPP – LV peak pressure, LV EDP/LV EDV – LV end-diastolic pressure/volume, SV – stroke volume, SW – stroke work.

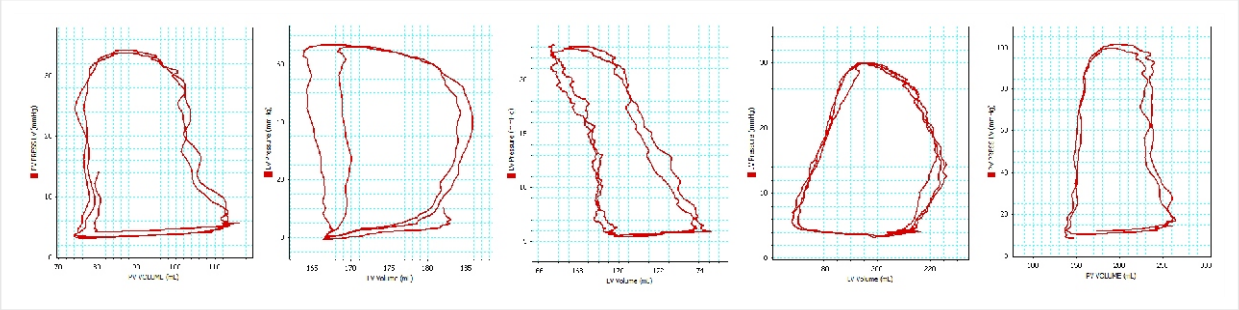

Figure 23. Pressure-volume measurements. Samples of direct left ventricular PV loops reflecting decompensated chronic heart failure. Of note, absence of isovolumic phase can be seen in some samples.

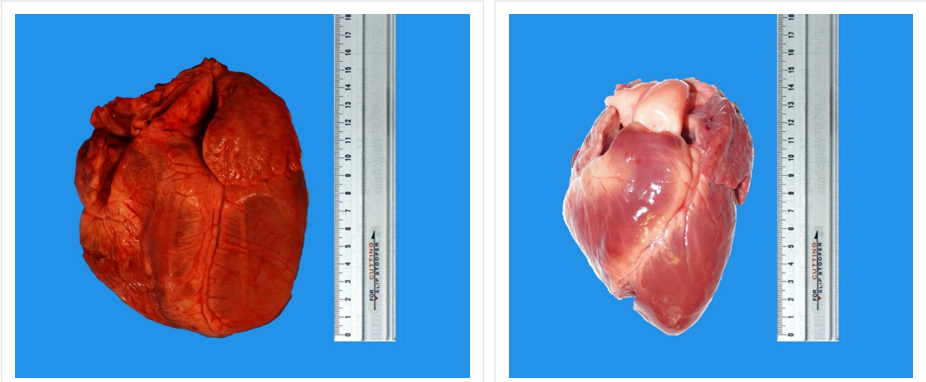

Figure 24. Photography of exposed heart. Cardiomegaly (left) after the TIC induction. Normal porcine heart sample for size comparison (right).

of them required defibrillation.

5.3 Characteristics of acute HF model induced by global coronary hypoxemia

This acute HF model was triggered by limiting lung ventilation and therefore low saturation in the blood ejected from LV and the coronary circulation. After approximately 1 hour of global myocardial hypoxia, severe cardiogenic shock developed on the grounds of reduced overall contractility. Cardiac output was reduced to 1.7 ± 0.7 L/min with increased heart rate of 106 ± 3 beats/min, LV ejection fraction to 22 ± 7%, and LVPP to

Parameter	***[Unit]***	**Value**
CO	*[L/min]*	2.81 ± 0.34
HR	*[beats/min]*	94 ± 4
LV EF	*[%]*	43 ± 3
LVPP	*[mmHg]*	60 ± 7

Table 4. Characteristics of acute heart failure model (induced by regional coronary hypoxemia) demonstrating cardiogenic shock.

Parameter	*[Units]*	Baseline	Cardiogenic shock	P
EDV	*[mL]*	130 ± 3.2	142 ± 3.8	0.073
ESV	*[mL]*	50.3 ± 1.8	116.6 ± 3.4	<0.001
SV	*[mL]*	79.7 ± 2.8	25.3 ± 2.3	<0.001
EDP	*[mmHg]*	13.6 ± 0.7	28.1 ± 1.7	<0.001
LVPP	*[mmHg]*	115.7 ± 2.4	63.5 ± 6.4	<0.001
LV EF	*[%]*	61.2 ± 1.2	17.7 ± 1.4	<0.001
HR	*[beats/min]*	82.8 ± 2.8	112 ± 4.6	<0.001
CO	*[L/min]*	6.61 ± 0.3	2.75 ± 0.2	0.001

Table 5. Characteristics of acute heart failure model (induced by the global coronary hypoxemia). Major hemodynamic and left ventricular performance parameters at baseline and after development of acute cardiogenic shock on subgroup of 12 animals.

64 ± 22 mmHg. Thereafter, continuous heart perfusion with hypoxemic blood enabled the maintenance of advanced myocardial dysfunction throughout the experimental protocol. Detailed effects of the global coronary hypoxemia on subgroup of 12 animals are presented in Table 5.

5.4 Characteristics of right-sided HF model

The right-sided HF model was induced by gradual obstruction of pulmonary artery. Mean PA pressure at the beginning of the experiment was normal but increased significantly (from 20 ± 5 to 33 ± 4 mmHg, $P < 0.01$) after the gradual PA vascular bed reduction. There was a significant decrease in SvO_2 to 55 ± 8%, $P < 0.01$, but arterial oxygen saturation remained stable with supplemental oxygen. Pulmonary hypertension caused significant changes to both ventricular dimensions and function (Figure 25).

Echocardiographic findings are summarized in Table 5. Compared to baseline, the RV enlarged in all cross-sectional dimensions, enlarged longitudinally, and formed a balloon-shaped chamber with septal bowing. The EDA and ESA increased significantly, but RV free wall thickness did not increase and systolic function worsened with severe reduction in TAPSE, FAC, and EF. Unlike the RV, the left ventricle retained its normal contractility, but decreased in size, reflecting reduced filling from decreased preload.

5.5 Effects of EBF on chronic HF

After connecting VA ECMO to the model of chronic heart failure, extracorporeal blood flow was changed according to the stepwise protocol from minimal to maximal flow rate in one liter increments. The ECMO flow induced gradual and dramatic changes in perfusion, oxygen saturation, and LV hemodynamic parameters. Summary results are in Figure 26, Table 7, and attached Documents 1 and 3 (Hala et al. 2016, Hála et al. 2020).

Regional tissue oximetry and arterial flow

With stepwise increase of EBF from minimal to maximal flow, we observed gradual increase in mean aortic blood pressure by 79% – from baseline 47 ± 22 mmHg to 84 ± 12 mmHg (for EBF 0 to EBF 5, $P < 0.001$). Similarly, arterial blood flow in-

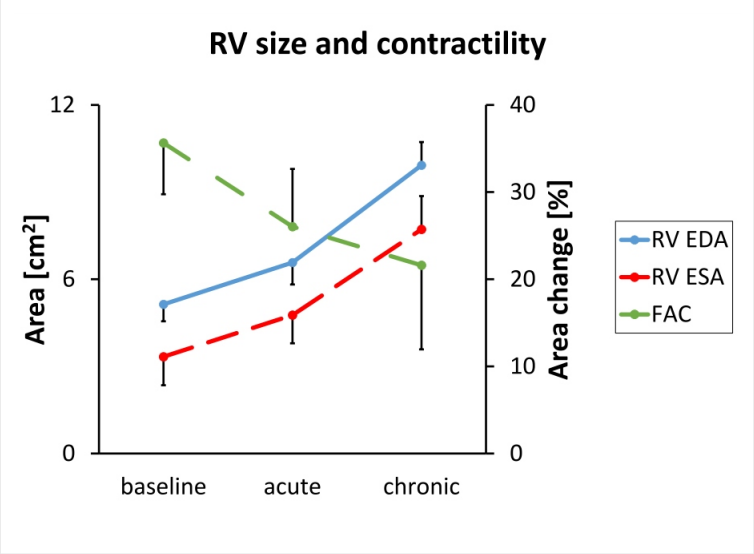

Figure 25. Effects of right pulmonary artery occlusion on right ventricular function and size. Periprocedural (acute) and final measurements after 7 days of disease progression (chronic). With right pulmonary artery occlusion, right ventricular size increased, while contractility decreased ($P < 0.05$). FAC – fractional area change, RV EDA/ESA – right ventricular end-diastolic/end-systolic area.

Parameter	***[Units]***	**Baseline**	**Acute**	**Chronic**	**Relative change (chronic)**	**P**
LV EDD	*[mm]*	32 ± 2	25 ± 1	25 ± 2	79%	0.03
RV EDD basal	*[mm]*	20 ± 1	26 ± 2	28 ± 1	136%	0.04
RV EDD mid	*[mm]*	15 ± 2	23 ± 0	24 ± 2	166%	0.03
RV EDD apical	*[mm]*	10 ± 1	14 ± 2	14 ± 0	148%	0.02
RV length	*[mm]*	36 ± 3	41 ± 2	45 ± 1	125%	0.02
TAPSE	*[mm]*	13 ± 2	11 ± 1	7 ± 1	52%	< 0.01
PA diameter	*[mm]*	15 ± 1	15 ± 2	19 ± 2	123%	0.12
RV EDA	*[cm^2]*	5 ± 1	7 ± 1	10 ± 1	193%	0.01
RV ESA	*[cm^2]*	3 ± 0	5 ± 1	8 ± 1	232%	0.01
FAC	*[%]*	36 ± 3	26 ± 7	22 ± 5	61%	0.04
RV EF	*[%]*	51 ± 4	31 ± 12	27 ± 8	53%	0.03

Table 6. Comparison of echocardiographic parameters at baseline, during acute perioperative temporal occlusion, and after 7 days of 100% right PA occlusion (chronic) in a chronic model of right-sided HF.

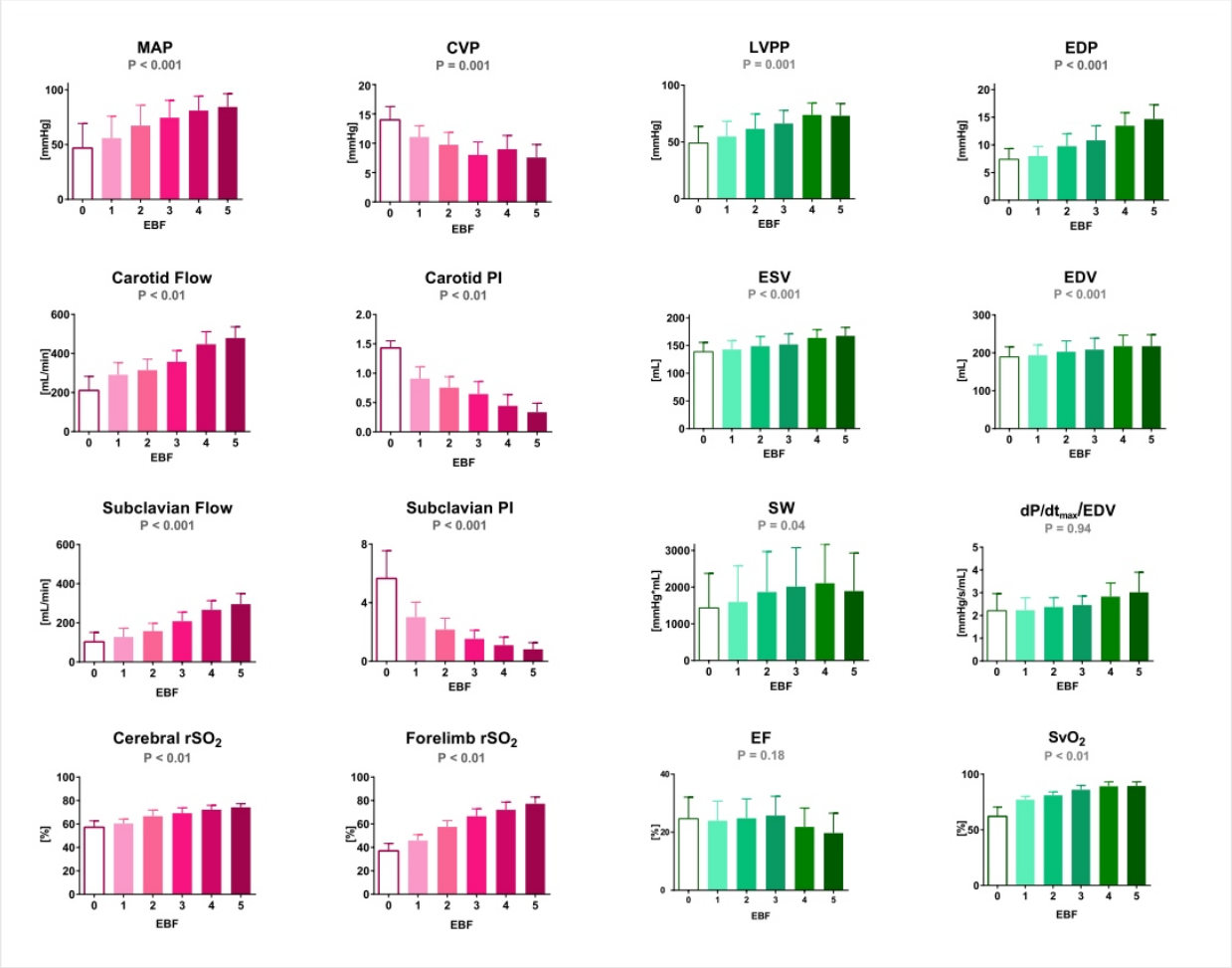

Figure 26. Effects of venoarterial extracorporeal membrane oxygenation blood flow (EBF in L/min) on hemodynamic parameters in a porcine model of chronic heart failure - regional tissue oximetry and arterial flow parameters (purple and left) and LV hemodynamics (green and right).

creased with every increase of EBF. In carotid artery it changed from 211 ± 72 mL/min to 479 ± 58 mL/min (by 127% from EBF 0 to EBF 5, $P < 0.01$) and in subclavian artery from 103 ± 49 mL/min to 296 ± 54 mL/min (by 187%, $P < 0.001$). For both arteries the pulsatility index (PI) was defined as calculated difference between the peak systolic and minimum diastolic velocities divided by the mean velocity during each cardiac cycle and as such represents the variability of arterial flow during cardiac cycle. Interestingly, baseline PI was considerably higher in subclavian than in carotid artery. A reduction of pulsatility indices by 76% (from 1.43 ± 0.12 to 0.34 ± 0.15, $P < 0.05$) in carotid and by 85% (from 5.7 ± 1.9 to 0.8 ± 0.5, $P < 0.001$) in the subclavian artery was observed from EBF 0 to EBF 5.

Baseline SvO_2 was 62 ± 8% which corresponded with inadequate tissue oxygen delivery in our model. It increased to 77 ± 3% with EBF 1 and reached > 80% with all higher EBF steps ($P < 0.01$). With increasing of EBF, the average value of CVP did gradually fall, but not under 7 mmHg, avoiding ECMO underfilling ($P = 0.001$).

Similarly, the regional tissue oxygenations both cerebral and on forelimb were low at baseline, but increased promptly with increase of EBF. Cerebral rSO_2 changed by 30% from 57 ± 6% to 74 ± 3% and forelimb rSO_2 changed in total by 108% from 37 ± 6% to

77 ± 6% (both P < 0.01).

Left ventricular hemodynamics

LVPP increased by 49% from 49 ± 15 mmHg to 55 ± 13, 61 ± 13, 66 ± 12, 74 ± 10, and 73 ± 11 mmHg (for EBF 0 to 5, P = 0.001) and EDP increased by 114% from 7 ± 2 mmHg to 8 ± 2, 10 ± 2, 11 ± 3, 13 ± 2, and 15 ± 3 mmHg (for EBF 0 to 5, P < 0.001). Every escalation of EBF emphasized LV dilation. ESV increased severely by 20% from 139 ± 17 mL to 143 ± 16, 148 ± 18, 152 ± 19, 164 ± 15, and 167 ± 15 mL and EDV by 15% from 189 ± 26 mL to 194 ± 27, 203 ± 29, 209 ± 30, 217 ± 29, and 218 ± 30 mL (both for EBF 0 to 5, P < 0.001). Graphically depicted on Figure 27.

On the other hand, SV and EF changed only with less significant mean differences and both reached highest values at EBF 3 L/min. In detail, SV changed from 51 ± 20 mL to 51 ± 20, 56 ± 20, 59 ± 20, 55 ± 21, and 52 ± 21 mL (P = 0.03), and EF from 25 ± 7% to 24 ± 6, 26 ± 7, 27 ± 7, 23 ± 6, and 21 ± 6% (P = 0.18). Mean HR tended to decline with every increase in EBF – from 101 ± 22 beats/min to 96 ± 19, 93 ± 17, 90 ± 13, 90 ± 14, and 86 ± 14 beats/min (for EBF 0 to 5, P = 0.34).

Left ventricular SW was calculated from measured pressure-volume loops and exhibited significant flow-dependent increases from 1434 ± 941 mmHg*mL to 1595 ± 987, 1867 ± 1102, 2014 ± 1062, 2105 ± 1060, and 1892 ± 1036 mmHg*mL (EBF 0 to 5, P = 0.04), reaching its maximal value at EBF 4. However, preload independent index of LV contractility represented by $dP/dt_{max}/EDV$ ratio showed no consistent trend during the ECMO protocol – from 2.2 ± 0.8 mmHg/s/mL to 2.2 ± 0.6, 2.4 ± 0.4, 2.5 ± 0.4, 2.8 ± 0.6, and 3.0 ± 0.9 mmHg/s/mL (EBF 0 to 5, P = 0.94).

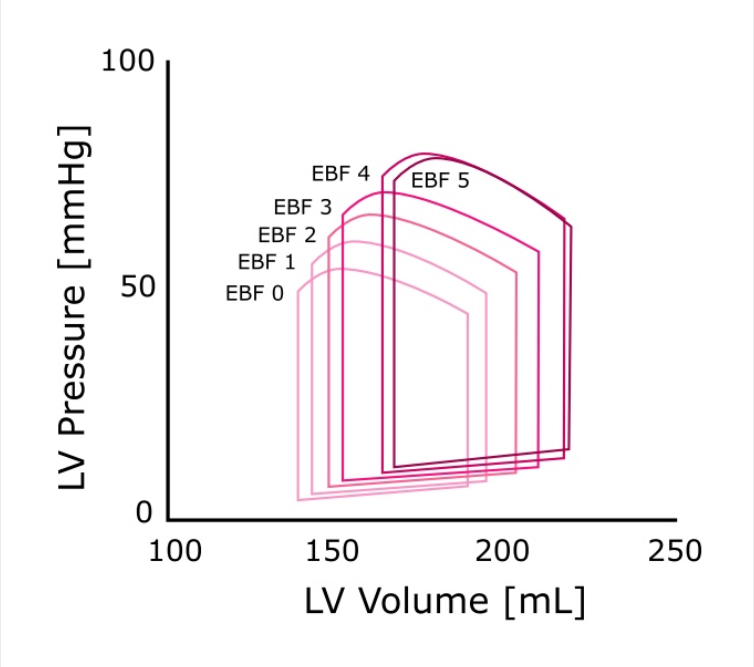

Figure 27. Schematic mean PV loop changes by effects of increasing VA ECMO flow. The left ventricular work parameters in a porcine model of chronic heart failure reveal a significant dependence on VA ECMO flow (EBF in L/min).

		VA ECMO blood flow in chronic HF model							Relative
Parameter	***Units***	**EBF 0**	**EBF 1**	**EBF 2**	**EBF 3**	**EBF 4**	**EBF 5**	**P**	EBF 0-5
Ventricular hemodynamics:									
LVPP	*mmHg*	49 ± 15	55 ± 13	61 ± 13	66 ± 12	$74 \pm 10*$	$73 \pm 11*$	0.001	49%
EDP	*mmHg*	7 ± 2	8 ± 2	10 ± 2	11 ± 3	$13 \pm 2*$	$15 \pm 3*$	< 0.001	114%
ESV	*mL*	139 ± 17	143 ± 16	148 ± 18	152 ± 19	$164 \pm 15*$	$167 \pm 15*$	< 0.001	20%
EDV	*mL*	189 ± 26	194 ± 27	203 ± 29	209 ± 30	$217 \pm 29*$	$218 \pm 30*$	< 0.001	15%
SV	*mL*	51 ± 20	51 ± 20	56 ± 20	59 ± 20	55 ± 21	52 ± 21	0.03	2%
EF	*%*	25 ± 7	24 ± 6	26 ± 7	27 ± 7	23 ± 6	21 ± 6	0.18	-16%
HR	*beats/min*	101 ± 22	96 ± 19	93 ± 17	90 ± 13	90 ± 14	86 ± 14	0.34	-15%
SW	*mmHg*mL*	1434 ± 941	1595 ± 987	1867 ± 1102	2014 ± 1062	$2105 \pm 1060*$	1892 ± 1036	0.04	32%
dP/dtmax/EDV	*mmHg/s/mL*	2.2 ± 0.8	2.2 ± 0.6	2.4 ± 0.4	2.5 ± 0.4	2.8 ± 0.6	3 ± 0.9	0.94	36%
Perfusion parameters:									
Carotid flow	*mL/min*	211 ± 72	291 ± 62	314 ± 57	356 ± 57	$447 \pm 64*$	$479 \pm 58*$	< 0.001	127%
Car. pulsatility index		1.43 ± 0.12	0.91 ± 0.2	0.75 ± 0.19	0.64 ± 0.21	$0.44 \pm 0.19*$	$0.34 \pm 0.15*$	< 0.01	-76%
Subclavian flow	*mL/min*	103 ± 49	128 ± 44	158 ± 40	208 ± 47	$266 \pm 47*$	$296 \pm 54*$	< 0.001	187%
Sbcl. pulsatility index		5.7 ± 1.9	3 ± 1	2.2 ± 0.8	1.5 ± 0.6	$1.1 \pm 0.5*$	$0.8 \pm 0.5*$	< 0.001	-86%
Cerebral rSO_2	*%*	57 ± 6	60 ± 4	67 ± 5	69 ± 5	$72 \pm 4*$	$74 \pm 3*$	< 0.001	30%
Forelimb rSO_2	*%*	37 ± 6	46 ± 5	58 ± 5	67 ± 6	$72 \pm 7*$	$77 \pm 6*$	< 0.001	108%
SvO_2	*%*	62 ± 8	77 ± 3	81 ± 3	86 ± 4	$89 \pm 4*$	$89 \pm 4*$	< 0.001	44%
CVP	*mmHg*	14 ± 2	11 ± 2	10 ± 2	$8 \pm 2*$	$9 \pm 2*$	$8 \pm 2*$	0.001	-43%

Table 7. Hemodynamic and pressure-volume characteristics on chronic HF model. For each step of increasing extracorporeal blood flow (EBF in L/min), hemodynamic values are expressed as mean ± SEM. Values significantly different from EBF 0 are marked with *.

5.6 Effects of EBF on acute HF

When the stepwise ramp protocol was applied to the model of acute heart failure induced by regional coronary hypoxemia, changes in hemodynamic parameters were similar, but still differed in some details compared to observations in the chronic HF model (see Document 4, Figure 28, and Table 8).

With increasing the flow rate from EBF 1 to EBF 5, changes were observed in LV workload. LVPP increased from 60 ± 7 mmHg to 72 ± 7, 81 ± 6, 89 ± 7, and 97 ± 8 mmHg (all for EBF 1, 2, 3, 4, and 5; $P < 0.001$) and HR decreased from 94 ± 4 beats/min to 89 ± 3, 84 ± 3, 80 ± 2, and 77 ± 2 beats/min ($P < 0.001$). Although there was only a numerical increase in EDP from 17.2 ± 1.4 mmHg to 18.2 ± 0.7, 18.6 ± 1.5, 18.9 ± 2.4, and 19.0 ± 2.9 mmHg, these differences were not statistically significant ($P = 0.87$).

Also, the LV volumes demonstrated dependence on the EBF. ESV increased from 64 ± 11 mL to 70 ± 11, 74 ± 11, 78 ± 12, and 83 ± 14 mL, ($P < 0.001$), but EDV did not change significantly – from 112 ± 19 mL to 115 ± 19, 116 ± 19, 119 ± 19, and 123 ± 20 mL ($P = 0.43$).

Finally, SW increased from 2096 ± 342 mmHg*mL to 2510 ± 335, 2752 ± 346, 3031 ± 404, and 2884 ± 412 mmHg*mL, respectively ($P < 0.001$).

		VA ECMO blood flow in acute HF model					
Parameter	***Units***	**EBF 1**	**EBF 2**	**EBF 3**	**EBF 4**	**EBF 5**	**P**
LVPP	*mmHg*	60 ± 7	72 ± 7	81 ± 6	89 ± 7	97 ± 8	< 0.001
EDP	*mmHg*	17.2 ± 1.4	18.2 ± 0.7	18.6 ± 1.5	18.9 ± 2.4	19 ± 2.9	0.87
ESV	*mL*	64 ± 11	70 ± 11	74 ± 11	78 ± 12	83 ± 14	< 0.001
EDV	*mL*	112 ± 19	115 ± 19	116 ± 19	119 ± 19	123 ± 20	0.43
SV	*mL*	48 ± 9	45 ± 9	42 ± 9	41 ± 9	40 ± 8	0.045
EF	*%*	43 ± 3	39 ± 2	36 ± 3	34 ± 3	32 ± 3	< 0.001
HR	*beats/min*	94 ± 4	89 ± 3	84 ± 3	80 ± 2	77 ± 2	< 0.001
SW	*mmHg*mL*	2096 ± 342	2510 ± 335	2752 ± 346	3031 ± 404	2884 ± 412	< 0.001
CO	L/min	4.3 ± 0.4	3.9 ± 0.5	3.5 ± 0.5	3.2 ± 0.4	3.0 ± 0.4	< 0.001

Table 8. Hemodynamic and pressure-volume characteristics on acute HF model. For each step of increasing extracorporeal blood flow (EBF in L/min), hemodynamic values are expressed as mean ± SEM.

Additional calculated parameters showed myocardial contractility change with increasing EBF. Both left ventricular stroke volume and ejection fraction decreased significantly: SV from 48 ± 9 mL to 45 ± 9, 42 ± 9, 41 ± 9, and 40 ± 8 mL ($P = 0.045$) and EF from 43 ± 3% to 39 ± 2, 36 ± 3, 34 ± 3, and 32 ± 3% ($P < 0.001$). Calculated cardiac output decreased from 4.31 ± 0.40 L/min to 3.90 ± 0.47, 3.49 ± 0.51, 3.21 ± 0.40, and 2.99 ± 0.38 L/min (again all for EBF 1 to 5; $P < 0.001$).

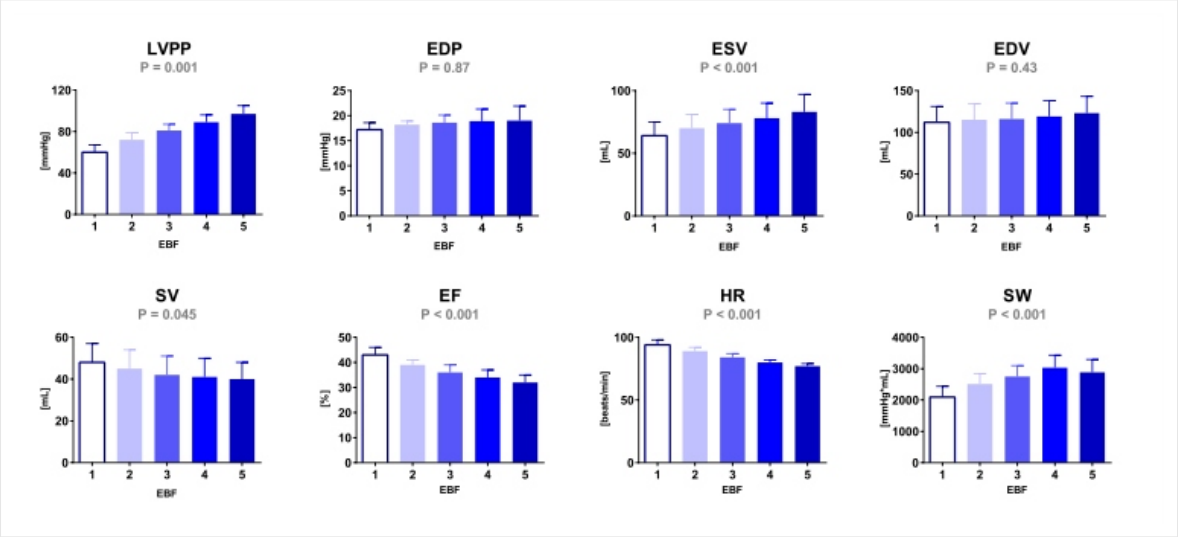

Figure 28. Effects of VA ECMO blood flow (EBF 1-5) on acute HF – hemodynamic and LV performance parameters in a porcine model of acute cardiogenic shock induced by regional coronary hypoxemia.

6 Discussion

To mimic severe circulatory failure, we first developed appropriate models of both acute and chronic heart failure. Then, ECMO was introduced and defined protocols of stepwise flow rates were applied to test its impacts on systemic perfusion parameters and ventricular hemodynamics. By precise monitoring, consequential circulation changes in chronic and acute forms of HF were described. Characteristics of developed animal models and the effects of various levels of extracorporeal blood flow are further discussed in detail. All attached documents also complement our discussions.

6.1 Comments on HF animal models

Heart failure is a major health problem that contributes greatly to morbidity and mortality. The pathogenesis and progression of HF in humans is complex, so an appropriate animal model is critical to investigate the underlying mechanisms and to test novel therapeutics that aim to interfere with native severe disease progression. To study the pathogenesis, multiple large animal models have been suggested for experimental testing.

Even though a significant part of VA ECMO clinical applications is for circulatory decompensation developed on grounds of previously present chronic heart disease, only minority of evidence comes from corresponding experiments. Furthermore, retrospective clinical studies have also revealed that outcome of patients treated by ECMO differs according to the “acuteness or chronicity” of cardiac disease (Tarzia et al. 2015).

For its suitability and bilateral heart failure, we used the model of TIC for chronic modelling and compared the measurements to two acute HF models induced by regional or global myocardial hypoxia.

Chronic HF model

In general, surgical models of chronic HF are useful to closely mimic the disease. When compared to models of acute HF, chronic HF models offer more insight into the long-term pathophysiology, but at the cost of time-consuming experimental preparation or higher mortality rates. From the variety of known chronic HF models, we are referring to an appropriate and easily manageable model, represented here by decompensated chronic HF induced by paced tachycardia.

It has been shown that in predisposed hearts long-lasting incessant tachyarrhythmias can lead to systolic dysfunction and dilation with decreased cardiac output. Such condition referred to as tachycardia-induced cardiomyopathy was firstly described in 1913 (Gossage and Braxton Hicks 1913), widely used in experiments since 1962 (Whipple et al. 1962), and is nowadays a well-known disorder. Its origin can lie in various types of arrhythmias - both supraventricular and ventricular tachycardia can lead to progressive deterioration of systolic function, biventricular dilation and progressive clinical signs of heart failure including ascites, edemas, lethargy and ultimately cardiac decompensation leading to terminal heart failure and, if not opposed, death.

Similar effects of circulatory suppression were observed by introduction of high rate cardiac pacing in animal models. In a porcine model, atrial or ventricular heart rate over 200 beats/min is potent to induce end-stage heart failure in a period of 3-5 weeks (progressive phase) with characteristics of TIC, but interindividual differences exist (Spinale et al. 1992, Shinbane et al. 1997). These findings correspond well to decompensated cardiomyopathy and the animal model of TIC offers multiple advantages for HF testing and treatment innovations. It offers to easily control the severity of chronic HF progression with titration of duration and rate of pacing protocol and, importantly, the heart failure persists also after cessation of the rapid pacing (chronic phase) (Moe et al. 1988, Cruz et al. 1990, Tomita et al. 1991, Shinbane et al. 1997, Takagaki et al. 2002, Umana et al. 2003, Schmitto et al. 2011).

The pacing electrode can be located in the ventricles or atria (Spinale et al. 1990, Shinbane et al. 1997). We omitted the supraventricular pacing site to prevent problems possibly caused by atrioventricular block during high pacing frequencies. The ventricular position also improved the stability of the pacing lead fixated in the ventricular apex compared to the atrial position and reduced occurrence of its dislocation.

In attached Document 2 (Hala et al. 2018) we present a detailed protocol with a video demonstration to produce a tachycardia-induced cardiomyopathy by long-term fast cardiac pacing in swine. This biomodel represents a potent way to study decompensated dilated cardiomyopathy, hemodynamics of progressive chronic HF with low cardiac output and effects of applied treatment. According to previous publications (Chow et al. 1990, Hendrick et al. 1990, Tomita et al. 1991) and the authors' experience, the pacing protocol was defined and started with pacing rate of 200 beats/min, which is above physiological rate of healthy swine in exercise or stress. Subsequently, the frequency was escalated and titrated between 200 and 240 beats/min with respect to individual HF progression (Shinbane et al. 1997, Moe and Armstrong 1999). Due to interindividual differences in response to fast pacing, the time needed to produce chronic HF with profound signs of decompensation varied from 4 to 8 weeks.

At the end of pacing protocol, all animals presented consistently with symptoms of chronic HF – tachypnea, fatigue, spontaneous tachycardia of > 150 beats/min, and systolic murmurs. At further investigation, ascites, pericardial and pleural effusions, nonsustained ventricular tachycardias, dilation of all heart chambers, and significant mitral and

tricuspid regurgitations were noticeable.

Hemodynamics of failing circulation was denoted by arterial hypotension, and due to poor contractility and low stroke volume, cardiac output was reduced to approximately 50% of a healthy animal's expected normal value (Wyler et al. 1979, Tranquilli et al. 1982). This model of tachycardia-induced cardiomyopathy matched well to poorly compensated dilated cardiomyopathy and was preserved also after the cessation of pacing (Cruz et al. 1990, Takagaki et al. 2002, Umana et al. 2003). Qualities of prepared model including neurohumoral dynamics, peripheral vascular abnormalities, and cardiac dysfunction reflected human chronic HF (Power and Tonkin 1999). As no anatomical shunts were found postmortem, the cardiac output was equally low in systemic as well as in pulmonary circulation.

Functional reflection is then the failing circulation and tissue hypoperfusion. The forelimb and cerebral regional tissue oxygen saturation as well as the regional blood flow in subclavian and carotid artery suggests centralization of the blood circulation. Their low values show severely reduced tissue perfusion in peripheral as well as in vital organs, which was confirmed by low SvO_2 when compared to the expected normal value of at least 65% (Xanthos et al. 2007). The general low tissue perfusion was in concordance with the measurements of low cardiac output.

Hemodynamics and mechanical work during each cardiac cycle of the left ventricle were well documented by the PV diagram obtained from PV catheter instant measurements. Poor myocardial strength was denoted by maximum LV peak pressure during systole and the $dP/dt_{max}/EDV$ ratio, a preload independent index of LV contractility. LV chamber volumes were enlarged during the whole cycle, thus the image of dilated cardiomyopathy. The end-diastolic LV pressure was not increased as high as would be expected in cardiogenic shock. The LV filling pressure remains low, most likely due to high compliance of the LV thin myocardial wall (Little 2005).

Bacterial infection complications are a major problem of implants in experimental settings. Generator pocket infections and infective endocarditis are both poor prognoses and would make the experiment futile. Due to porcine anatomy, the jugular region is exposed and if a pacemaker generator was placed here, healing and preventing contamination would be a difficult task in long-survival experiments. The usage of subcutaneous tunneling enables to relocate the pacemaker generator pocket to the dorsal region, which is accessible and can easily be kept in a hygienic state. There, the pacemaker is also not within the animal's reach, which considerably improves healing. Also, the use of in-house modified "Y" connecting part allowed for high pacing frequencies with the use of a single pacing lead and regular pacemaker.

Acute HF models

Two models of acute HF were used for the presented experiments – a model of regional coronary hypoxemia and a model of global coronary hypoxemia. Both led to myocardial hypoxia, contractility dysfunction, and progression to acute circulatory decompensation. The amount of oxygen delivery to the myocardium was titrated by the oxygen saturation and coronary blood flow in the perfused region to reach conditions of cardiogenic shock.

In comparisn to other frequently used ways to induce acute HF like coronary artery ligation or embolization with subsequent myocardial infarction which are associated with a very high acute mortality rate, the concept of regional or global coronary hypoxemia allowed reversibility of the developed HF and successfully prevented mortality. Although

severe acute cardiogenic shock was successfully induced in all animals with CO reduction to $< 50\%$, there was no need for defibrillation and zero mortality.

In an earlier perfusion study of VA ECMO support, the coronary arterial flow was predominantly derived from left ventricular ejection, despite proximal placement of the reinfusion cannula (Kinsella et al. 1992). With poor or no gas exchange in the lungs, global myocardial hypoxia led to acute HF in the latter of our models. Similar to the "Harlequin syndrome", hypoxia of the whole upper body was a limitation of this design. Thus, we cannot exclude the possibility that the hypoxia of central nervous system and upper body parts influenced the circulation.

Both presented acute HF models were developed and served well for the hemodynamic studies. The evaluations between chronic and acute HF models provide stable grounds for our conclusions. Compared to the chronic model of TIC, regional myocardial hypoxia led to resultant ESV and EDV of far smaller dimensions (46% for ESV, 58% for EDV) and lower LV pressures.

Right-sided HF model

Additionally, a model of right-sided HF was developed by gradual pulmonary artery occlusion. The echocardiographic findings described well developed eccentric RV dilation with diminished contractility as reaction to extreme afterload. After the 7 days of disease progression, increase in afterload were demonstrated by tricuspid regurgitation and its high gradient and the compensatory mechanisms were partially developed. We used TAPSE as a well-established method of RV longitudinal contractility and FAC to evaluate overall systolic function due to the asymmetric shape and remodeling of RV. Both parameters showed severe systolic dysfunction after the rPA was gradually occluded.

This model reflects well pediatric or neonatal pulmonary hypertension with right-sided HF and suites well for testing of hemodynamic circulatory support designed for CO_2 removal. Low pressure drop gas exchange units, which are currently under development (Thompson et al. 2019), can be applied and passively perfused in parallel to the native pulmonary circulation, and thus alleviate RV work load – with no blood pump needed.

The ECMO protocol was not applied to the right-sided HF model.

6.2 EBF effects on chronic HF

VA ECMO is being used as an ultimate method in cases of severe circulatory decompensation, but multiple clinical and experimental studies have documented adverse changes in LV function with the increased EBF (Soleimani and Pae 2012, Burkhoff et al. 2015, Ostadal et al. 2015, Brogan et al. 2017) for both cardiac (Truby et al. 2017) and respiratory (Tanke et al. 2005) compromised patients. The incidences of these complications vary widely between 12 to 68% (Cheng et al. 2014, Truby et al. 2017, Kim et al. 2019, Na et al. 2019) and are still believed to be underreported (Cheng et al. 2014, Truby et al. 2017).

The goal of our experimental work was to assess the response of hemodynamic parameters and LV workload to different levels of EBF. We chose a porcine model of TIC, developed by long-term fast ventricular pacing, over weeks resulting in symptoms and signs of anatomical, functional, and neurohumoral profiles similar to human chronic HF. As far as we are informed, this study was unique in that it describes the hemodynamic effects of VA ECMO in decompensated chronic HF model. An important feature of our

protocol is also adequate lung ventilation, which ensures that coronary arteries receive well-oxygenated blood during all rates of EBF. Therefore, reported changes in LV hemodynamics should not be attributed to coronary ischemia as a result of poor oxygenation.

Ventricular hemodynamics

With initiation of the extracorporeal circulation and stepwise increase of EBF, progressive dilation of LV was observed. Affected were both the end-diastolic (in total by 15% from EBF 0 to 5) and even more, the end-systolic volume (by 20%). This increase in LV dimensions was strongly pronounced between EBF 0 to EBF 4; by increasing the flow beyond this point, left ventricle did not significantly further dilate.

LV pressures demonstrated upward trends as well. LVPP increased by 49% but still remained abnormally low despite high EBF. LV EDP was initially elevated to 7 mmHg due to abnormal LV filling dynamics, but when compared to the models of acute HF, the EDP elevation during low EBF in TIC was pointedly lower. This may be explained by the chronicity of our HF model which led to massive ventricular dilation without appreciable thickening of its wall, higher ventricular compliance, and thus less pronounced EDP elevation. With ECMO flows from EBF 0 to 5, EDP increased significantly further by over 114% leading to high preload and high end-diastolic wall tension, possibly opposing coronary perfusion (Kato et al. 1996). Similar ventricular pressure trends were described by (Seo et al. 1991) with the conclusion that VA ECMO flow should be kept as low as possible, in view of undesirable hemodynamic effects on both ventricles.

On the other hand, SV and EF had a different course when increasing EBF. Both these measures of LV ejection showed increase from EBF 1 to EBF 3, but with higher EBF, their mean values decreased. Systolic ejection trended to maximum at middle levels and to minimum at the highest levels of VA ECMO support. This trend will be further compared to acute HF models.

SW, defined as the area of PV loop and representing the instant LV workload, was expected to be proportional to ventricular systolic pressure and SV (Glower et al. 1985, Burkhoff et al. 2005). In our measurements, demands on the LV work measured by SW showed significant increase by 40% from EBF 0 to EBF 4, and with further escalation of ECMO flow to EBF 5, declined. In fact, SW is well respecting the trend of LVPP and SV.

The maximal positive LV pressure change is considered to be one of isovolumetric phase contractility indices. Due to severe LV dilation in our experiment, we used this index normalized to EDV, $dP/dt_{max}/EDV$ ratio, as recommended for its high sensitivity for global inotropic state, irrespective of ventricular loading conditions (Little 1985, Kass et al. 1987, Burkhoff et al. 2005). It has been confirmed that its linear relation is affected less by afterload compared to the end-systolic PV ratio (Little 1985). As expected, the initial value in our TIC model was significantly below normal. Further across the stepwise protocol of EBF, the ratio of $dP/dt_{max}/EDV$ continued to increase but did not meet statistical significance. For isovolumetric phase of contraction, this could imply that LV did not lose its ability to contract. In individuals where the $dP/dt_{max}/EDV$ ratio did not decrease with higher EBF, this could be explained by unrestricted or at least, sufficient coronary perfusion and secondarily by preserved potential of contractility. A similarly designed study reported hemodynamic effects of VA ECMO, but applied to healthy canine circulation (Kato et al. 1996). Although they reported reduction of coronary flow with increasing EBF, myocardial oxygen consumption was not reduced. In a similar sense, our data did not indicate critically inadequate myocardial perfusion on any of EBF levels.

Blood propelled to the aortic root, especially potentiated by aortic and mitral regurgitations, often leads to increased left atrial pressure (Fuhrman et al. 1999). Yet, in none of our cases, progression into pulmonary edema was observed, which could be due to the short-term duration of extracorporeal support and sufficient right heart unloading.

The combination of increasing SW and not declining $dP/dt_{max}/EDV$ ratio demonstrate increased demands on LV work, placed by the high afterload, and this increase in LV work occurs concurrently with LV dilation (Burkhoff et al. 2005).

These observations support our first hypothesis.

Perfusion and regional saturation

As the metabolic rate and hematocrit remain unchanged, systemic organ perfusion can be predicted by arterial flows and mixed venous blood saturation. In Dokument 1 we reported linear correlation of tissue saturation and regional arterial flow in VA ECMO support of chronic HF. Both tissue saturation and regional arterial flow demonstrated significant increases with respect to EBF (Hala et al. 2016). Low initial value of SvO_2 improved already at level of EBF 1, suggesting sufficient systemic perfusion with only minor extracorporeal support. Not surprisingly, with every higher EBF step, average SvO_2 and carotid arterial flow rose, but the pulsatility index gradually decreased, demonstrating loss of aortic pulse pressure and the dominance of ECMO blood flow in systemic circulation (Belohlavek et al. 2012, Hala et al. 2016). Practically, the value of regional tissue saturation together with SvO_2 have the potential to serve as additional methods to secure vital organ perfusion in ECMO therapy guidance.

Namely, brain and peripheral tissue oxygenation levels were represented by near-infrared spectroscopy with sensors placed on forehead and right forelimb. This transcutaneous technique is widely used for bedside monitoring of relative local oxyhemoglobin concentration changes. As a non-invasive method it has been validated both in experimental and clinical studies for microcirculation assessments (Ito et al. 2012, Ostadal et al. 2014). Blood flow to matching regions was measured by circumjacent probes on right carotid and right subclavian artery.

An overlook of our results confirms that with stepwise increase of the EBF, arterial blood flow in carotid and subclavian artery increase in a manner respecting the increase of mean aortic blood pressure. As both pulsatile systemic and non-pulsatile extracorporeal circulations are concomitantly meeting in the thoracic aorta, with increasing of EBF, the relative contribution of LV ejection to arterial flow is decreasing. Due to the increase of LV end-diastolic pressure, excessive afterload may not be accompanied by increase in coronary perfusion, which may further contribute to loss of pulsatility observed in both arteries (Kato et al. 1996). Though, we did not see a trend in $dP/dt_{max}/EDV$.

In the chronic HF, baseline cerebral perfusion through the right carotid artery was 211 $\pm$ 72 mL/min, which is approximately 59% of flow reported previously in healthy animals with identical methodology (Mlcek et al. 2016). Interindividual variability of carotid flow does not seem to correlate with body size. Instantaneous increase of arterial flow is provided by setting higher EBF. This increase is again more prominent in subclavian compared to carotid artery (by 187% vs. 127%). Similarly, respecting the local flow, baseline regional tissue oxygenation of the arm is lower compared to the forehead ($P = 0.08$), but it increases by 108% compared to only 30% increase on the forehead. These observations are reflecting peripheral hypoperfusion and the ability to compensate intracranial circulation at baseline conditions of cardiogenic shock. Both brain and

brachial tissue oxygenation demonstrate linear correlation with local perfusion throughout the whole protocol, which supports the constant local oxygen consumption.

Mean cerebral oxygenation in healthy animal is referred to reach 65% (Xanthos et al. 2007). In our work, already during low to mild circulatory support of EBF 2 or 3 L/min, the tissue oxygenation, arterial flow, and mixed venous oxygen saturation steeply comes close to normal values. Further increase to high rates of EBF then seems to provide only moderate improvement.

As stated by our second hypothesis, these experimental results could imply, that in decompensated chronic heart failure of matching severity, low to mild EBF may be of enough circulatory support to cover adequate tissue needs and at the same time protecting the LV from possibly harming overload.

6.3 EBF effects on acute HF

A similar ECMO protocol was applied to the acute HF model developed by regional myocardial hypoxemia and the hemodynamic effects were analyzed and compared to chronic HF (see Figure 29).

In comparison to chronic HF study, baseline LV volumes were far smaller (46% for ESV, 58% for EDV) and the effect of faster EBF was different – by increasing EBF, ESV increased by 31% (64 ± 11 mL to 83 ± 14 mL, $P < 0.001$), but EDV only by 10% (112 ± 19 mL to 123 ± 20 mL, $P = 0.43$, both for EBF 1 to 5). Likewise, increase of LVPP was more pronounced (by 67%; from 60 ± 7 mmHg to 97 ± 8 mmHg, $P < 0.001$), but changes of EDP were only mild (17.2 ± 1.4 mmHg to 19.0 ± 2.9 mmHg, $P = 0.87$, both for EBF 1 to 5). In both studies, SW followed the same trend, reaching the highest value at EBF 4, and HR declined with every increment of EBF.

In the acute model induced by regional myocardial hypoxemia supported by stepwise VA ECMO, trend of LV EF continued to decline. This was observed neither in the chronic HF model, nor in the model of global myocardial hypoxia. Interestingly, in the latter experiment, this trend was not observed regardless of pulsatile or non-pulsatile ECMO flows.

In Figure 29, PV characteristics of regional myocardial hypoxic model are plotted against the chronic TIC model. Values of EDV, ESV, EDP, and LVPP for corresponding EBF steps reveal linear relations with dissimilar slopes ($r = 0.94$, $r = 0.97$, $r = 0.92$, and $r = 0.97$, respectively, all $P < 0.05$).

In another model of acute HF generated by hypoxic myocardial perfusion, Shen et al. (2001) reported a decline of dP/dtmax and of LVPP associated with VA ECMO flow, but in their settings all of the coronary vascular bed received hypoxemic blood.

When summarized, in the chronic HF model, EDP was lower at baseline but increased more with higher EBF, and end-diastolic dilation was more pronounced. EF and SV were proved to decline only in the case of acute regional hypoxic HF. One possible explanation is that in the ECMO protocol, high extracorporeal flows improve the coronary perfusion with oxygen rich blood, in contrast to the acute models, where a major portion of LV myocardium is perfused by constant flow of oxygen-poor blood, stunned, and therefore cannot keep pace and eject against increasing afterload. Long-term adaptation to chronic HF conditions with humoral activation during TIC model induction could be another possible explanation.

Findings of these innovative animal HF models were also confirmed by computer modeling (Broome and Donker 2016) – the effects of increasing EBF on LV hemodynamics

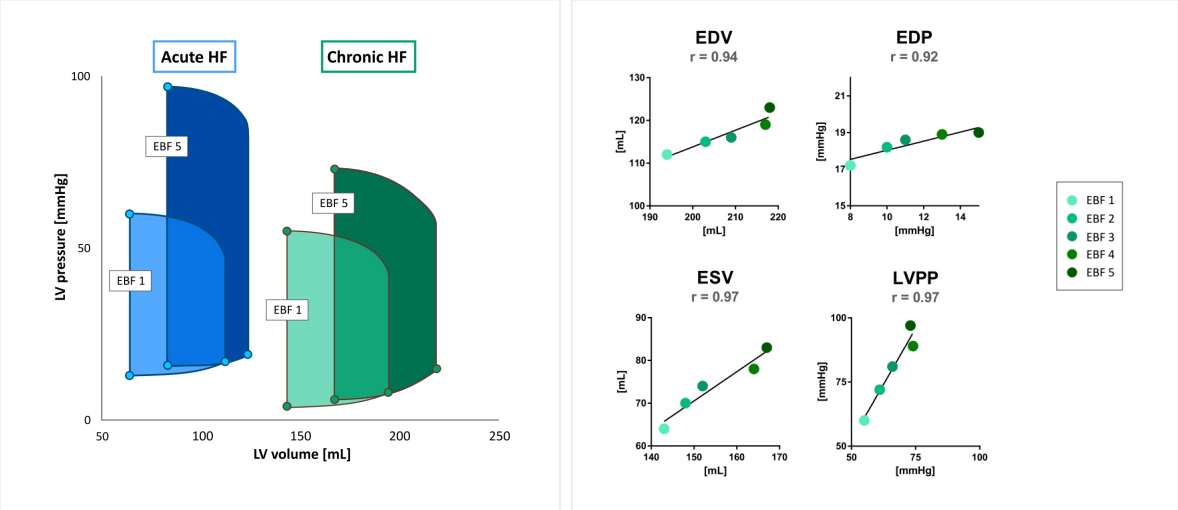

Figure 29. Effect of increasing EBF on acute (blue) and chronic (green) heart failure. Left – averaged PV loops for EBF 1 and EBF 5 are demonstrating the change of LV parameters increasing EBF. Right – scatter plots of LV pressure-volume parameters, increasing EBF effects on chronic (horizontal axes) and on hypoxic acute heart failure (vertical axes). In each graph, both axis (horizontal and vertical) have identical scales. For all, $P < 0.05$.

were reported. Figure 29 is depicting PV loops of acute and chronic model reactions to VA ECMO flow which can offer insights into hemodynamic changes in both chronic and acute HF models. Effects of different levels of EBF on LV work load, mean arterial pressure, and coronary flow is also well documented by review of previously published studies (Table 1).

6.4 Correlation of tissue saturation and perfusion

The brain and peripheral tissue oxygenation levels were represented by near-infrared spectroscopy. Blood flow to the corresponding regions was measured by circumjacent probes on right carotid and right subclavian artery.

The perfusion and regional tissue oxygenation of forelimb and brain are visualized on Figure 30 and demonstrate a linear relationship. Carotid flow correlated with brain oxygenation ($r = 0.75$, $P < 0.001$) and subclavian flow correlated with corresponding forelimb oxygenation ($r = 0.94$, $P < 0.001$). As both methods can be considered reliable and reproducible (Wolf et al. 2007, Ito et al. 2012, Ostadal et al. 2014), the well demonstrated linearity confirms a relation of saturation and perfusion in both central and peripheral organs.

Both figures are scaled to equal axis ranges. Notably, as the relation slopes are steeper for forelimb, this is proposing a stronger autoregulation of the brain perfusion and centralization of cardiac output. With the lowest level of extracorporeal support, brain saturation was higher by approximately 20 percent points but this difference diminished with higher ECMO flows. This trend occurred simultaneously with significant drop in pulsatility.

Our results of cerebral perfusion are similar to clinical study reported by Liem et al. (1995). In infants undergoing VA ECMO for cardiorespiratory failure, they evidenced increased total cerebral blood flow accompanied by increased cerebral blood volume and

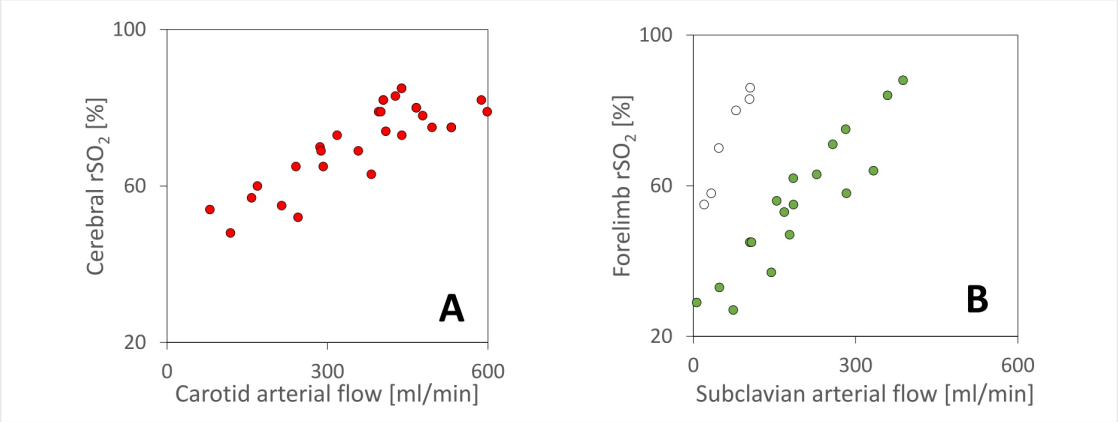

Figure 30. Correlation of carotid (A) and subclavian (B) arterial flow and corresponding regional tissue oxygenation. Correlation coefficients r = 0.75 (for A) and r = 0.94 (B), P < 0.001 for both; omitting one outlying subject – in white color.

also loss of pulsatility assessed by transcranial Doppler ultrasound. On contrary, different observations were reported by Stolar and Reyes (1988) in healthy lambs – two hours of high flow VA ECMO narrowed pulse pressure, but caused no significant changes of carotid flow. The use of healthy animals, absence of increase in mean arterial pressure or cannulas' position can explain this discrepancy. Notably, link of cerebral hyperperfusion and intracranial hemorrhage is suspected (van de Bor et al. 1990).

6.5 Effects of flow pulsatility

With the high rates of venoarterial bypass flow, significant drops of pulsatility indices were observed. Both circulations are set in paralel, thus the combination of increasing EBF and consequently decreasing ventricular ejection, not surprisingly, reduces the pulse pressure and pulsatility of flow in all systemic arteries.

Pulsatility indices were calculated for the subclavian and carotid arteries. Before ECMO initiation, pulsatility index of carotid flow was considerably lower compared to the subclavian, but with increase of EBF to 5 L/min, the carotid PI dropped less than in subclavian artery (by 76% vs. 85%).

In general, PI is to be influenced by transaortic LV ejection, vascular resistance, arterial carbon dioxide tension and aortic and arterial wall stiffness, which can be considered low as we studied young animals. To suppress their effects, blood gas parameters were maintained in physiological ranges in extracorporeal and also native circulation. Insufficiency of the aortic valve, another contributor to pulsatility, was present in our model due to the insertion of transaortic catheter. But, according to echocardiography, this was of little significance.

Similar gradual decline of PI in newborns was observed at higher EBF and remained low also shortly after the VA ECMO decannulation, suggesting changes in vascular resistance (van de Bor et al. 1990). Whether deficiency of pulsatile flow in arteries negatively affects organ perfusion remains a controversial topic. Some studies reported benefits of pulsatility on microcirculation (Orime et al. 1996, Orime et al. 1999).

Pulsatile form of VA ECMO (PECMO) support has been introduced to preclinical and clinical testing. Different mechanisms lead to pulse pressure generation. ECG synchronization and increasing pump rotation speed during diastole and decreasing the speed

during systole cause diastolic augmentation in arterial blood flow. Another mechanism would be utilizing a secondary blood pump (Foerster et al. 2018) or alternating constriction of the reinfusion line. In recent reports, these applications were associated with improved systemic perfusion and decreasing LV demands (Karaci et al. 2011, Wang et al. 2015, Itoh et al. 2016, Ostadal et al. 2018). An overview of pulsatile and non-pulsatile ECMO studies is available in Table 9.

In attached Document 6 (Ostadal et al. 2018) hemodynamic effects of ECG-synchronized pulsatile VA ECMO support are presented. By alternating blood pump speed, extracorporeal flow pulsatility was associated with a significant reduction in LV end-systolic volume (by 6.7%), an increase in LV stroke volume (by 17.4%), higher EF (by 18.8 percent points), cardiac output (by 17.1%), and mean arterial pressure (by 5.5%) when compared to continuous flow (all $P < 0.05$). Interestingly, these changes were accompanied by significant increase of coronary flow, as measured by coronary Doppler wire.

6.6 Clinical considerations

Although the impact of LV overload on clinical outcomes is mostly unknown and the literary evidence limited, it is expected that it negatively affects patients' recovery (Truby et al. 2017, Donker et al. 2019) and in minority of patients, the status can further progress into pulmonary congestion or edema (Soleimani and Pae 2012, Boulate et al. 2013, Truby et al. 2017, Donker et al. 2019). In addition, recent small clinical and experimental series have shown that the severity of LV overload and distention correlates well with the rate of EBF (Walther et al. 1990, Aissaoui et al. 2012, Ostadal et al. 2015).

As mentioned above, our results of cerebral perfusion are similar to clinical study reported by Liem et al. (1995). The authors evidenced increased total cerebral blood flow accompanied by increased cerebral blood volume and also loss of PI assessed by transcranial Doppler ultrasound in infants undergoing VA ECMO for cardiorespiratory failure. Importantly, the cerebral hyperperfusion was associated to intracranial hemorrhage (van de Bor et al. 1990).

In clinical settings, echocardiography can serve as a method of choice to evaluate the ventricular response to volume loading during or while weaning from ECMO (Walther et al. 1990, Aissaoui et al. 2012, Donker et al. 2019). Assessments of SV and filling pressures, together with pulmonary wedge pressure, lung fluid accumulation, and regional saturations, are available measures which should be operated on daily basis (Truby et al. 2017, Donker et al. 2018, Donker et al. 2019). Having these in hands, partial flows of extracorporeal support in conjunction with aggressive inotropic support have been suggested in effort to prevent LV overload (Ostadal et al. 2015, Hala et al. 2016, Truby et al. 2017).

In the presented study we showed how VA ECMO increases the demands on LV work and that despite significant increase of EDP, negative effect on load-independent contractility was not observed, suggesting sufficient myocardial oxygenated blood supply. Several methods have been proposed to unload the ventricles under VA ECMO therapy but are associated with increased rate of complications and the clinical evidence is limited to few single center small cohorts and case reports (Barbone et al. 2011, Soleimani and Pae 2012, Boulate et al. 2013, Truby et al. 2017, Donker et al. 2019). In a recent report, 15 out of 36 patients with LV distention on VA ECMO required some venting strategy to reduce wall stress (Truby et al. 2017). It has also been shown that even a small venting

	ECLS type	HF	setting	sample size	assessed parameters/main findings
Hala et al. 2020	non-pulsatile	chronic HF	experimental (porcine)	5	EBF puts higher demands on LV work
Hala et al. 2016	non-pulsatile	chronic HF	experimental (porcine)	5	perfusion and rSO_2 correlate w/EBF
Ostadal et al. 2018	pulsatile	acute HF	experimental (porcine)	16	pulsatile flow improves coronary perfusion
Ostadal et al. 2015	non-pulsatile	acute HF	experimental (porcine)	5	excessive EBF increases demands on LV
Aissaoui et al. 2012	non-pulsatile	mixed	clinical	22	echocardiographic assessments, tissue Doppler
Kato et al. 1996	non-pulsatile	-	experimental (canine)	14	coronary perfusion decreases w/higher EBF
Seo et al. 1991	non-pulsatile	-	experimental (canine)	16	EDP increases w/higher EBF
Shen et al. 2001	non-pulsatile	-	experimental (porcine)	8	myocardial function is not reduced by EBF
Kinsela et al. 1992	non-pulsatile	-	experimental (ovine)	7	>90% of coronary flow is from LV
Cremers et al. 2015	pulsatile	cardiac arrest	experimental (porcine)	8	pulsatile flow improves coronary perfusion
Itoh et al. 2016	pulsatile	cardiac arrest	experimental (porcine)	14	pulsatile flow improves brain saturation
Orime at al. 1996	pulsatile	acute HF	experimental (porcine)	14	pulsatile flow improves microcirculation
Orime at al. 1999	pulsatile	-	clinical	18	pulsatile flow reduces endothelial damage

Table 9. Review of hemodynamic studies of extracorporeal blood flow pathophysiology. EBF – extracorporeal blood flow, LV – left ventricle, ECLS – extracorporeal life support, EDP – end-diastolic pressure, HF – heart failure.

catheter of 7 or 8 Fr in left atrium (Kim et al. 2019) or LV (Barbone et al. 2011) might be sufficient and that its early applications result in lower mortality (Soleimani and Pae 2012, Na et al. 2019). However, the clinical relevance of these effects still remains uncertain.

6.7 Study limitations

In order to cover wide spectrum of situations, ECMO was applied to three different models of HF – both acute models simulate the clinical conditions in patients with cardiogenic shock caused by acute myocardial ischemia or fulminant myocarditis - and the chronic (TIC) model which mimics more situation of advanced dilated cardiomyopathy.

Although the HF models were adequately reliable, we realize several limitations. As mentioned earlier, nonsustained ventricular tachycardias are a sign of successful HF induction, but if long-lasting, they also produce risk of sudden cardiac death. During anesthesia one of the animals required resuscitation and defibrillation. Differences in animal body weight can slightly contribute to dispersion of model characteristics. Also the necessity of anesthesia has to be taken under consideration when using the models, especially its influence on HR and blood pressure. On the other hand it also reflects the real life situations of sedated patients. Blood levels of porcine specific markers could be useful for assessing the degree of HF progression and cardiac remodeling, but adequate evidence is still lacking.

Regional myocardial hypoxia proved to develop a reliable HF model, but can also lead to different extent of injury due to variations in coronary anatomy. We overcame this by including another model induced by global hypoxia and by titration of the circulatory failure progression.

Although the ECMO studies were prepared carefully and the total numbers of studied animals were adequately reasonable, several limitations of the ECMO protocol must be considered. First, real isovolumetric phase was absent on recorded PV loops, as it could only be seen in cases with intact heart valves. In real measurements, LV volume may never stay constant due to valve insufficiency. The aortic regurgitation in our experiments was caused by PV loop catheter and was not considered severe on echocardiography. Second, contractility indices (like $dP/dt_{max}/EDV$ ratio) are highly sensitive but are also known to have a low reproducibility for contractile status. Therefore, myocardial perfusion cannot be directly deducted. In future studies, coronary arterial flow and oxygen consumption should be included. A third limitation could be seen in the relatively brief duration of extracorporeal support used in this study compared to common durations of ECMO therapy. To test long-term effects, experiments should be extended, and lung fluid content assessed. Lastly, right ventricular workload and the pulmonary circulation or pulmonary edema should also be considered.

7 Conclusions

Large animal models of acute and chronic forms of heart failure were successfully developed. The design allowed for wide range of titration and in all experiments extracorporeal circulatory support was then applied to decompensated states of circulatory failure. Thanks to a constant methodology of heart failure models preparation, highly reproducible measurements were obtained.

A set of hemodynamic monitoring tools were used to assess left ventricular workload and systemic perfusion. Particularly pressure-volume loop analyses, regional tissue saturation, and invasive arterial flow measurements were used to describe circulatory status.

Effects of different levels of circulatory support were tested by a stepwise protocol and main changes caused by extracorporeal flow increments were observed – with already mild flows, the regional tissue saturations and systemic flow improved, but on the other hand ventricular dilation, increases in pressures, and thus increased left ventricular work were observed with every step-up of extracorporeal flow. Overall, similar trends were seen in both acute and chronic heart failure models, but small differences like differences in end-diastolic pressures or myocardial contractility deserve to be pointed out.

Based on obtained results, we can confirm both our hypotheses were correct. Venoarterial extracorporeal membrane oxygenation causes significant changes to hemodynamics by putting higher demands on the left ventricular work. Though, this might be accompanied by sufficient coronary perfusion.

Although experiments were performed on severely compromised circulation, systemic perfusion parameters improved already with low to mild extracorporeal blood flow support. The results imply that even submaximal flows can provide hemodynamic support and in matching settings, high rates of EBF may not only be unnecessary, but also harmful to the heart.

Considering the experimental results, we propose that to decrease the risk of LV overload, VA ECMO flow should be maintained at the lowest level securing adequate tissue perfusion.

8 List of attached documents

Document 1
Hala P., Mlcek M., Ostadal P., Janak D., Popkova M., Boucek T., Lacko S., Kudlicka J., Neuzil P., and Kittnar O. (2016). "Regional tissue oximetry reflects changes in arterial flow in porcine chronic heart failure treated with venoarterial extracorporeal membrane oxygenation." Physiological Research 65(Supplementum 5): S621-S631.

Document 2
Hala P., Mlcek M., Ostadal P., Janak D., Popkova M., Boucek T., Lacko S., Kudlicka J., Neuzil P., and Kittnar O. (2018). "Tachycardia-Induced Cardiomyopathy as a Chronic Heart Failure Model in Swine." Journal of Visualized Experiments 132(e57030).

Document 3
Hála P., Mlček M., Ošťádal P., Popková M., Janák D., Bouček T., Lacko S., Kudlička J., Neužil P., and Kittnar O. (2020). "Increasing venoarterial extracorporeal membrane oxygenation flow puts higher demands on left ventricular work in a porcine model of chronic heart failure." Journal of Translational Medicine 18(1).

Document 4
Ostadal P., Mlcek M., Kruger A., Hala P., Lacko S., Mates M., Vondrakova D., Svoboda T., Hrachovina M., Janotka M., Psotova H., Strunina S., Kittnar O., and Neuzil P. (2015). "Increasing venoarterial extracorporeal membrane oxygenation flow negatively affects left ventricular performance in a porcine model of cardiogenic shock." Journal of Translational Medicine 13: 266.

Document 5
Ostadal P., Mlcek M., Strunina S., Hrachovina M., Kruger A., Vondrakova D., Janotka M., Hala P., Kittnar O., and Neuzil P. (2016). "Novel porcine model of acute severe cardiogenic shock developed by upper-body hypoxia." Physiological Research 65(4): 711-715.

Document 6
Ostadal P., Mlcek M., Gorhan H., Simundic I., Strunina S., Hrachovina M., Kruger A., Vondrakova D., Janotka M., Hala P., Mates M., Ostadal M., Leiter J. C., Kittnar O., and Neuzil P. (2018). "Electrocardiogram-synchronized pulsatile extracorporeal life support preserves left ventricular function and coronary flow in a porcine model of cardiogenic shock." PLoS One 13(4): e0196321.

Document 7
Carr B. D., Poling C. J., Hala P., Caceres Quinones M., Prater A. R., McLeod J. S., Bartlett R. H., Rojas-Pena A., and Hirschl R. B. (2019). "A Model of Pediatric End-Stage Lung Failure in Small Lambs <20 kg." ASAIO Journal. DOI: 10.1097/MAT.0000000000001017

9 Abstract

Introduction:

Venoarterial extracorporeal membrane oxygenation (VA ECMO) is widely used in the treatment of circulatory failure, but repeatedly, its negative effects on the left ventricle (LV) have been observed. The purpose of this study is to assess the influence of extracorporeal blood flow (EBF) on systemic hemodynamic changes and LV performance parameters during VA ECMO therapy of decompensated heart failure.

Methods:

Porcine models of low-output chronic and acute heart failure were developed by long-term fast cardiac pacing and coronary hypoxemia, respectively. Profound signs of circulatory decompensation were defined by reduced cardiac output and tissue hypoperfusion. Subsequently, under total anesthesia and artificial ventilation, VA ECMO was introduced. LV performance and organ specific parameters were recorded at different levels of EBF using an LV pressure-volume loop analysis, arterial flow probes on carotid and subclavian arteries, and transcutaneous probes positioned to measure cerebral and forelimb regional tissue oxygen saturations.

Results:

Conditions of severely decompensated heart failure led to systemic hypotension, low tissue and mixed venous oxygen saturations, and increase in LV end-diastolic pressure. By increasing the EBF from minimal flow to 5 L/min, we observed a gradual increase of LV peak pressure, reduced arterial flow pulsatility, and an improvement in organ perfusion. On the other hand, cardiac performance parameters revealed higher demands put on LV function: LV end-systolic volume and end-diastolic pressure and volume all significantly increased (all $P < 0.001$). Consequently, the LV stroke work increased ($P < 0.05$) but LV ejection fraction did not. Also, the isovolumetric contractility index did not change significantly.

Conclusions:

In decompensated chronic and acute heart failure, excessive VA ECMO flow increases demands on left ventricular workload and can be potentially harmful. To protect the myocardium, VA ECMO flow should be adjusted with respect to not only systemic perfusion, but also to LV parameters.

Key words:

Extracorporeal membrane oxygenation; Heart failure; Hemodynamics; Heart ventricles; Artificial cardiac pacing

10 Abstrakt

Úvod:

Venoarteriální mimotělní membránová oxygenace (VA ECMO) je široce využívaná metoda v léčbě závažného oběhového selhání, avšak opakovaně byl pozorován také její negativní vliv na levou komoru srdeční (LV). Cílem práce je zhodnotit vliv průtoku mimotělní podporou (EBF, extracorporeal blood flow) na systémovou hemodynamiku během VA ECMO terapie dekompensovaného srdečního selhání.

Metody:

Biomodel (prase domácí) srdečního selhání s nízkým srdečním výdejem byl vytvořen dlouhodobou rychlou stimulací myokardu (chronické srdeční selhání) a koronární hypoxemií (akutní srdeční selhání). Známky dekompensovaného srdečního selhání byly definovány sníženým srdečním výdejem a tkáňovou hypoperfusí. Následně bylo v celkové anestezii zavedeno VA ECMO a během různých průtoků mimotělní podporou byla pomocí PV diagramu hodnocena práce levé komory. Orgánově specifické parametry byly monitorovány regionální tkáňovou oxygenací a měřením průtoku krve v karotické a subklaviální arterii.

Výsledky:

Závažné dekompensované srdeční selhání vedlo k systémové hypotensi, nízké tkáňové oxygenaci, nízké saturaci smíšené venosní krve a ke zvýšení end-diastolického tlaku v levé komoře. Zvyšováním EBF od minimálního průtoku až na 5 l/min došlo k výraznému zvýšení systolického tlaku v levé komoře, snížení pulsatility v tepnách a zlepšení orgánové perfuse. Na druhou stranu ale byly zjištěny zvýšené nároky na funkci levé komory: významně se zvýšily end-systolický a end-diastolický objem a end-diastolický tlak (pro všechny $P < 0.001$). V důsledku toho vzrostla práce levé komory ($P < 0.05$), avšak ejekční frakce se neměnila. Významně se nezměnil ani isovolumický index kontraktility.

Závěr:

U modelu dekompensovaného chronického i akutního srdečního selhání se při vyšších průtocích VA ECMO zvyšují nároky na práci levé komory. Vysoký průtok VA ECMO tak může být potenciálně nebezpečný a pro ochranu myokardu by měl být průtok mimotělní podporou nastaven nejen s ohledem na systémovou perfusi, ale také na parametry levé komory.

Klíčová slova:

Mimotělní membránová oxygenace; srdeční selhání; hemodynamika; srdeční komory; kardiostimulace

11 References

1. Jackson G., Gibbs C. R., Davies M. K., and Lip G. Y. (2000). "ABC of heart failure. Pathophysiology." BMJ 320(7228): 167-170.

2. Abrams D., Combes A., and Brodie D. (2014). "Extracorporeal membrane oxygenation in cardiopulmonary disease in adults." J Am Coll Cardiol 63(25 Pt A): 2769-2778.

3. Brogan T. V., Lequier L., Lorusso R., MacLaren G., and Peek G. (2017). Extracorporeal Life Support: The ELSO Red Book.

4. Pranikoff T., Hirschl R. B., Steimle C. N., Anderson H. L., 3rd, and Bartlett R. H. (1994). "Efficacy of extracorporeal life support in the setting of adult cardiorespiratory failure." ASAIO J 40(3): M339-343.

5. Combes A., Leprince P., Luyt C. E., Bonnet N., Trouillet J. L., Leger P., Pavie A., and Chastre J. (2008). "Outcomes and long-term quality-of-life of patients supported by extracorporeal membrane oxygenation for refractory cardiogenic shock." Crit Care Med 36(5): 1404-1411.

6. Seo T., Ito T., Iio K., Kato J., and Takagi H. (1991). "Experimental study on the hemodynamic effects of veno-arterial extracorporeal membrane oxygenation with an automatically driven blood pump on puppies." Artif Organs 15(5): 402-407.

7. Aissaoui N., Guerot E., Combes A., Delouche A., Chastre J., Leprince P., Leger P., Diehl J. L., Fagon J. Y., and Diebold B. (2012). "Two-dimensional strain rate and Doppler tissue myocardial velocities: analysis by echocardiography of hemodynamic and functional changes of the failed left ventricle during different degrees of extracorporeal life support." J Am Soc Echocardiogr 25(6): 632-640.

8. Burkhoff D., Sayer G., Doshi D., and Uriel N. (2015). "Hemodynamics of Mechanical Circulatory Support." J Am Coll Cardiol 66(23): 2663-2674.

9. Broome M., and Donker D. W. (2016). "Individualized real-time clinical decision support to monitor cardiac loading during venoarterial ECMO." J Transl Med 14(1): 4.

10. Truby L. K., Takeda K., Mauro C., Yuzefpolskaya M., Garan A. R., Kirtane A. J., Topkara V. K., Abrams D., Brodie D., Colombo P. C., Naka Y., and Takayama H. (2017). "Incidence and Implications of Left Ventricular Distention During Venoarterial Extracorporeal Membrane Oxygenation Support." ASAIO J 63(3): 257-265.

11. Barbone A., Malvindi P. G., Ferrara P., and Tarelli G. (2011). "Left ventricle unloading by percutaneous pigtail during extracorporeal membrane oxygenation." Interact Cardiovasc Thorac Surg 13(3): 293-295.

12. Soleimani B., and Pae W. E. (2012). "Management of left ventricular distension during peripheral extracorporeal membrane oxygenation for cardiogenic shock." Perfusion 27(4): 326-331.

13. Boulate D., Luyt C. E., Pozzi M., Niculescu M., Combes A., Leprince P., and Kirsch M. (2013). "Acute lung injury after mechanical circulatory support implantation in patients on extracorporeal life support: an unrecognized problem." Eur J Cardiothorac Surg 44(3): 544-549; discussion 549-550.

14. Na S. J., Yang J. H., Yang J. H., Sung K., Choi J. O., Hahn J. Y., Jeon E. S., and Cho Y. H. (2019). "Left heart decompression at venoarterial extracorporeal membrane oxygenation initiation in cardiogenic shock: prophylactic versus therapeutic strategy." J Thorac Dis 11(9): 3746-3756.

15. Ošťádal B., and Vízek M. (2005). Patologická fyziologie srdce a cév.

16. Reil J. C., and Bohm M. (2008). "BEAUTIFUL results–the slower, the better?" Lancet 372(9641): 779-780.

17. Davies C. H., Davia K., Bennett J. G., Pepper J. R., Poole-Wilson P. A., and Harding S. E. (1995). "Reduced contraction and altered frequency response of isolated ventricular myocytes from patients with heart failure." Circulation 92(9): 2540-2549.

18. Packer M. (1992). "The neurohormonal hypothesis: a theory to explain the mechanism of disease progression in heart failure." J Am Coll Cardiol 20(1): 248-254.

19. Gardner R. S., Ozalp F., Murday A. J., Robb S. D., and McDonagh T. A. (2003). "N-terminal pro-brain natriuretic peptide. A new gold standard in predicting mortality in patients with advanced heart failure." Eur Heart J 24(19): 1735-1743.

20. Watson R. D., Gibbs C. R., and Lip G. Y. (2000). "ABC of heart failure. Clinical features and complications." BMJ 320(7229): 236-239.

21. Uretsky B. F., Thygesen K., Armstrong P. W., Cleland J. G., Horowitz J. D., Massie B. M., Packer M., Poole-Wilson P. A., and Ryden L. (2000). "Acute coronary findings at autopsy in heart failure patients with sudden death: results from the assessment of treatment with lisinopril and survival (ATLAS) trial." Circulation 102(6): 611-616.

22. Werdan K., Gielen S., Ebelt H., and Hochman J. S. (2014). "Mechanical circulatory support in cardiogenic shock." Eur Heart J 35(3): 156-167.

23. Fuhrman B. P., Hernan L. J., Rotta A. T., Heard C. M., and Rosenkranz E. R. (1999). "Pathophysiology of cardiac extracorporeal membrane oxygenation." Artif Organs 23(11): 966-969.

24. Millane T., Jackson G., Gibbs C. R., and Lip G. Y. (2000). "ABC of heart failure. Acute and chronic management strategies." BMJ 320(7234): 559-562.

25. Power J. M., and Tonkin A. M. (1999). "Large animal models of heart failure." Aust N Z J Med 29(3): 395-402.

26. Dixon J. A., and Spinale F. G. (2009). "Large animal models of heart failure: a critical link in the translation of basic science to clinical practice." Circ Heart Fail 2(3): 262-271.

27. Trahanas J. M., Witer L. J., Alghanem F., Bryner B. S., Iyengar A., Hirschl J. R., Hoenerhoff M. J., Potkay J. A., Bartlett R. H., Rojas-Pena A., Owens G. E., and Bocks M. L. (2016). "Achieving 12 Hour Normothermic Ex Situ Heart Perfusion: An Experience of 40 Porcine Hearts." ASAIO J 62(4): 470-476.

28. Church J. T., Alghanem F., Deatrick K. B., Trahanas J. M., Phillips J. P., Song M. H., Perkins E. M., Bartlett R. H., Rojas-Pena A., Bocks M. L., and Owens G. E. (2017). "Normothermic Ex-Vivo Heart Perfusion: Effects of Live Animal Blood and Plasma Cross-Circulation." ASAIO J.

29. Ostadal P., Mlcek M., Strunina S., Hrachovina M., Kruger A., Vondrakova D., Janotka M., Hala P., Kittnar O., and Neuzil P. (2016). "Novel porcine model of acute severe cardiogenic shock developed by upper-body hypoxia." Physiol Res 65(4): 711-715.

30. Lacko S., Mlcek M., Hala P., Popkova M., Janak D., Hrachovina M., Kudlicka J., Hrachovina V., Ostadal P., and Kittnar O. (2018). "Severe acute heart failure - experimental model with very low mortality." Physiol Res 67(4): 555-562.

31. Bavaria J. E., Ratcliffe M. B., Gupta K. B., Wenger R. K., Bogen D. K., and Edmunds L. H., Jr. (1988). "Changes in left ventricular systolic wall stress during biventricular circulatory assistance." Ann Thorac Surg 45(5): 526-532.

32. Shen I., Levy F. H., Vocelka C. R., O'Rourke P. P., Duncan B. W., Thomas R., and Verrier E. D. (2001). "Effect of extracorporeal membrane oxygenation on left ventricular function of swine." Ann Thorac Surg 71(3): 862-867.

33. Mlcek M., Ostadal P., Belohlavek J., Havranek S., Hrachovina M., Huptych M., Hala P., Hrachovina V., Neuzil P., and Kittnar O. (2012). "Hemodynamic and metabolic parameters during prolonged cardiac arrest and reperfusion by extracorporeal circulation." Physiol Res 61 Suppl 2: S57-65.

34. Ostadal P., Kruger A., Vondrakova D., Janotka M., Psotova H., and Neuzil P. (2014). "Non-invasive assessment of hemodynamic variables using near-infrared spectroscopy in patients experiencing cardiogenic shock and individuals undergoing venoarterial extracorporeal membrane oxygenation." J Crit Care 29(4): 690 e611-695.

35. Ostadal P., Mlcek M., Kruger A., Hala P., Lacko S., Mates M., Vondrakova D., Svoboda T., Hrachovina M., Janotka M., Psotova H., Strunina S., Kittnar O., and Neuzil P. (2015). "Increasing venoarterial extracorporeal membrane oxygenation flow negatively affects left ventricular performance in a porcine model of cardiogenic shock." J Transl Med 13: 266.

36. Tarzia V., Bortolussi G., Bianco R., Buratto E., Bejko J., Carrozzini M., De Franceschi M., Gregori D., Fichera D., Zanella F., Bottio T., and Gerosa G. (2015). "Extracorporeal life support in cardiogenic shock: Impact of acute versus chronic etiology on outcome." J Thorac Cardiovasc Surg 150(2): 333-340.

37. Howard R. J., Stopps T. P., Moe G. W., Gotlieb A., and Armstrong P. W. (1988). "Recovery from heart failure: structural and functional analysis in a canine model." Can J Physiol Pharmacol 66(12): 1505-1512.

38. Moe G. W., and Armstrong P. (1999). "Pacing-induced heart failure: a model to study the mechanism of disease progression and novel therapy in heart failure." Cardiovasc Res 42(3): 591-599.

39. Schmitto J. D., Mokashi S. A., Lee L. S., Popov A. F., Coskun K. O., Sossalla S., Sohns C., Bolman R. M., 3rd, Cohn L. H., and Chen F. Y. (2011). "Large animal models of chronic heart failure (CHF)." J Surg Res 166(1): 131-137.

40. Hala P., Mlcek M., Ostadal P., Janak D., Popkova M., Boucek T., Lacko S., Kudlicka J., Neuzil P., and Kittnar O. (2018). "Tachycardia-Induced Cardiomyopathy As a Chronic Heart Failure Model in

Swine." J Vis Exp 132(e57030).

41. Spinale F. G., Hendrick D. A., Crawford F. A., Smith A. C., Hamada Y., and Carabello B. A. (1990). "Chronic supraventricular tachycardia causes ventricular dysfunction and subendocardial injury in swine." Am J Physiol 259(1 Pt 2): H218-229.

42. Chow E., Woodard J. C., and Farrar D. J. (1990). "Rapid ventricular pacing in pigs: an experimental model of congestive heart failure." Am J Physiol 258(5 Pt 2): H1603-1605.

43. Howard R. J., Moe G. W., and Armstrong P. W. (1991). "Sequential echocardiographic-Doppler assessment of left ventricular remodelling and mitral regurgitation during evolving experimental heart failure." Cardiovasc Res 25(6): 468-474.

44. Lillehei C. W. (1993). "History of the developement of extracorporeal circulation, in Arensman RM, Cornish JD, eds. Extracorporeal Life Support in Critical Care (1st edition), Boston: Blackwell Publications."

45. Bartlett R. H. (2014). "John H Gibbon Jr Lecture. Extracorporeal life support: Gibbon fulfilled." J Am Coll Surg 218(3): 317-327.

46. Kanto W. P., and Shapiro M. B. (1995). "The development of prolonged extracorporeal circulation, in Zwischenberger J B, Bartlett RHH, eds. ECMO: Extracorporeal Cardiopulmonary Support in Critical Care, Ann Arbor, MI."

47. Kolff W. J., Effler D. B., Groves L. K., Peereboom G., and Moraca P. P. (1956). "Disposable membrane oxygenator (heart-lung machine) and its use in experimental surgery." Cleve Clin Q 23(2): 69-97.

48. Kammermeyer K. (1957). "Silicone rubber as a selective barrier." Ind Eng Chem. 49:1685.

49. Bartlett R. H., Isherwood J., Moss R. A., Olszewski W. L., Polet H., and Drinker P. A. (1969). "A toroidal flow membrane oxygenator: four day partial bypass in dogs." Surg Forum 20: 152-153.

50. Hill J. D., O'Brien T. G., Murray J. J., Dontigny L., Bramson M. L., Osborn J. J., and Gerbode F. (1972). "Prolonged extracorporeal oxygenation for acute post-traumatic respiratory failure (shock-lung syndrome). Use of the Bramson membrane lung." N Engl J Med 286(12): 629-634.

51. Bartlett R. H., Gazzaniga A. B., Jefferies M. R., Huxtable R. F., Haiduc N. J., and Fong S. W. (1976). "Extracorporeal membrane oxygenation (ECMO) cardiopulmonary support in infancy." Trans Am Soc Artif Intern Organs 22: 80-93.

52. Bartlett R. H., Gazzaniga A. B., Fong S. W., Jefferies M. R., Roohk H. V., and Haiduc N. (1977). "Extracorporeal membrane oxygenator support for cardiopulmonary failure. Experience in 28 cases." J Thorac Cardiovasc Surg 73(3): 375-386.

53. Bartlett R. H. (2017). "Esperanza: The First Neonatal ECMO Patient." ASAIO J 63(6): 832-843.

54. Zapol W. M., Snider M. T., Hill J. D., Fallat R. J., Bartlett R. H., Edmunds L. H., Morris A. H., Peirce E. C., 2nd, Thomas A. N., Proctor H. J., Drinker P. A., Pratt P. C., Bagniewski A., and Miller R. G., Jr. (1979). "Extracorporeal membrane oxygenation in severe acute respiratory failure. A randomized prospective study." JAMA 242(20): 2193-2196.

55. Makdisi G., and Wang I. W. (2015). "Extra Corporeal Membrane Oxygenation (ECMO) review of a lifesaving technology." J Thorac Dis 7(7): E166-176.

56. Bartlett R. H. (1997). "Extracorporeal Life Support Registry Report 1995." ASAIO J 43(1): 104-107.

57. Haines N. M., Rycus P. T., Zwischenberger J. B., Bartlett R. H., and Undar A. (2009). "Extracorporeal Life Support Registry Report 2008: neonatal and pediatric cardiac cases." ASAIO J 55(1): 111-116.

58. Thiagarajan R. R., Barbaro R. P., Rycus P. T., McMullan D. M., Conrad S. A., Fortenberry J. D., and Paden M. L. (2017). "Extracorporeal Life Support Organization Registry International Report 2016." ASAIO J 63(1): 60-67.

59. Church J. T., Coughlin M. A., Perkins E. M., Hoffman H. R., Barks J. D., Rabah R., Bentley J. K., Hershenson M. B., Bartlett R. H., and Mychaliska G. B. (2018). "The artificial placenta: Continued lung development during extracorporeal support in a preterm lamb model." J Pediatr Surg 53(10): 1896-1903.

60. McLeod J. S., Church J. T., Coughlin M. A., Carr B., Poling C., Sarosi E., Perkins E. M., Quinones M. C., Hala P., Rabah R., Freiheit E., Rojas-Pena A., Bartlett R. H., and Mychaliska G. B. (2019). "Splenic development and injury in premature lambs supported by the artificial placenta." J Pediatr Surg 54(6): 1147-1152.

61. Peek G. J., Mugford M., Tiruvoipati R., Wilson A., Allen E., Thalanany M. M., Hibbert C. L., Truesdale A., Clemens F., Cooper N., Firmin R. K., Elbourne D., and collaboration C. t. (2009). "Efficacy and economic assessment of conventional ventilatory support versus extracorporeal membrane

oxygenation for severe adult respiratory failure (CESAR): a multicentre randomised controlled trial." Lancet 374(9698): 1351-1363.

62. Swol J., Belohlavek J., Haft J. W., Ichiba S., Lorusso R., and Peek G. J. (2016). "Conditions and procedures for in-hospital extracorporeal life support (ECLS) in cardiopulmonary resuscitation (CPR) of adult patients." Perfusion 31(3): 182-188.

63. Haas N. L., Coute R. A., Hsu C. H., Cranford J. A., and Neumar R. W. (2017). "Descriptive analysis of extracorporeal cardiopulmonary resuscitation following out-of-hospital cardiac arrest-An ELSO registry study." Resuscitation 119: 56-62.

64. Richardson A. S., Schmidt M., Bailey M., Pellegrino V. A., Rycus P. T., and Pilcher D. V. (2017). "ECMO Cardio-Pulmonary Resuscitation (ECPR), trends in survival from an international multicentre cohort study over 12-years." Resuscitation 112: 34-40.

65. Spinelli E., Davis R. P., Ren X., Sheth P. S., Tooley T. R., Iyengar A., Sowell B., Owens G. E., Bocks M. L., Jacobs T. L., Yang L. J., Stacey W. C., Bartlett R. H., Rojas-Pena A., and Neumar R. W. (2016). "Thrombolytic-Enhanced Extracorporeal Cardiopulmonary Resuscitation After Prolonged Cardiac Arrest." Crit Care Med 44(2): e58-69.

66. Chen Y.-S., Lin J.-W., Yu H.-Y., Ko W.-J., Jerng J.-S., Chang W.-T., Chen W.-J., Huang S.-C., Chi N.-H., Wang C.-H., Chen L.-C., Tsai P.-R., Wang S.-S., Hwang J.-J., and Lin F.-Y. (2008). "Cardiopulmonary resuscitation with assisted extracorporeal life-support versus conventional cardiopulmonary resuscitation in adults with in-hospital cardiac arrest: an observational study and propensity analysis." The Lancet 372(9638): 554-561.

67. Wang C. H., Chou N. K., Becker L. B., Lin J. W., Yu H. Y., Chi N. H., Hunag S. C., Ko W. J., Wang S. S., Tseng L. J., Lin M. H., Wu I. H., Ma M. H., and Chen Y. S. (2014). "Improved outcome of extracorporeal cardiopulmonary resuscitation for out-of-hospital cardiac arrest–a comparison with that for extracorporeal rescue for in-hospital cardiac arrest." Resuscitation 85(9): 1219-1224.

68. Belohlavek J., Kucera K., Jarkovsky J., Franek O., Pokorna M., Danda J., Skripsky R., Kandrnal V., Balik M., Kunstyr J., Horak J., Smid O., Valasek J., Mrazek V., Schwarz Z., and Linhart A. (2012). "Hyperinvasive approach to out-of hospital cardiac arrest using mechanical chest compression device, prehospital intraarrest cooling, extracorporeal life support and early invasive assessment compared to standard of care. A randomized parallel groups comparative study proposal. "Prague OHCA study"." J Transl Med 10: 163.

69. Lamhaut L., Hutin A., Puymirat E., Jouan J., Raphalen J. H., Jouffroy R., Jaffry M., Dagron C., An K., Dumas F., Marijon E., Bougouin W., Tourtier J. P., Baud F., Jouven X., Danchin N., Spaulding C., and Carli P. (2017). "A Pre-Hospital Extracorporeal Cardio Pulmonary Resuscitation (ECPR) strategy for treatment of refractory out hospital cardiac arrest: An observational study and propensity analysis." Resuscitation 117: 109-117.

70. Jacobs J. V., Hooft N. M., Robinson B. R., Todd E., Bremner R. M., Petersen S. R., and Smith M. A. (2015). "The use of extracorporeal membrane oxygenation in blunt thoracic trauma: A study of the Extracorporeal Life Support Organization database." J Trauma Acute Care Surg 79(6): 1049-1053; discussion 1053-1044.

71. Baratto F., Pappalardo F., Oloriz T., Bisceglia C., Vergara P., Silberbauer J., Albanese N., Cireddu M., D'Angelo G., Di Prima A. L., Monaco F., Paglino G., Radinovic A., Regazzoli D., Silvetti S., Trevisi N., Zangrillo A., and Della Bella P. (2016). "Extracorporeal Membrane Oxygenation for Hemodynamic Support of Ventricular Tachycardia Ablation." Circ Arrhythm Electrophysiol 9(12).

72. ELSO (2019). Extracorporeal Life Support Registry Report. Available online: https://www.elso.org/Registry/Statistics/ published January 30, 2019

73. Soar J., Nolan J. P., Bottiger B. W., Perkins G. D., Lott C., Carli P., Pellis T., Sandroni C., Skrifvars M. B., Smith G. B., Sunde K., Deakin C. D., and Adult advanced life support section C. (2015). "European Resuscitation Council Guidelines for Resuscitation 2015: Section 3. Adult advanced life support." Resuscitation 95: 100-147.

74. Itoh H., Ichiba S., Ujike Y., Douguchi T., Obata H., Inamori S., Iwasaki T., Kasahara S., Sano S., and Undar A. (2016). "Effect of the Pulsatile Extracorporeal Membrane Oxygenation on Hemodynamic Energy and Systemic Microcirculation in a Piglet Model of Acute Cardiac Failure." Artif Organs 40(1): 19-26.

75. Ostadal P., Mlcek M., Gorhan H., Simundic I., Strunina S., Hrachovina M., Kruger A., Vondrakova D., Janotka M., Hala P., Mates M., Ostadal M., Leiter J. C., Kittnar O., and Neuzil P. (2018). "Electrocardiogram-synchronized pulsatile extracorporeal life support preserves left ventricular function and coronary flow in a porcine model of cardiogenic shock." PLoS One 13(4): e0196321.

76. Brodie D., Slutsky A. S., and Combes A. (2019). "Extracorporeal Life Support for Adults With Respiratory Failure and Related Indications: A Review." JAMA 322(6): 557-568.

77. Bartlett R. H. (2016). "Physiology of Gas Exchange During ECMO for Respiratory Failure." J Intensive Care Med.

78. Augustin S., Horton A., Butt W., Bennett M., and Horton S. (2010). "Centrifugal pump inlet pressure site affects measurement." Perfusion 25(5): 313-320.

79. Thompson A. J., Ma L. J., Plegue T. J., and Potkay J. A. (2019). "Design Analysis and Optimization of a Single-Layer PDMS Microfluidic Artificial Lung." IEEE Trans Biomed Eng 66(4): 1082-1093.

80. Cheng R., Hachamovitch R., Kittleson M., Patel J., Arabia F., Moriguchi J., Esmailian F., and Azarbal B. (2014). "Complications of extracorporeal membrane oxygenation for treatment of cardiogenic shock and cardiac arrest: a meta-analysis of 1,866 adult patients." Ann Thorac Surg 97(2): 610-616.

81. Janak D., Hala P., Mlcek M., Popkova M., Lacko S., Kudlicka J., and Kittnar O. (2017). "Detection of microembolic signals in the common carotid artery using Doppler sonography in the porcine model of acute heart failure treated by veno-arterial extracorporeal membrane oxygenation." Physiol Res 66(Supplementum 4): S529-S536.

82. Kinsella J. P., Gerstmann D. R., and Rosenberg A. A. (1992). "The effect of extracorporeal membrane oxygenation on coronary perfusion and regional blood flow distribution." Pediatr Res 31(1): 80-84.

83. Kamimura T., Sakamoto H., and Misumi K. (1999). "Regional blood flow distribution from the proximal arterial cannula during veno-arterial extracorporeal membrane oxygenation in neonatal dog." J Vet Med Sci 61(4): 311-315.

84. Sidebotham D., Allen S., McGeorge A., and Beca J. (2012). "Catastrophic left heart distension following initiation of venoarterial extracorporeal membrane oxygenation in a patient with mild aortic regurgitation." Anaesth Intensive Care 40(3): 568-569.

85. Shen I., Levy F. H., Benak A. M., Rothnie C. L., O'Rourke P. P., Duncan B. W., and Verrier E. D. (2001). "Left ventricular dysfunction during extracorporeal membrane oxygenation in a hypoxemic swine model." Ann Thorac Surg 71(3): 868-871.

86. Buckberg G. D., Fixler D. E., Archie J. P., and Hoffman J. I. (1972). "Experimental subendocardial ischemia in dogs with normal coronary arteries." Circ Res 30(1): 67-81.

87. Brazier J., Cooper N., and Buckberg G. (1974). "The adequacy of subendocardial oxygen delivery: the interaction of determinants of flow, arterial oxygen content and myocardial oxygen need." Circulation 49(5): 968-977.

88. Kato J., Seo T., Ando H., Takagi H., and Ito T. (1996). "Coronary arterial perfusion during venoarterial extracorporeal membrane oxygenation." J Thorac Cardiovasc Surg 111(3): 630-636.

89. Cremers B., Link A., Werner C., Gorhan H., Simundic I., Matheis G., Scheller B., Bohm M., and Laufs U. (2015). "Pulsatile venoarterial perfusion using a novel synchronized cardiac assist device augments coronary artery blood flow during ventricular fibrillation." Artif Organs 39(1): 77-82.

90. Glower D. D., Spratt J. A., Snow N. D., Kabas J. S., Davis J. W., Olsen C. O., Tyson G. S., Sabiston D. C., Jr., and Rankin J. S. (1985). "Linearity of the Frank-Starling relationship in the intact heart: the concept of preload recruitable stroke work." Circulation 71(5): 994-1009.

91. Rihal C. S., Naidu S. S., Givertz M. M., Szeto W. Y., Burke J. A., Kapur N. K., Kern M., Garratt K. N., Goldstein J. A., Dimas V., and Tu T. (2015). "2015 SCAI/ACC/HFSA/STS Clinical Expert Consensus Statement on the Use of Percutaneous Mechanical Circulatory Support Devices in Cardiovascular Care (Endorsed by the American Heart Association, the Cardiological Society of India, and Sociedad Latino Americana de Cardiologia Intervencion; Affirmation of Value by the Canadian Association of Interventional Cardiology-Association Canadienne de Cardiologie d'intervention)." J Card Fail 21(6): 499-518.

92. Hala P., Mlcek M., Ostadal P., Janak D., Popkova M., Boucek T., Lacko S., Kudlicka J., Neuzil P., and Kittnar O. (2016). "Regional tissue oximetry reflects changes in arterial flow in porcine chronic heart failure treated with venoarterial extracorporeal membrane oxygenation." Physiol Res 65(Supplementum 5): S621-S631.

93. Hála P., Mlček M., Ošťádal P., Popková M., Janák D., Bouček T., Lacko S., Kudlička J., Neužil P., and Kittnar O. (2020). "Increasing venoarterial extracorporeal membrane oxygenation flow puts higher demands on left ventricular work in a porcine model of chronic heart failure." J Transl Med 18(1).

94. Strunina S., and Ostadal P. (2016). "Left ventricle unloading during veno-arterial extracorporeal membrane oxygenation." Curr Res Cardiol 1(3): 5-8.

95. Ošťádal P., Bělohlávek J., Balík M., and Říha H. (2018). Extracorporeal embrane Oxygenation - Manual for use in Adult Patients.

96. Seib P. M., Faulkner S. C., Erickson C. C., Van Devanter S. H., Harrell J. E., Fasules J. W., Frazier E. A., and Morrow W. R. (1999). "Blade and balloon atrial septostomy for left heart decompression in patients with severe ventricular dysfunction on extracorporeal membrane oxygenation." Catheter Cardiovasc Interv 46(2): 179-186.

97. Donker D. W., Brodie D., Henriques J. P. S., and Broome M. (2019). "Left ventricular unloading during veno-arterial ECMO: a review of percutaneous and surgical unloading interventions." Perfusion 34(2): 98-105.

98. Avalli L., Maggioni E., Sangalli F., Favini G., Formica F., and Fumagalli R. (2011). "Percutaneous left-heart decompression during extracorporeal membrane oxygenation: an alternative to surgical and transeptal venting in adult patients." ASAIO J 57(1): 38-40.

99. Fumagalli R., Bombino M., Borelli M., Rossi F., Colombo V., Osculati G., Ferrazzi P., Pesenti A., and Gattinoni L. (2004). "Percutaneous bridge to heart transplantation by venoarterial ECMO and transaortic left ventricular venting." Int J Artif Organs 27(5): 410-413.

100. Doll N., Kiaii B., Borger M., Bucerius J., Kramer K., Schmitt D. V., Walther T., and Mohr F. W. (2004). "Five-year results of 219 consecutive patients treated with extracorporeal membrane oxygenation for refractory postoperative cardiogenic shock." Ann Thorac Surg 77(1): 151-157; discussion 157.

101. Brechot N., Demondion P., Santi F., Lebreton G., Pham T., Dalakidis A., Gambotti L., Luyt C. E., Schmidt M., Hekimian G., Cluzel P., Chastre J., Leprince P., and Combes A. (2018). "Intra-aortic balloon pump protects against hydrostatic pulmonary oedema during peripheral venoarterial-extracorporeal membrane oxygenation." Eur Heart J Acute Cardiovasc Care 7(1): 62-69.

102. Nikolaidis L. A., Hentosz T., Doverspike A., Huerbin R., Stolarski C., Shen Y. T., and Shannon R. P. (2001). "Mechanisms whereby rapid RV pacing causes LV dysfunction: perfusion-contraction matching and NO." Am J Physiol Heart Circ Physiol 281(6): H2270-2281.

103. Gupta S., and Figueredo V. M. (2014). "Tachycardia mediated cardiomyopathy: pathophysiology, mechanisms, clinical features and management." Int J Cardiol 172(1): 40-46.

104. Hala P., Mlcek M., Ostadal P., Janak D., Popkova M., Boucek T., Lacko S., Kudlicka J., Neuzil P., and Kittnar O. (2018). "Tachycardia-Induced Cardiomyopathy As a Chronic Heart Failure Model in Swine." J Vis Exp(132).

105. Hendrick D. A., Smith A. C., Kratz J. M., Crawford F. A., and Spinale F. G. (1990). "The pig as a model of tachycardia and dilated cardiomyopathy." Lab Anim Sci 40(5): 495-501.

106. Tomita M., Spinale F. G., Crawford F. A., and Zile M. R. (1991). "Changes in left ventricular volume, mass, and function during the development and regression of supraventricular tachycardia-induced cardiomyopathy. Disparity between recovery of systolic versus diastolic function." Circulation 83(2): 635-644.

107. Shinbane J. S., Wood M. A., Jensen D. N., Ellenbogen K. A., Fitzpatrick A. P., and Scheinman M. M. (1997). "Tachycardia-induced cardiomyopathy: a review of animal models and clinical studies." J Am Coll Cardiol 29(4): 709-715.

108. Carr B. D., Poling C. J., Hala P., Caceres Quinones M., Prater A. R., McLeod J. S., Bartlett R. H., Rojas-Pena A., and Hirschl R. B. (2019). "A Model of Pediatric End-Stage Lung Failure in Small Lambs <20 kg." ASAIO J.

109. Wolf M., Ferrari M., and Quaresima V. (2007). "Progress of near-infrared spectroscopy and topography for brain and muscle clinical applications." J Biomed Opt 12(6): 062104.

110. Little W. C. (1985). "The left ventricular dP/dtmax-end-diastolic volume relation in closed-chest dogs." Circ Res 56(6): 808-815.

111. Kass D. A., Maughan W. L., Guo Z. M., Kono A., Sunagawa K., and Sagawa K. (1987). "Comparative influence of load versus inotropic states on indexes of ventricular contractility: experimental and theoretical analysis based on pressure-volume relationships." Circulation 76(6): 1422-1436.

112. Burkhoff D., Mirsky I., and Suga H. (2005). "Assessment of systolic and diastolic ventricular properties via pressure-volume analysis: a guide for clinical, translational, and basic researchers." Am J Physiol Heart Circ Physiol 289(2): H501-512.

113. Walley K. R. (2016). "Left ventricular function: time-varying elastance and left ventricular aortic coupling." Crit Care 20: 270.

114. Bartlett R. H., Gazzaniga A. B., Huxtable R. F., Schippers H. C., O'Connor M. J., and Jefferies M. R. (1977). "Extracorporeal circulation (ECMO) in neonatal respiratory failure." J Thorac Cardiovasc Surg 74(6): 826-833.

115. Gossage A. M., and Braxton Hicks J. A. (1913). "On auricular fibrillation." Quarterly Journal of Medicine 6: 435-440.

116. Whipple G. H., Sheffield L. T., Woodman E. G., Theophilis C., and Friedman S. (1962). "Reversible congestive heart failure due to chronic rapid stimulation of the normal heart." Proceedings of the New England Cardiovascular Society 20(1): 39-40.

117. Spinale F. G., Grine R. C., Tempel G. E., Crawford F. A., and Zile M. R. (1992). "Alterations in the myocardial capillary vasculature accompany tachycardia-induced cardiomyopathy." Basic Res Cardiol 87(1): 65-79.

118. Moe G. W., Stopps T. P., Howard R. J., and Armstrong P. W. (1988). "Early recovery from heart failure: insights into the pathogenesis of experimental chronic pacing-induced heart failure." J Lab Clin Med 112(4): 426-432.

119. Cruz F. E., Cheriex E. C., Smeets J. L., Atie J., Peres A. K., Penn O. C., Brugada P., and Wellens H. J. (1990). "Reversibility of tachycardia-induced cardiomyopathy after cure of incessant supraventricular tachycardia." J Am Coll Cardiol 16(3): 739-744.

120. Takagaki M., McCarthy P. M., Tabata T., Dessoffy R., Cardon L. A., Connor J., Ochiai Y., Thomas J. D., Francis G. S., Young J. B., and Fukamachi K. (2002). "Induction and maintenance of an experimental model of severe cardiomyopathy with a novel protocol of rapid ventricular pacing." J Thorac Cardiovasc Surg 123(3): 544-549.

121. Umana E., Solares C. A., and Alpert M. A. (2003). "Tachycardia-induced cardiomyopathy." Am J Med 114(1): 51-55.

122. Wyler F., Kaslin M., Hof R., Beglinger R., Becker M., and Stalder G. (1979). "[The Gottinger minipig as a laboratory animal. 5. Communication: cardiac output, its regional distribution and organ blood flow (author's transl)]." Res Exp Med (Berl) 175(1): 31-36.

123. Tranquilli W. J., Manohar M., Parks C. M., Thurmon J. C., Theodorakis M. C., and Benson G. J. (1982). "Systemic and regional blood flow distribution in unanesthetized swine and swine anesthetized with halothane + nitrous oxide, halothane, or enflurane." Anesthesiology 56(5): 369-379.

124. Xanthos T., Bassiakou E., Koudouna E., Tsirikos-Karapanos N., Lelovas P., Papadimitriou D., Dontas I., and Papadimitriou L. (2007). "Baseline hemodynamics in anesthetized landrace-large white swine: reference values for research in cardiac arrest and cardiopulmonary resuscitation models." J Am Assoc Lab Anim Sci 46(5): 21-25.

125. Little W. C. (2005). "Diastolic dysfunction beyond distensibility: adverse effects of ventricular dilatation." Circulation 112(19): 2888-2890.

126. Tanke R. B., Daniels O., van Heijst A. F., van Lier H., and Festen C. (2005). "Cardiac dimensions during extracorporeal membrane oxygenation." Cardiol Young 15(4): 373-378.

127. Kim S., Kim J. S., Shin J. S., and Shin H. J. (2019). "How small is enough for the left heart decompression cannula during extracorporeal membrane oxygenation?" Acute Crit Care 34(4): 263-268.

128. Belohlavek J., Mlcek M., Huptych M., Svoboda T., Havranek S., Ost'adal P., Boucek T., Kovarnik T., Mlejnsky F., Mrazek V., Belohlavek M., Aschermann M., Linhart A., and Kittnar O. (2012). "Coronary versus carotid blood flow and coronary perfusion pressure in a pig model of prolonged cardiac arrest treated by different modes of venoarterial ECMO and intraaortic balloon counterpulsation." Crit Care 16(2): R50.

129. Ito N., Nanto S., Nagao K., Hatanaka T., Nishiyama K., and Kai T. (2012). "Regional cerebral oxygen saturation on hospital arrival is a potential novel predictor of neurological outcomes at hospital discharge in patients with out-of-hospital cardiac arrest." Resuscitation 83(1): 46-50.

130. Mlcek M., Belohlavek J., Huptych M., Boucek T., Belza T., Lacko S., Krupickova P., Hrachovina M., Popkova M., Neuzil P., and Kittnar O. (2016). "Head-up tilt rapidly compromises hemodynamics in healthy anesthetized swine." Physiol Res 64 Suppl 5: S677-683.

131. Liem K. D., Hopman J. C., Oeseburg B., de Haan A. F., Festen C., and Kollee L. A. (1995). "Cerebral oxygenation and hemodynamics during induction of extracorporeal membrane oxygenation as investigated by near infrared spectrophotometry." Pediatrics 95(4): 555-561.

132. Stolar C. J., and Reyes C. (1988). "Extracorporeal membrane oxygenation causes significant changes in intracranial pressure and carotid artery blood flow in newborn lambs." J Pediatr Surg 23(12): 1163-1168.

133. van de Bor M., Walther F. J., Gangitano E. S., and Snyder J. R. (1990). "Extracorporeal membrane oxygenation and cerebral blood flow velocity in newborn infants." Crit Care Med 18(1): 10-13.

134. Orime Y., Shiono M., Nakata K., Hata M., Sezai A., Yamada H., Iida M., Kashiwazaki S., Nemoto M., Kinoshita J., Kojima T., Saito T., and Sezai Y. (1996). "The role of pulsatility in end-organ

microcirculation after cardiogenic shock." ASAIO J 42(5): M724-729.

135. Orime Y., Shiono M., Hata H., Yagi S., Tsukamoto S., Okumura H., Nakata K., Kimura S., Hata M., Sezai A., and Sezai Y. (1999). "Cytokine and endothelial damage in pulsatile and nonpulsatile cardiopulmonary bypass." Artif Organs 23(6): 508-512.

136. Foerster K., Benk C., Beyersdorf F., Cristina Schmitz H., Wittmann K., Taunyane I., Heilmann C., and Trummer G. (2018). "Twenty minutes of normothermic cardiac arrest in a pig model: the role of short-term hypothermia for neurological outcome." Perfusion 33(4): 270-277.

137. Karaci A. R., Sasmazel A., Aydemir N. A., Saritas T., Harmandar B., Tuncel Z., and Undar A. (2011). "Comparison of parameters for detection of splanchnic hypoxia in children undergoing cardiopulmonary bypass with pulsatile versus nonpulsatile normothermia or hypothermia during congenital heart surgeries." Artif Organs 35(11): 1010-1017.

138. Wang S., Izer J. M., Clark J. B., Patel S., Pauliks L., Kunselman A. R., Leach D., Cooper T. K., Wilson R. P., and Undar A. (2015). "In Vivo Hemodynamic Performance Evaluation of Novel Electrocardiogram-Synchronized Pulsatile and Nonpulsatile Extracorporeal Life Support Systems in an Adult Swine Model." Artif Organs 39(7): E90-E101.

139. Walther F. J., van de Bor M., Gangitano E. S., and Snyder J. R. (1990). "Left and right ventricular output in newborn infants undergoing extracorporeal membrane oxygenation." Crit Care Med 18(2): 148-151.

140. Donker D. W., Meuwese C. L., Braithwaite S. A., Broome M., van der Heijden J. J., Hermens J. A., Platenkamp M., de Jong M., Janssen J. G. D., Balik M., and Belohlavek J. (2018). "Echocardiography in extracorporeal life support: A key player in procedural guidance, tailoring and monitoring." Perfusion 33(1 suppl): 31-41.